DECODING CALCIUM ENCODING THROUGH BI-DIRECTIONAL OPTOGENETIC CONTROL OVER G_q-PROTEIN SIGNALING

Pimkhuan Hannanta-anan

A DISSERTATION

in

Bioengineering

Presented to the Faculties of the University of Pennsylvania

in

Partial Fulfillment of the Requirements for the

Degree of Doctor of Philosophy

2018

Supervisor of Dissertation

_____

Brian Chow, Ph.D., Assistant Professor of Bioengineering

Graduate Group Chairperson

_____

Ravi Radhakrishnan, Professor of Bioengineering

Dissertation Committee

Arjun Raj, Ph.D, Associate Professor of Bioengineering

Scott Diamond, Ph.D, Professor of Chemical and Biomolecular Engineering

Matthew Good, Ph.D, Assistant Professor of Cell and Developmental Biology

DECODING CALCIUM ENCODING THROUGH BI-DIRECTIONAL OPTOGENETIC CONTROL OVER G_q-PROTEIN SIGNALING

COPYRIGHT

2018

Pimkhuan Hannanta-anan

ACKNOWLEDGEMENTS

First and foremost, I'd like to thank my advisor, Dr. Brian Chow, who welcomed me into his lab as one of his first students and believed in me throughout my PhD. Brian consistently encouraged me to step out of my comfort zone and supported me in trying new things. It has helped me tremendously to view things differently and to realize that I can do almost anything I put my mind towards. His encouragement and his firm belief in my abilities have been crucial and have helped me to become the confident and independent scientist I am today. Additionally, I'd like to thank my committee members - Dr. Arjun Raj, Dr. Scott Diamond, and Dr. Matthew Good - for providing guidance throughout the course of my Thesis.

Secondly, I'd like to acknowledge all my labmates who were sources of enjoyment, wisdom, and motivation. I'd like to give a special thanks to Ranganath Parthasarathy, my lab and life mentor, who patiently listened to me share my challenges, who guided me in finding solutions for every problem, and who is filled with wisdom that always helped put things in perspective. His insights were immensely instrumental to the completion of this thesis. I'd also like to acknowledge Spencer Glantz, Michael Magaraci, and Erin Berlew for their scientific support, countless hours of thoughtful conversations, and friendship. This thesis would have not been completed without them. They have all made the lab an enjoyable and meaningful place to work.

Lastly, I could not feel more grateful for my friends and family who have been consistent sources of love and support through good and hard times. I'd like to thank my Dad, who since I was young, instilled in me a deep interest in math and science and my

Mom, for her immeasurable amount of care in my well-being, embodied in the countless international calls across numerous time zones to make sure I was always doing well. I'd also like to thank Paul Cheh for the emotional support and companionship. They all have been instrumental to my accomplishments, and I am forever grateful.

ABSTRACT

DECODING CALCIUM ENCODING THROUGH BI-DIRECTIONAL OPTOGENETIC CONTROL OVER G_q-PROTEIN SIGNALING

Pimkhuan Hannanta-anan

Brian Chow

Calcium is a fundamental secondary messenger responsible for relaying information from the extracellular space to the cell interior. Extracellular cues are temporally encoded through calcium signals, which often arise in the form of oscillations. These oscillations are then decoded to inform cellular decisions and regulate cellular functions. Despite its crucial role in cell signaling, the encoding and decoding of calcium oscillations is poorly understood. The current biological tools and methods used to study calcium signaling lack the temporal precision and specificity necessary to precisely manipulate, perturb, and dissect calcium signaling circuits. To address this need, we developed a new set of optogenetic techniques to regulate calcium signaling circuits and study calcium encoding and decoding. First, we created optogenetic RGS2 (opto-RGS2) for studying calcium encoding. A light-induced hetero-dimerization system was engineered to recruit the RGS2 domain to the membrane where it interacted with its cognate G protein. Using our engineered opto-RGS2 cell line, we revealed that RGS2 reduced periodicity and stochasticity of G-protein coupled calcium oscillations and acted as a feedback regulator in this signaling circuit. Our opto-RGS2 addresses the need for better tools to perturb calcium signaling circuits and will enable future studies in calcium encoding. Next, we developed an optogenetic method to dissect mechanisms of calcium decoding. The amplitude, frequency, and duty cycle of calcium oscillations are the

principal components driving calcium-coupled cellular functions. However, how these components individually contribute to the overall calcium decoding is unknown. Using a mathematical model, an optogenetically-engineered cell line, and custom hardware, we optically re-created patterns of calcium oscillations that independently varied a single waveform component. By monitoring calcium-coupled transcription, we revealed that the calcium-dependent transcription factor NFAT was more sensitive to the duty cycle of calcium oscillations as opposed to the oscillation frequency. Therefore, NFAT acted primarily as a signal integrator rather than a frequency decoder as previously hypothesized. With our new optogenetic approach, we isolated the role of individual signaling components and resolved a prevailing and controversial question in calcium decoding.

TABLE OF CONTENTS

LIST OF TABLES

LIST OF FIGURES

CHAPTER 1 : Background and Motivations

1.1 Intracellular signaling dynamics

Cells maintain proper functions and survival by sensing and responding to their changing environments. They are equipped with cascades of signal transduction proteins that convert extracellular information into intracellular signals and inform cell decisions. One ubiquitous signaling architecture is an organization in which multiple extracellular stimuli pass information along through a shared signaling channel (or a common messenger), yet are able to trigger selective cellular responses (**Figure 1.1A**). It is speculated that the response specificity is obtained in part through the distinctive temporal dynamics of the messenger signaling (*7*, *13*, *65*, *84*, *92*, *113*, *128*, *142*, *180*).

Calcium serves as one of these most prevalent messengers that modulate diverse cellular functions, including hormone secretion, contraction, chemotaxis, proliferation, differentiation, survival, and apoptosis (*14*, *15*, *42*, *51*, *94*, *140*, *169*). Different type and concentration of external stimuli have been observed to trigger distinct temporal dynamics of calcium signals which often arise in the form of oscillatory signals. It suggests that the extracellular information is encoded in the temporal patterns of the calcium oscillations, a process termed “calcium encoding” (*10*, *42*, *52*, *54*). In addition, the distinct dynamics of these oscillations have been observed to be associated with specific cellular outcomes. It is believed that downstream calcium effectors are capable of interpret or decode these calcium temporal profiles to activate specific cellular responses (*29*, *37*, *38*, *44*, *121*, *137*, *150*). This process is termed “calcium decoding”

(**Figure 1.1B**). Together, calcium encoding and decoding allow cells to create a unique form of communication that elicits cellular responses specific to individual stimuli.

Given the importance of calcium dynamics in determining cellular decisions, we wished to investigate and gain more understanding of the principles of calcium encoding and decoding. One of the main barriers that limits the study of calcium signaling problems is the lack of tools that can precisely perturb calcium signaling and calcium signaling circuits with high temporal precision and specificity. Traditional genetic perturbation methods, such as overexpression and gene knockout that are commonly used for evaluating the roles of a specific protein within a pathway, are irreversible and sometimes create other unintended effects that confound experimental studies. Small molecules or pharmacological perturbations are often nonspecific and too slow to precisely fine-tune calcium waveforms (*44*, *102*, *165*). Having tools that overcome these limitations and enable studies of calcium encoding and decoding would be desirable.

Optogenetics serves as an ideal approach for such needs. Combining the use of optical stimulation with genetic engineering, optogenetic tools offer precise control over space and time and exhibit high target specificity, while create no toxicity to the cells (*5*, *79*, *154*, *164*, *165*, *181*). Recognizing the advantages of optogenetics, we wished to further develop existing optogenetic tools and engineer novel ones for use in studying calcium encoding and decoding.

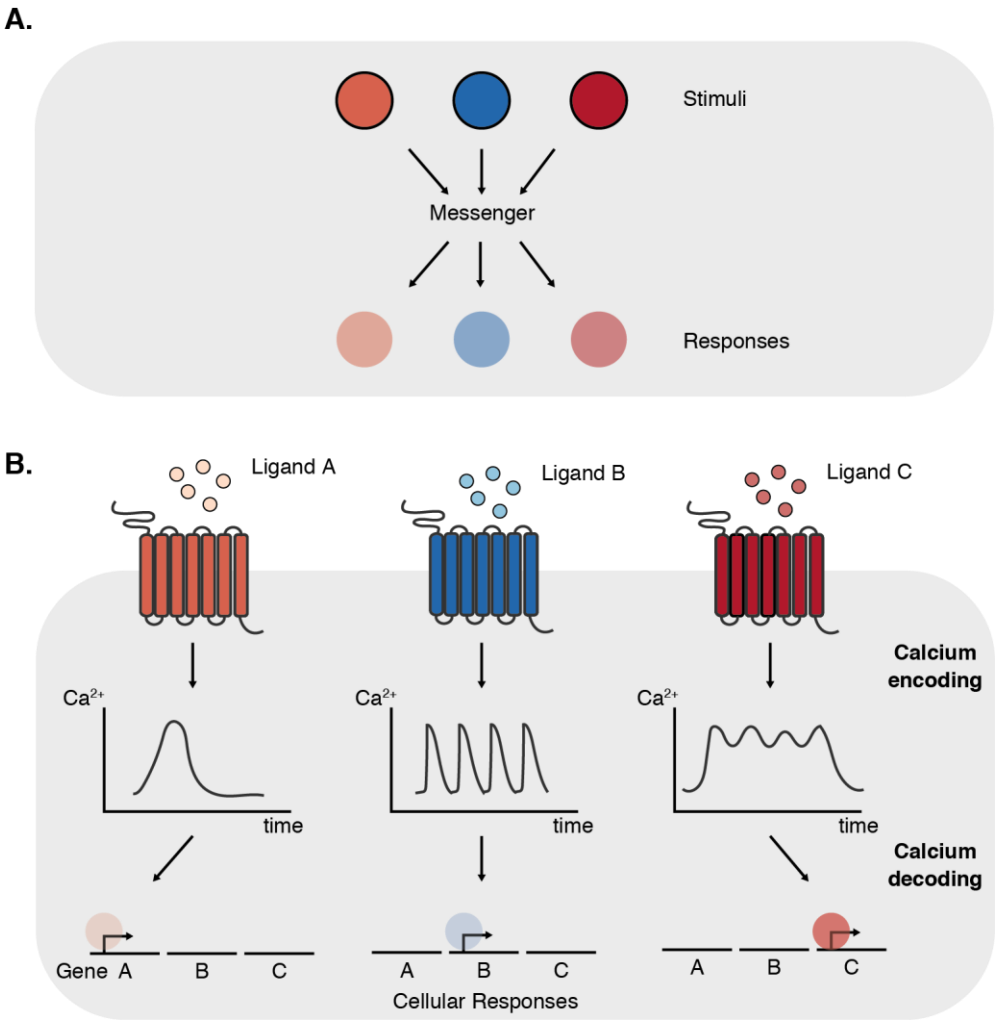

Figure 1.1. Signal transduction network architecture with mutual messengers.

(A) Multiple extracellular ligands send signals through a shared signaling channel. One of the most common channels is calcium.
(B) Cells achieve response specificity through temporal dynamics of the calcium signals. Cells encode information of external ligands in the temporal pattern of calcium signals. The signals are then decode to determine cellular responses/functions. The process by which cells create and interpret calcium signaling patterns specific to the extracellular ligand is termed calcium encoding and decoding, respectively.

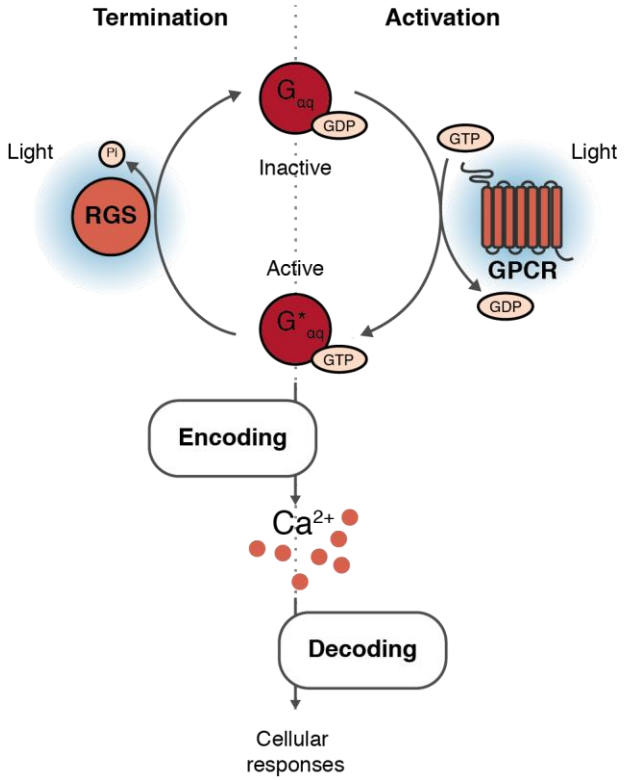

Figure 1.2. Bi-directional optogenetic control of G_q-modulated calcium signaling.

G protein-coupled receptors (GPCRs) mobilize calcium signaling through $G_{\alpha q}$ proteins. $G_{\alpha q}$ proteins are inhibited by regulators of G-protein signaling (RGS), resulting in termination of calcium signaling. Optogenetic manipulation through GPCRs and RGS proteins allows bi-directional control of G_q-modulated calcium signaling for the study of calcium encoding and decoding.

Recognizing the power of optogenetics for elucidating calcium signaling principles, we centered this thesis study around the development of bi-directional optogenetic approaches for regulating calcium signaling and circuitry (**figure 1.2**). One component of this thesis is focused on creating a novel optogenetic tool for resolving the

mechanism of calcium encoding while the other component homes in on determining primary calcium decoding principles.

1.1.1 Calcium encoding

Engagement of different types and concentrations of external ligands gives rise to intracellular calcium oscillations of distinctive patterns. This is possible because of the complex calcium signaling machinery that works together to fine-tune oscillation signals that are unique to each stimulus (*10*, *14*, *20*, *52*). The exact mechanism of the interplay of these signaling molecules is, however, unclear as the existing models fail to comprehensively explain the behavior of the calcium signals observed in non-excitable cells (*42*, *162*).

Original encoding models treat calcium signaling as a deterministic process that provides a mathematical model to explain average behavior of the system (*4*, *34*, *35*, *42*, *43*, *52*, *109*, *157*). A recent model, in contrast, views the calcium signaling as a stochastic process because the calcium signals are initiated from a few IP_3R cluster sites, suggesting that the global process can be subjected to the uncertainty of the opening properties of a few IP_3R channels (*41*, *45*, *148*, *161*, *162*). The stochastic model, therefore, should better describe the true physiological calcium signals. Despite the improvement on the incorporation of the stochastic component, none of the existing models are yet able to resolve the calcium signaling circuit that can give rise to oscillation signals with certain characteristics that have been observed in experiments.

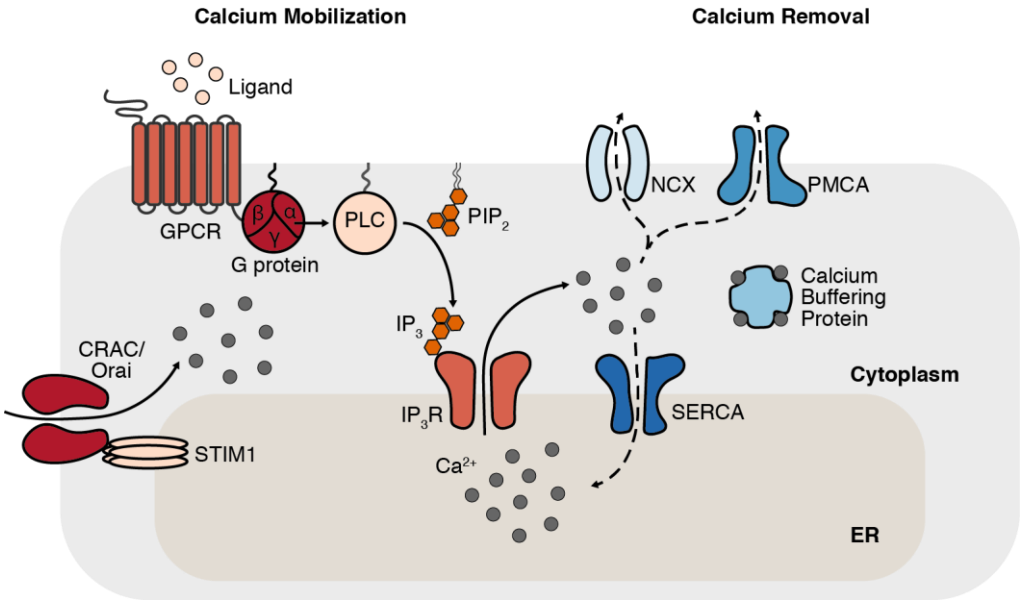

Figure 1.3. Calcium signaling pathway

Engagement of extracellular ligands to the cell-surface receptor GPCRs triggers the releases of calcium from the ER store through the G protein, PLC and IP_3 signaling cascade. Depletion of calcium in the ER, in turn, induces calcium influx from the extracellular space through CRAC/Orai calcium channels, further elevating the intracellular calcium levels. For calcium removal, calcium ions are pumped back into the ER store through SERCA pumps, and removed from the cells through PMCA pumps and NCX transporters. Additionally, cytosolic calcium buffering proteins bind and sequester free cytosolic calcium ions.

In non-excitable cells, calcium mobilization is typically triggered by engagement of extracellular ligands to cell-surface receptors. A repertoire of proteins is involved in regulating calcium levels. Binding of an external ligand to the G-protein coupled receptor (GPCR) activates the heterotrimeric G-protein complexes which are constituted of alpha (α), beta (β), and gamma (γ) subunits bound to the inner surface of the cell membrane. Upon stimulation, the G_α subunit dissociates to activate phospholipase C (PLC) enzyme which subsequently hydrolyses the membrane phospholipid phosphatidylinositol 4,5-bisphosphate (PIP_2) to form inositol trisphosphate (IP_3). IP_3 binds to the calcium channel IP_3 receptors (IP_3R) at the endoplasmic reticulum (ER) membrane, causing the release

of calcium from the ER to the cytosol, elevating the intracellular calcium level. Depletion of calcium from the ER store leads to additional calcium influx from extracellular space through calcium release-activated calcium (CRAC) or Orai channels. The calcium influx induced by the depletion of calcium from the ER is termed store-operated calcium entry (SOCE). On the other hand, calcium removal components consist of calcium pumps and exchangers that act rapidly to terminate calcium elevations. Sarco-endoplasmic reticulum ATPase (SERCA) is a pump located at the ER membrane; it functions to transfer cytosolic calcium back to the internal store. Plasma membrane calcium ATPase (PMCA) pumps and the Na^{+}/Ca^{2+} exchangers (NCX) function to extrude calcium out of cells. In addition, calcium buffering proteins are distributed around the calcium channels and throughout the cytoplasm to bind and sequester free calcium ions (*14*, *24*, *28*) (**Figure 1.3**).

In order for calcium oscillations to occur, these components of machinery must interact with each other in a specific way to allow cycles of rapid calcium increase followed by slow calcium removal. Many deterministic models have been proposed to explain such phenomena. All of these models share a common principle: a fast positive feedback paired with a delayed negative feedback is required to create oscillatory signals (*21*, *53*, *84*, *168*). The existing well-accepted deterministic models can be categorized into two different classes. What differentiates the two classes of model are 1) the point of regulation to which the calcium feedback is coupled and 2) the behavior of the calcium dynamics in relative to IP_3 (*42*).

The first class assumes that oscillations occur through the bi-phasic property of IP_3R (*16*, *46*), in which calcium can both increase and decrease the open probability of

the IP_3R. This unique property permits positive feedback at low calcium levels and a delayed negative feedback at high calcium levels on the IP_3R (*4*, *35*, *40*, *96*, *157*). High activation through positive feedback allows IP_3R to rapidly release calcium to the cytosol, while the accumulation of calcium, in turn, promotes the negative feedback to slow down or terminate the calcium release from IP_3R, leading to the reduction in calcium **(Figure 1.4A)**. The cycles of rapid positive feedback on IP_3R, followed by the slow negative feedback, essentially form a basis for calcium oscillations. With this assumption, calcium oscillations arise at a constant IP_3 level. In this model, the oscillation period should be determined by how fast IP_3R recovers from the negative feedback and re-gains its initial sensitivity which is in the timescale of less than 10 seconds (*30*, *46*, *49*). However, most non-excitable cells exhibit oscillations with much longer periods (*73*), which suggests that additional negative feedback is required to extend the suppression of the calcium level before the next signal spike arises.

The second model assumes that oscillations are modulated through alterations in the production or degradation of IP_3 levels. The elevation of calcium raises the PLC activity, resulting in the increase in IP_3 production and, as a consequence, more calcium is released from the internal stores. Meanwhile, calcium can also activate IP_3 3-kinases that slowly metabolize IP_3 to IP_4 lowering the activity of the IP_3R and, in turn, lowering the accumulation of intracellular calcium **(Figure 1.4B)**. This class of model suggests that IP_3 signals oscillate with the calcium signals (*34*, *109*, *126*). Even though this model can explain the long recovery period as the signal recovery is governed by the rate of IP_3 re-production, it falls short of proving experimentally that the calcium-coupled activity of the PLC beta (β) isoform (*130*), is coupled to G-protein pathways to mobilize the release of ER calcium. As a result, the calcium feedback remains unverified.

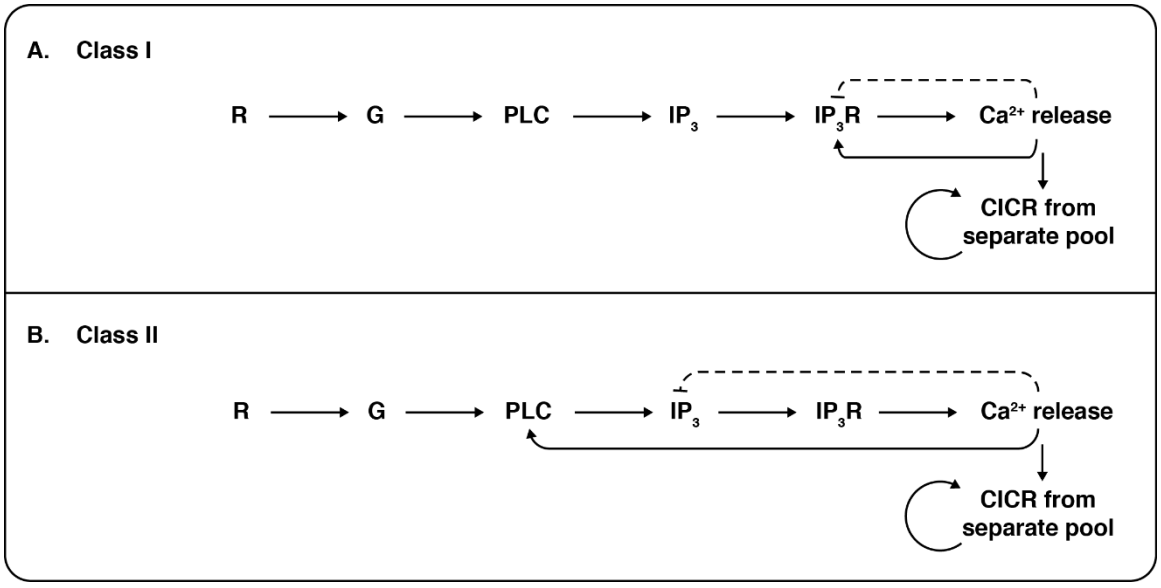

Figure 1.4. Deterministic models of calcium encoding

Calcium oscillations are created through a mixed feedback mechanism of a fast positive feedback and a delayed negative feedback loops. Fast positive feedback allows initial elevation of calcium level which is subsequently suppressed by the slow negative feedback loop. Series of these positive and negative regulation mechanism enable generation of calcium oscillation signals. Two classes of deterministic models have been proposed:
(A) Class I model. The positive and negative feedbacks are coupled through IP_3R. At low calcium concentrations, IP_3Rs are highly sensitive to IP_3 and calcium releases, whereas high calcium levels desensitize IP_3Rs, significantly lowering or inhibiting calcium releases.
(B) Class II model. Calcium elevations enhance PLC catalytic activities while exerts a slow negative regulation by catalyzing the degradation of IP_3.

On the other hand, the stochastic model suggests that calcium signaling should be stochastic as signals are initiated from a few IP_3R clusters (*45*, *148*, *161*). IP_3Rs are arranged in the form of clusters throughout the ER membrane. Binding of IP_3, formed during ligand-evoked GPCR stimulation, to the IP_3Rs increases the probability of IP_3R channel openings. If enough IP_3R within a cluster and the adjacent clusters are open at the same time, enough calcium can be released to generate global calcium signaling (*12*, *20*, *160*). Calcium signals can, therefore, be triggered from a few IP_3R channels.

Calcium signals also demonstrate properties of a stochastic process, in that the periods between calcium spikes, or interspike intervals (ISIs), are independent of each other and vary too drastically (~80%) for the signaling to be deterministic (*45*, *148*, *162*). With this framework, the global negative feedback that regulates the oscillation periods is still missing, but this feedback would also determine the variability of the ISI or the stochasticity of the oscillation signals.

Given this key unknown, one part of this thesis is devoted to resolving the crucial negative feedback that determines prolonged periodicity and regulates the stochasticity of calcium oscillations.

1.1.2 Calcium decoding

It has been observed that different temporal patterns of calcium oscillations result in unique cellular responses. These temporal dynamics are, therefore, speculated to confer cellular response specificity. Such selectivity may potentially be achieved through the existence of multiple calcium effectors (or calcium decoders) that are capable of interpreting information carried in the calcium waveforms (*29*, *121*, *128*, *150*, *166*). Calcium oscillations are often compared to electronic signals in which information is modulated through amplitude (amplitude modulation, AM) or frequency (frequency modulation, FM) (*150*). Receivers can then decode the signals according to the arranged mode of communication (*7*, *121*). Traditional views suggest that the calcium decoders act as the electrical receivers to decode the calcium waveforms using either an AM or FM mode of modulations. However, this view presents one caveat: true frequency

modulation may not exist in biological systems (*135*, *150*). Therefore, an interesting question that we sought to answer is: how exactly do calcium effectors decode the calcium waveform; and, specifically, how does each component of the waveform affect the activities of the calcium decoders. The other component of this thesis is, therefore, focused on uncovering these decoding principles.

AM signaling discriminates signals based on signal amplitude. In the context of calcium signaling, amplitude decoding is determined predominantly by the calcium affinity and the number of calcium binding sites of the calcium decoders (*7*, *52*, *121*, *135*). The decoders with high calcium binding affinity would be activated by just a small elevation of calcium, while the ones with low affinity would require a significantly higher increase in calcium level. In addition to the binding affinity, most calcium effectors show multiple calcium binding sites that allow cooperative binding of calcium ions, giving the effectors a switch-like response upon the calcium binding (*121*, *135*, *136*).

FM communication differentiates signals based on frequency. For calcium decoders, the molecular mechanism for frequency decoding is mostly involved in activation and inactivation or on/off kinetics of the decoder proteins by calcium-dependent kinases and phosphatases. If the oscillation frequency is faster than the typical on-off rates of the proteins, the proteins will integrate the signals resulting in a large accumulated responses. On the other hand, if the oscillation frequency is much lower than the required rate, signal integration will not occur and the signal will simply be decoded as a sum of calcium spikes (*32*, *88*, *119*, *121*, *135*, *150*). Under this mechanism, the oscillation frequency determines if the decoders integrate over spike signals and result in amplified protein activities. However, this calcium decoding is

slightly different from electronic FM in that the decoder activities are still dependent on the amplitude or the calcium load of the calcium signals in addition to the frequency (*135*, *150*).

In addition to amplitude and frequency, duty ratio, defined as a fraction of active signal within an oscillation period, is another characteristic that defines oscillation signals (*135*, *150*). In electronics, most oscillatory signals are purely frequency encoding where frequency changes with constant duty ratio. Electrical receivers are considered true frequency decoders that differentiate frequency changes independent of the duty ratio. In biology, however, most oscillation signals are varied in both frequency and duty ratio (*135*, *150*), while calcium effector activities may also rely on both parameters. Therefore, the role of each waveform component that governs the calcium effector activities is unclear. *As a result, the second half of this thesis seeks to examine the decoding principles that primarily regulate activities of the calcium decoders.*

1.2 Optogenetic tools

1.2.1 Optogenetic tools for studying negative feedback in calcium encoding and regulation of stochasticity

We first aimed to uncover the calcium-coupled feedback loop that controls calcium oscillation and stochasticity. To do that, we first identified possible negative feedback regulation that can potentially terminate calcium elevations. Previous studies suggested that the feedback could potentially be coupled at the following calcium regulation points and mechanisms: (i) GPCR receptors through protein kinase C (PKC)

(*34*), (ii) G proteins through PKC (*34*), (iii) G proteins through regulator of G-protein signaling (RGS) (*69*, *70*, *101*), (iv) PLC (*162*), (v) IP_3R change in sensitivity (*4*, *35*, *96*, *162*), (vi) IP_3R phosphorylation by CaMKII (*48*), and (vii) SERCA (*162*). Recent analyses ruled out PLC, IP_3R and SERCA as perturbations of these protein activities did not alter stochasticity of the calcium oscillations (*162*). The experimental evidence, instead, pointed to the upstream direction closer to the GPCR or G protein as a potential point of negative feedback.

Past studies show more concrete evidence supporting RGS as a calcium-coupled negative feedback regulating periodicity of calcium oscillations. Early theoretical mathematic models incorporate PKC as a possible negative feedback regulator to explain the oscillatory behavior of calcium signals (*34*). There is, however, no experimental proof of PKC inhibition of GPCR and G-protein in response to calcium elevation. In contrast, experiments have shown that RGS plays a role in generating calcium oscillations (*101*, *167*), and its activity is coupled to calcium elevation through calcium binding protein calmodulin (CaM) (*69–71*). By the process of elimination and supporting experimental evidence, RGS is the most plausible negative feedback regulator that controls oscillation periods and stochasticity.

To test this hypothesis, one needs a reversible control of RGS activity. To date, a preliminary optogenetic RGS tool has been made (*118*). It is, however, of a different RGS isoform non-specific to G_α subtype coupled to calcium signaling. Therefore, in this thesis, we set out to create an optogenetic RGS protein that enables light-regulation of specific RGS activity to study its role in regulating oscillation and stochasticity of calcium encoding.

1.2.2 Optogenetic tools for investigation of calcium decoding principles

In order to investigate decoding mechanisms of calcium effectors, one needs an approach to generate calcium oscillations of arbitrary waveforms in which the amplitude, frequency, and duty ratio can be precisely fine-tuned. To fulfill such requirements, an optogenetic tool must be sufficiently fast and sensitive to create of calcium oscillations with amplitudes and frequencies within physiological ranges.

There exist various types of optogenetic tools for controlling calcium signaling. Some are natural light-sensitive proteins found in human photoreceptor cells or other organisms, while others were engineered to incorporate different types of photoreceptors and effectors to regulate calcium signaling (*102*). Each of the tools perturbs calcium signaling at a different point in the pathway and, as a result, exhibits distinct kinetics and properties that are suitable for different applications. To date, there are four general approaches to optogenetic calcium perturbation (*102*):

1.2.2.1 Photo-activated calcium releaser (PACR)

PACR functions through photo-induced release of calcium ions. It is constructed from a plant-derived LOV2 photoreceptor fused to the mammalian calcium binding protein calmodulin (CaM-M13). In the dark, PARC shows extremely high calcium affinity, with dissociation constant (K_d) ~16nm, sequestering calcium within the calmodulin domain. Upon blue light irradiation, PARC changes its conformation lowering its calcium affinity by 200 folds and, therefore, releasing calcium to the cytosol (**Figure 1.5B-i**). PARC then reverses back to its initial state within 41.7s after the blue light is removed

(*50*). Kinetics of less than one minute, such as this, is considered fast compared to other optogenetic calcium tools. However, PARC possesses significant limitations on calcium releasing capacity and its potential crosstalk with the host physiology. PARC can release calcium with the maximum cytosolic concentration of ~ 90nm, which is considerably smaller than the physiological active calcium level (*50*, *102*). It is, therefore, challenging to use PARC to recreate calcium signals equivalent to what is observed in cells under natural hormone stimulations.

1.2.2.2 Photo-activated calcium mobilization through cell-surface receptors

This class consists of natural G_q-coupled opsins and engineered GPCR chimera, opto-α_1AR. These natural opsins carry a retinal chromophore that undergoes isomerization when exposed to light illumination. The isomerization of the chromophore then induces conformational change of the opsins leading to activation of $G_{\alpha q}$ proteins and consequently calcium signals (*57*, *120*, *177*) (**Figure 1.5B-ii**). These opsins are found in arthropods, vertebrates, and human retinal ganglion cells (*131*, *144*, *145*). The variant that is found in vertebrates, called melanopsin (or OPN4), has been expressed and proven to successfully activate calcium in a light-dependent manner in other cell types (*90*, *108*, *120*, *129*, *178*). On the other hand, opto-α_1AR was engineered by replacing the intracellular region of G_t-coupled bovine rhodopsin with that of a human adrenergic receptor to allow intracellular engagement with $G_{\alpha q}$ protein (*2*). This chimera is a proof of concept and is not as sensitive as the natural G_q-coupled opsins. The natural opsins are extremely light sensitive as the signal from the receptor is amplified through a series of signaling cascades to mobilize the calcium signals (*90*, *120*). The

kinetics is relatively slower compared to the tools constructed from LOV domain (*102*), but it is sufficiently fast for our application.

1.2.2.3 Light-gated calcium channels (CatCh)

CatCh is an engineered variant of the algae-derived light-gated non-selective cation Channelrhodopsin-2 (ChR2). CatCh was made by a ChR2 L132C mutation to enhance permeability for calcium ions. Light exposure induces the channel opening resulting in an influx of calcium ions (*87*) (**Figure 1.5B-iii**). Despite its improved calcium permeability, CatCh can conduct only a small amount of calcium ions compared to other cations, making it unsuitable for mobilizing a large calcium load for our intended application.

1.2.2.4 Photo-activated store-operated calcium entry (SOCE)

Optogenetic tools were engineered to directly probe the opening of the membrane Orai channels to imitate the SOCE process without depleting the ER calcium store. SOCE is a process by which the depletion of calcium in the ER store, initiated by the cell-surface receptors, induces calcium influx through plasma membrane CRAC channels (*28*, *122*). CRAC channels comprise two protein families: 1) Orai channel as pore-forming subunit at the plasma membrane and 2) stromal interaction molecule (STIM) as an ER calcium sensor. The depletion of calcium in the ER induces structural reorganization of STIM, causing them to oligomerize. Oligomerized STIM then translocates to the plasma membrane to engage with Orai channels, opening the calcium gate (*28*, *97*, *99*, *151*, *182*). Taking advantage of the existing plant

photoreceptors, two engineering strategies were employed to light-activate SOCE: light-induced oligomerization of STIM1 and light-switchable engagement of Orai.

Light-inducible STIM1 oligomerization: STIM1 consists of a luminal domain responsible for ER calcium sensing and an Orai engagement domain. To induce oligomerization of STIM with light, independent of ER calcium, the luminal calcium-sensing domain was replaced by a plant-derived photoreceptor *Arabidopsis* cryptochrome (CRY2). The tool is termed optoSTIM1. Under light exposure, optoSTIM1 oligomerizes and translocates to activate the calcium influx through CRAC channels (*91*) (**Figure 1.5B-iv**). This approach is highly sensitive, but relatively slow. It requires minutes for the calcium signals to completely reverse back to the basal level in the dark and, therefore, may not be a suitable tool for studying fast calcium kinetics.

Light-switchable Orai engagement: Another strategy is to directly activate the Orai channels with the STIM1 cytosolic (STIM1ct) component (*59*, *72*, *102*, *125*). A fragment of STIM1 bearing a minimal sequence for activating Orai was fused to the truncated light-sensitive LOV2 domain from *A. sativa* phototropin 1 (AsLOV2). AsLOV2 carries a PAS (Period-ARNT-Singleminded) core that forms a binding pocket with flavin mononucleotide (FMN) chromophore and a J_α helix that serves as a linker between the AsLOV2 and the STIM1ct fragment. In the dark, the STIM1ct fragment is inactive, as its Orai interaction interface is protected by the AsLOV2. Under illumination, FMN forms a covalent bond with the PAS core, which in turn induces a conformational change in AsLOV2. As a result, J_α helix and the STIM1ct fragment are relieved from the PAS core, exposing the Orai interaction site and thus allowing gating of calcium influx through the Orai channels (**Figure 1.5B-iv**). The kinetics of this design is generally fast due to the

rapid unhinging mechanism of the AsLOV2 domain. The calcium mobilizing capacity , however, is low compared to opsins or optoSTIM1 and may not be sufficient to elevate calcium concentrations to the desired level.

Three different versions of this design have been created, including LOVS1K (*125*), BACCS (*72*), and Opto-CRAC (*59*). LOVS1K is the earliest version constructed from $LOV2_{402-546}$ fused to $STIM1_{233-450}$. LOVS1K, however, showed relatively low dynamic range and failed to respond to blue light in some of the commonly used cell lines. BACCS is a later variation that contains slightly different truncated sequences of $AsLOV2_{404-538}$ and $STIM1ct_{347-448}$ fragments. Two additional variants of BACCS were designed that include co-expression of human BACCS dimers with human Orai channels (hBACCS2) and *Drosophila* BACCS dimers with *Drosophila* Orai channel (dmBACCS2). Of all the variants, dmBACCS2 exhibited the fastest and highest dynamic range, a considerable improvement over LOVS1K. Similarly, Opto-CRAC took upon the similar design but it also coupled the AsLOV2 domain to lanthanide-doped upconversion nanoparticles (UCNP), which extends the spectra sensitivity of opto-CRAC to a near-infrared range for improved light transmission for in vivo studies.

Among the available options, cell-surface receptor opsins would be the most appropriate tool for generating precise calcium waveforms for the study of calcium decoding principles. In the second portion of this thesis, we will discuss our optogenetic approach that built upon a natural opsin and its application to resolve our key calcium decoding question.

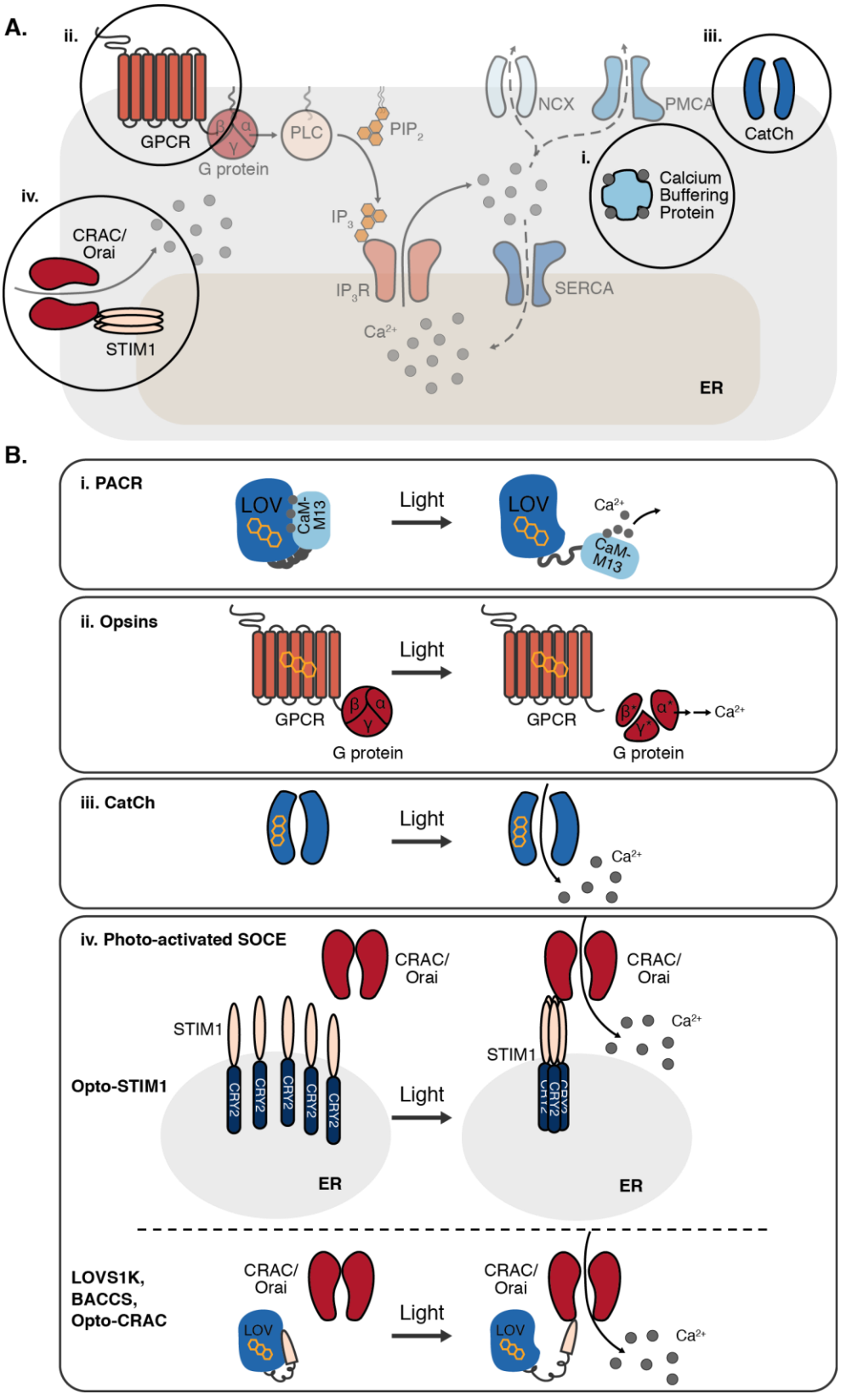
A.
ii.
GPCR
G protein
PLC
PIP2
NCX
PMCA
iii.
CatCh
i.
Calcium Buffering Protein
iv.
CRAC/ Orai
STIM1
IP3
IP3R
SERCA
Ca2+
ER
B.
i. PACR
LOV
CaM-M13
Light
ii. Opsins
GPCR
G protein
iii. CatCh
iv. Photo-activated SOCE
Opto-STIM1
CRY2
LOVS1K, BACCS, Opto-CRAC

1.3 Problem statement

As discussed, calcium signaling is remarkably versatile; it can regulate diverse cellular processes, while maintaining its selectivity through variations of its temporal patterns. We were particularly interested in how this level of signaling sophistication is encoded and decoded to create distinct cellular responses. Numerous hypotheses have been proposed to explain the underlying mechanisms of such encoding and decoding processes. Nonetheless, a number of key questions remain unanswered. As a result, we wished to investigate these key unknowns to gain more understanding of the calcium encoding and decoding that governs an extraordinary number of cellular actions.

Given the dynamic nature of calcium signals, we sought to modify and develop novel optogenetic methods for investigating calcium signaling problems. The first component of this thesis, presented in chapter 2, focuses on the calcium encoding problem; we created optogenetic RGS as a tool to resolve the negative feedback regulation and stochasticity of calcium encoding. The second component of this thesis, presented in chapter 3, describes an optogenetic approach we established that allows

---

Figure 1.5. Optogenetic tools for the regulation of calcium signals

(A) Four classes of optogenetic tools enable light-induced calcium elevations through (i) calcium buffering proteins (ii) cell surface receptor (iii) light-gated ion channel (iv) SOCE
(B) Optogenetic tool mechanism of functions. (i) PACR; calcium buffering domain CaM-M13 is fused to LOV photoreceptor. Light sensing of the LOV domain relieves CaM-M13 and, as a result, releases the bound calcium. (ii) Cell-surface receptor opsins; opsins undergo conformational change upon optical illumination that, in turn, activates $G_{\alpha q}$ proteins and calcium signaling downstream. (iii) CatCh; a high calcium permeable variant of light-gated cation channelrhodopsin ChR2. (iv) Photo-activated SOCE; (*top*) cytosolic STIM1 domains are conjugated to CRY2 photoreceptors. Light induces oligomerization of STIM1 which subsequently engages to the CRAC/Orai channels and promotes the channel openings. (*Bottom*) Minimal STIM1 fragments are fused to LOV domains. Under illumination, STIM1 fragments detach from the LOV domain to gate the openings of CRAC/Orai channels.

for precise re-creation of arbitrary calcium oscillation signals that we applied to reveal the mechanism of calcium decoding of calcium effectors. The developments of these optogenetic approaches to answer the key calcium signaling questions offer novel techniques for studying dynamic systems in cell signaling, and the findings answered by the studies enhance the understanding of how cells create and interpret calcium oscillatory signals that are crucial to the regulation of many important cellular processes.

CHAPTER 2 : Development of Light-Activated Regulator of G-protein Signaling (RGS) for Revealing Its Role in the Feedback Regulation of Calcium Encoding

2.1 Introduction

2.1.1 Calcium encoding

Calcium encoding is an important cellular process whereby cells convert information from the external stimuli into unique patterns of intracellular calcium oscillation signals. These characteristic temporal patterns of the calcium signals inform proper cellular responses (*7*, *13*, *65*, *84*, *92*, *113*, *128*, *142*, *180*). In chapter 1, we discussed signaling machinery orchestrated to regulate calcium signals and presented deterministic models proposed to explain the interplays of the signaling machinery that enable creation of oscillatory signals. Yet the models fall short of describing the calcium oscillations with relatively long periods commonly observed in non-excitable cells.

A number of recent studies have incorporated stochastic aspects to the calcium modeling to capture the unexplained component of the deterministic models. They believe calcium signaling is stochastic as the signals are initiated from a few number of inositol trisphosphate receptor (IP_3R) clusters (*45*, *148*, *149*, *161*). Binding of IP_3 following the extracellular stimulation generally increases the probability of the IP_3 channel opening. If enough channels within a cluster and neighboring clusters open at the same time, sufficient calcium will be released to create global signaling. Because

global calcium waves are often initiated from a small number of IP_3R clusters, the stochastic fluctuations from a few IP_3R can affect the behavior of the whole system. In this framework, the negative feedback controls the stochasticity of the oscillations in addition to the oscillation periods (*162*). Enhancing the negative feedback reduces the signal stochasticity and, in turn, improves signal decodability by the downstream calcium effectors. Therefore, this negative feedback plays a crucial role in the regulation of calcium encoding.

Intermediate signaling proteins such as IP_3R, SERCA, and PLC have been previously investigated, but were proven to have no role in regulating such negative feedback (*162*). Instead, studies suggest that the negative regulation might be further upstream and closer to the G-protein coupled receptors (GPCRs) (*162*). Regulators of G-protein signaling (RGSs) are one of the main negative regulators that exhibit a crucial role in the inhibition of G-protein signaling (*60*, *114*, *147*, *170*, *183*). Studies demonstrate that RGS proteins are necessary for cells to exhibit oscillation signals (*101*, *167*, *176*). In addition, their activities have shown to couple to calcium through calcium binding protein calmodulin (CaM) (*69–71*). Upon activation of G proteins, RGS proteins are sequestered through their interactions with PIP_3. Calcium elevations resulting from the G protein activation promote CaM calcium binding; calcium-bound CaM relieve RGS proteins from PIP_2 allowing them to inhibit G proteins and calcium signaling (*101*, *167*). Given this knowledge, we hypothesized that RGS proteins are the key missing negative feedback regulator of calcium oscillations and stochasticity. In this study, we set out to examine the roles of RGS proteins in the regulation of calcium encoding and stochasticity.

2.1.2 RGS protein functions and mechanisms

RGS proteins are the main negative regulators of G-protein signaling. Upon external stimulation of GPCRs, G proteins are activated by exchanging their bound GDP for GTP, releasing G-protein alpha subunit (G_α) to initiate a cascade of signaling downstream. RGS proteins act as GTPase-accelerating proteins (GAPs) that bind to G_α to catalyze the release of the phosphate (pi) group from the G_α-bound GTP and, therefore, inhibit the G-protein signaling (*60*, *75*, *107*, *114*, *147*, *170*, *183*). Four main subclasses of G_α proteins exist: G_s, $G_{i/o}$, G_q, and $G_{12/13}$. Activation of these G_α protein

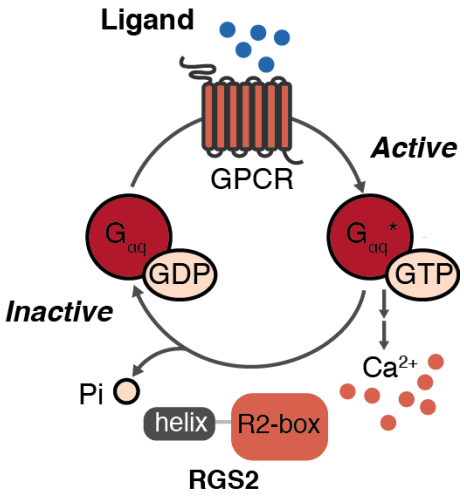

Figure 2.1. RGS2 inhibition of $G_{\alpha q}$ –mediated calcium signaling.

Binding of the external stimuli to G_q-coupled GPCRs activates $G_{\alpha q}$ proteins, which, in turn, trigger the downstream signaling cascade that leads to an increase in intracellular calcium level. RGS2 proteins inactivate the $G_{\alpha q}$ proteins by catalyzing the hydrolysis of the $G_{\alpha q}$ -bound GTP, resulting in the inhibition of $G_{\alpha q}$ and calcium signaling.

classes leads to distinct signaling events including cAMP production, cAMP reduction, intracellular calcium mobilization, and regulation of proton influx (*75*, *183*). Depending on the ligand and GPCRs, unique G_α protein and cellular events will be activated.

RGS proteins comprise a large and diverse family of multi-domain proteins. They all carry a sequence resembling highly conserved RGS domain and additional targeting domains that are distinct among the protein family (*170*, *175*). As a result, RGS proteins have different specificity towards each of the G_α proteins. We are particularly interested in the RGS protein subtype 2 (RGS2) (**Figure 2.1**). RGS2 exhibits highest targeting specificity to G-protein alpha q ($G_{\alpha q}$) (*63*, *85*, *114*, *153*), the G_α subclass that is coupled to the calcium signaling pathway. Active $G_{\alpha q}$ activates phospholipase C (PLC), which in turn, hydrolyzes phosphatidylinositol 4,5-bisphosphate or PtdIns(4,5)P_2 (PIP2) to produce an inositol trisphosphate (IP_3) molecule. IP_3 binds to the calcium channel IP_3 receptors on the endoplasmic reticulum (ER) membrane resulting in the release of the store calcium to the cytosol, elevating the intracellular calcium level. An increase in RGS2 activity inhibits $G_{\alpha q}$ signaling and, as a result, terminates calcium signaling.

2.1.3 RGS perturbation approaches

Appropriate RGS perturbation tools are necessary for studying the roles of RGS in calcium encoding. However, temporally precise technologies for probing the regulatory roles of specific RGS are lacking, subtype-selective pharmacological agents are challenging to create, and traditional genetic manipulation techniques are prone to compensatory confounds from RGS of non-interest and from signaling changes that maintain basal second messenger load (*80*, *86*, *132*, *147*, *171*). With the ability to

dynamically recapitulate protein function in response to light, optogenetic approaches are ideal for fulfilling such needs.

2.1.4 Problem statement

As RGS2 serves key dynamic roles in regulating the frequency of resting and agonist-induced intracellular calcium oscillations (*8*, *101*, *171*), we set out to engineer an optogenetic RGS2 (opto-RGS2) for temporally precise termination of $G\alpha_q$-signaling and downstream store-operated release of calcium from the endoplasmic reticulum (ER) (*9*, *61–63*, *68*, *82*). We examined two different Opto-RGS2 designs and their light-induced calcium inhibition capabilities. The best design was selected and applied to study a role of RGS2 in negative feedback control in calcium encoding. By emulating brief pharmacological stimulation of RGS2 in the absence of available selective agonists, this work expands the optogenetic toolbox for GPCR signaling and reveals how RGS impact cellular dynamics through inhibitory regulation of oscillatory calcium signals.

2.2 Results and discussion

2.2.1 Opto-RGS2 design

2.2.1.1 Opto-RGS2 general architecture and approach

RGS2 is composed of two domains: α-helix on the N-terminus and a conserved RGS domain on the C-terminus. The RGS domain is highly conserved and responsible for GTPase-accelerating (GAP) function, whereas the N-terminal α-helix regulates

subcellular localization of the RGS proteins (*9*, *61–63*, *85*, *112*) **(Figure 2.2A)**. The α-helix sequences are varied among the RGS members and therefore determine their unique subcellular localizations. Experiments have shown that the RGS domains alone without the α-helix are lost in cytoplasm and unable to effectively carry out its GAP functions.

One approach to manipulate activities of the RGS proteins is to sequester RGS domain within the cytoplasm and recruit them to the membrane where GPCRs and G proteins are located. To make this recruitment optically-regulated, we employed photo-inducible hetero-dimerization proteins where association of the two protein subunits can be induced upon illumination(*55*, *74*, *81*, *83*, *93*, *156*, *158*). The RGS domain was fused to one subunit of the photoreceptor, and the α-helix targeting domain was fused to the photoreceptor binding partner **(Figure 2.2A)**. In the absence of light, the component with

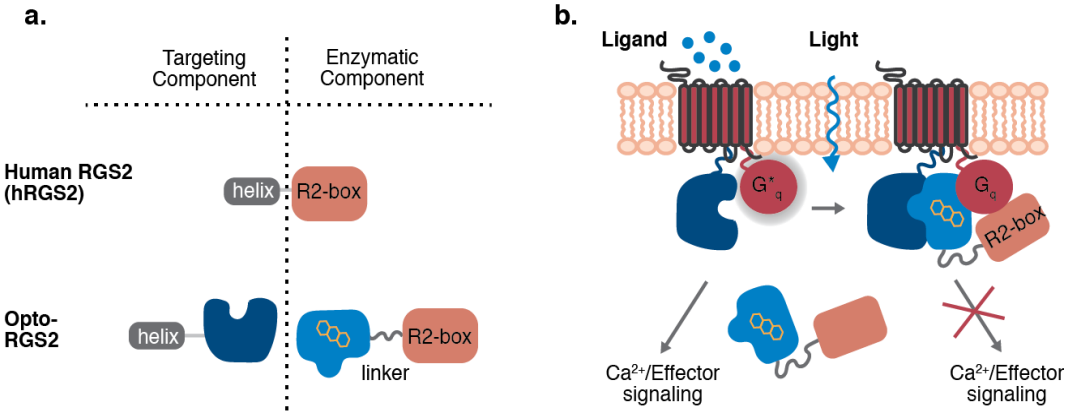

Figure 2.2 Design of optogenetic RGS2 (opto-RGS2).

(A) Opto-RGS2 splits the catalytic box and N-terminal amphipathic helix of human RGS2, and individually fuses them to a dimerization photoreceptor and its interaction partner.
(B) R2box photoreceptor fusion is sequestered in the cytosol in the dark. Light induces hetero-dimerization of the split components, reconstituting a functional membrane-localized complex.

targeting domain are localized at the membrane, while the component with the RGS domain are distributed in the cytoplasm. Optical stimulation will recruit the RGS domain to the membrane enabling it to act on the G proteins and terminate the signaling **(Figure 2.2B)**.

2.2.1.2 Choice of dimerization photoreceptors

To design photo-activated RGS systems based on light-inducible protein association approach, we first considered choices of dimerization photoreceptors based on their broad kinetic range (turn-on and turn-off rates), high dynamic range, no chromophore requirement, and small size. It is advantageous particularly for in vivo applications if the photoreceptors require no exogenous supplement of a chromophore. Small protein size reduces chance of steric hindrance to the interaction between RGS domain and G proteins and can also lead to better cellular expression (*117*, *164*, *181*, *185*). Based on these factors, we selected two photoreceptor candidates - naturally derived *Arabidopsis* cryptochrome 2 proteins (*83*, *158*) and a synthetic LOV-domain based iLID system (*55*, *56*) – for constructing our initial models of our opto-RGS2 systems.

Cryptochrome pairs are the most widely and successfully used photoproteins for applications involved light induced subcellular locations. They consist of two subunits – CRY2 and CIB1- that use flavin adenine dinucleotide (FAD) cofactor for light sensing. This cofactor is naturally present in mammalian cells, and no additional supplement is therefore required for this system (*22*, *83*, *95*, *158*). Many variants of cryptochrome pairs have recently been developed for fast and slow kinetics, improved dynamic range,

reduced dark background, and reduced size. These variants possess relatively wide range of kinetics in which association can be induced under illumination within seconds or minutes, whereas the dissociation happens spontaneously in the dark within minutes depending on the variants (*158*). Broad kinetic range can be useful for engineering light-

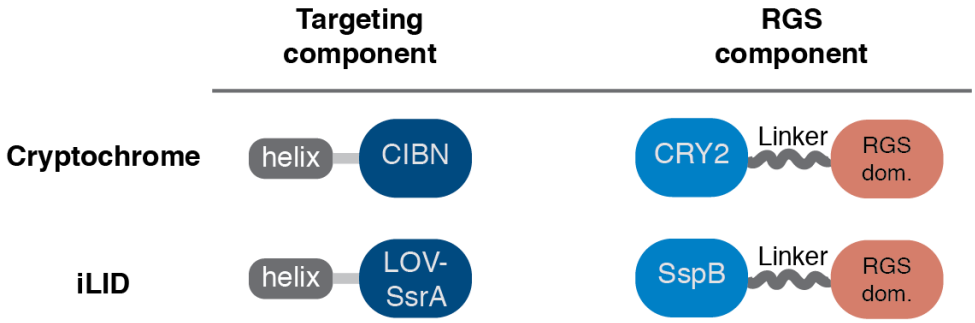

Figure 2.3. Cryptochrome- and iLID-based opto-RGS2.

RGS2 domain and α-helix were respectively fused to CRY2 and its interaction partner, CIBN, for the cryptochrome-based design (*top*). For the iLID-based system, CRY2 and CIBN were replaced with SspB and LOV-SsrA, respectively (*bottom*).

activated RGS with variable kinetics that are suitable for different applications. The cryptochrome systems also exhibit reasonable dynamic range based on cellular membrane recruitment assay (*56*). CRY2 and CIBN were respectively fused to the RGS2 domain and the RGS α-helix to construct cryptochrome-based opto-RGS2 **(Figure 2.3)**.

iLID is an engineered LOV-domain based dimerization between two bacterial peptides – SsrA and SspB. SsrA is fused to a Jα-helix of the light-switchable LOV domain so that interaction surface of SsrA peptide is buried in the dark. Light then induces conformational change to the LOV domain relieving the SsrA peptide to interact

with its dimer partner SspB peptide. The system is attractive due to its exceptionally high dynamic range, ~50 fold-change in light-to-dark activity, of its newly developed variants. The two subunits are shorter than 250 amino acids considered to be small compared to other photo-dimerization proteins. Association rate upon illumination and dissociation rate in the dark are in second timescale, the fastest of all the existing dimerization pairs (*55*, *56*). Its fast kinetics will enable better control over dynamic of the protein activity within a cell. To construct an iLID-based opto-RGS, we fused the N-terminal α-helix to the LOV-SsrA subunit and the RGS2 domain to the SspB subunit. Linkers were inserted between SspB and RGS domain to improve expression and RGS activities **(Figure 2.3)**.

2.2.1.3 Linker analysis to improve protein folding and expression

Ones of the major challenges in designing synthetic multi-domain proteins for applications in mammalian systems are poor expression yield and low biological activity. These issues arise particularly when the domains are in close proximity where one domain can interfere with the folding and structural stability of the adjacent domains and can create steric hindrance preventing interaction of the functional domain with its target. In these instances, insertion of peptide linkers is often necessary to lengthen the distances between the domains in order to improve the stability and overall functionality of the protein (*26*). This is specifically relevant for the component containing the RGS domain, as it requires extensive interaction with Gα protein to efficiently perform inhibitory activity.

We explored two key properties of the domain linkers: length and rigidity. The optimal linker length usually ranges from 5-20 amino acids depending on the size and

the function of the conjugated proteins. In term of rigidity, linkers can be classified into two types: flexible and rigid. The flexible linkers are generally employed when certain degree of mobility is required for protein-protein interactions, whereas rigid linkers are useful when further domains separation and firm orientation of the protein are required for the protein interaction (*26*). To date, there are no universal rules for determining suitable types of linkers for constructing multi-domain proteins. We therefore empirically examined the most widely used linkers from each category: (GGGGS) as a flexible linker and (EAAAK) and (AP) as rigid linkers with four varying lengths: 5, 10, 15, and 20 amino acids.

The cryptochrome-based system opto-RGS2 was constructed with 12 different linkers with varying length and rigidity and expressed in HEK293t cells. The expression of each variant was imaged with fluorescence microscopy to observe protein folding and subcellular distribution, and quantitatively assessed using flow cytometry. Our analysis showed that linkers are strictly necessary for yielding reasonable expression and functional opto-RGS2. The CRY2PHR-RGS without a linker was poorly expressed and not properly folded as indicated by formations of puncta and protein aggregation. Insertions of linkers, on the other hand, significantly improved the construct expression and protein stability as indicated by uniform distribution of protein expression throughout the cytoplasm (**Figure 2.4A**). CRY2-R2box with $(GGGGS)_3$ linker was expressed at a slightly higher level than the other linkers of the same length (**Figure 2.4C**), while linker length showed no effect on the expression for all linker types (**Figure 2.4B**). We next looked at the expression stochiometery of the two components. A plasmid construct carrying both cryptochrome units separated by the 2A ribosomal skipping site (labeled as “2A” site was used a reference for equimolar expression. G/S rich linker was

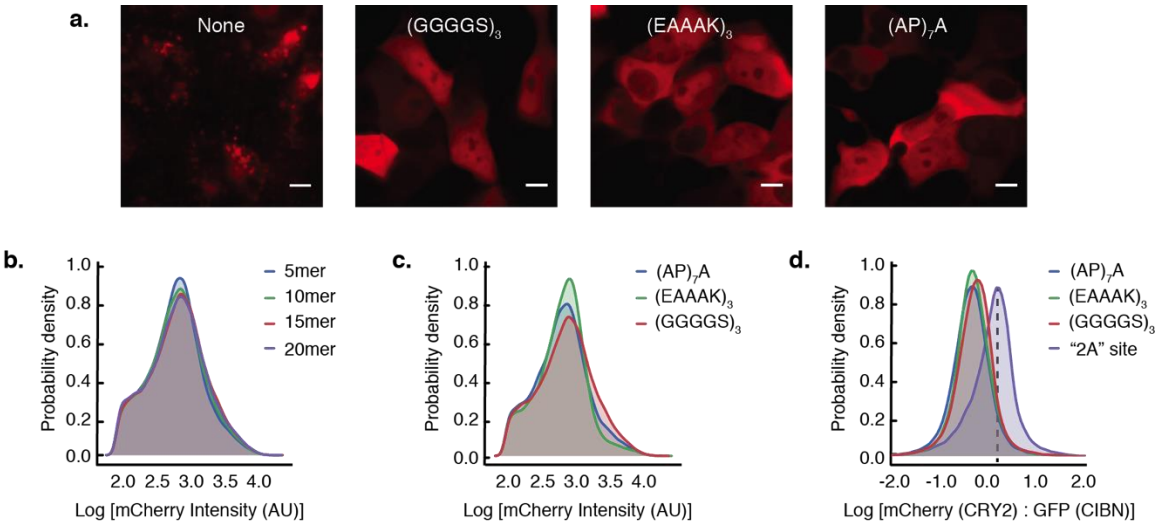

Figure 2.4. Linker analysis for improvement of CRY2-R2box expression.

(A) Fluorescence micrographs of HEK293t cells expressing mCherry-tagged CRY2-R2box of different linker variants. Scale bar = 10 μm. Insertion of a linker between CRY2 and R2box significantly improved protein folding and, consequently, enhanced expression of CRY2-R2box.
(B-D) Probability density distributions of mCherry-tagged CRY2-R2box and GFP-tagged R2helix-CIBN expression monitored by flow cytometry fluorescence analysis.
(B) CRY2-R2box with G/S-rich linker of varying lengths. Similar linker length-dependent distribution trends were observed with rigid (EAAAK)n and (AP)n repeat linkers (not shown).
(C) CRY2-R2box with varying 15-mer linker types.
(D) Ratio CRY2-R2box vs. R2helix-CIBN, where constructs were delivered on separate plasmids.

expressed at better stoichiometry (when co-expressed with R2helix-CIBN) as compared to the other two **(Figure 2.4-D).** R2helix-CIBN was in ~40% excess of the R2helix-CIBN unit. Because of its higher expression and improved stoichiometry, G/S-rich linker was selected for our final opto-RGS2 design.

2.2.2 Light-induced translocation

We first evaluated the properties of the photo-activated RGS system variants

through their light-induced membrane translocation activities, which can serve as an initial functional measurement of the opto-R2 variants.

2.2.2.1 iLID system

iLID system possesses two versions of the SspB unit which differs by its binding affinity towards LOV-SsrA. The “nano” SspB exhibits its largest dynamic range within the nanomolar range, whereas the “micro” SspB shows its optimal binding at the micromolar range. Because the absolute expression level of the system was unknown in our HEK293t cell model, we examined both variants for the initial opto-RGS2 design.

HEK293t cells were co-expressed with the GFP-tagged α-helix-LOV-SsrA and either “nano” or “micro” version of mCherry-tagged SspB-R2box and imaged under fluorescence microscopy. α-helix-LOV-SsrA was predominantly concentrated around the membrane and in the nucleus similar to the subcellular localization pattern of the native hRGS2. The SspB-R2box was, on the other hand, distributed more evenly throughout the cells. Saturated illumination did not appear to induce membrane translocation of the SspB-R2box as indicated by no significant change in the fluorescence intensity profile across the cell membrane for both iLID variants (**Figure 2.5**).

We suspected that fusion of the R2 α-helix to the N-terminus of the LOV-SsrA may have interfere with the photo-switchability of the LOV domain, as iLID-based optogentic tools constructed previously have only fused a small domain to the C-terminus of the LOV-SsrA. Therefore, we examined the dimerization ability of the SspB-R2 to C-terminal fusion membrane targeting sequence (CaaX) LOV-SsrA. Our analysis

showed that the same light condition did induce the translocation of the SspB-R2 to dimerize with LOV-SsrA-CaaX at the membrane (data not shown). These results indicated that N-terminal fusion of α-helix disrupted the light-inducible dimerization capability of the iLID system, suggesting that iLID was not an appropriate photoreceptor for this particular Opto-RGS2 design.

2.2.2.2 Cryptochrome system

We next evaluated the membrane recruitment activity of the cryptochrome-based opto-R2. GFP-tagged α-helix-CIBN and mCherry-tagged CRY2-R2 were co-expressed in HEK293t cells and imaged under fluorescence microscopy. α-helix-CIBN was accumulated largely at the plasma membrane and inside the nucleus similar to the subcellular localization pattern of the human RGS2 (**Figure 2.6A-B**). The cells were exposed to a saturated blue illumination epoch (0.5s ON, 5s OFF for 60s) and translocation of CRY2-R2 was monitored overtime through mCherry fluorescence imaging. The CRY2-R2 component was successfully recruited to the membrane upon illumination to co-localize with the α-helix-CIBN, reconstituting a full-length hRGS2 (**Figure 2.6C**).

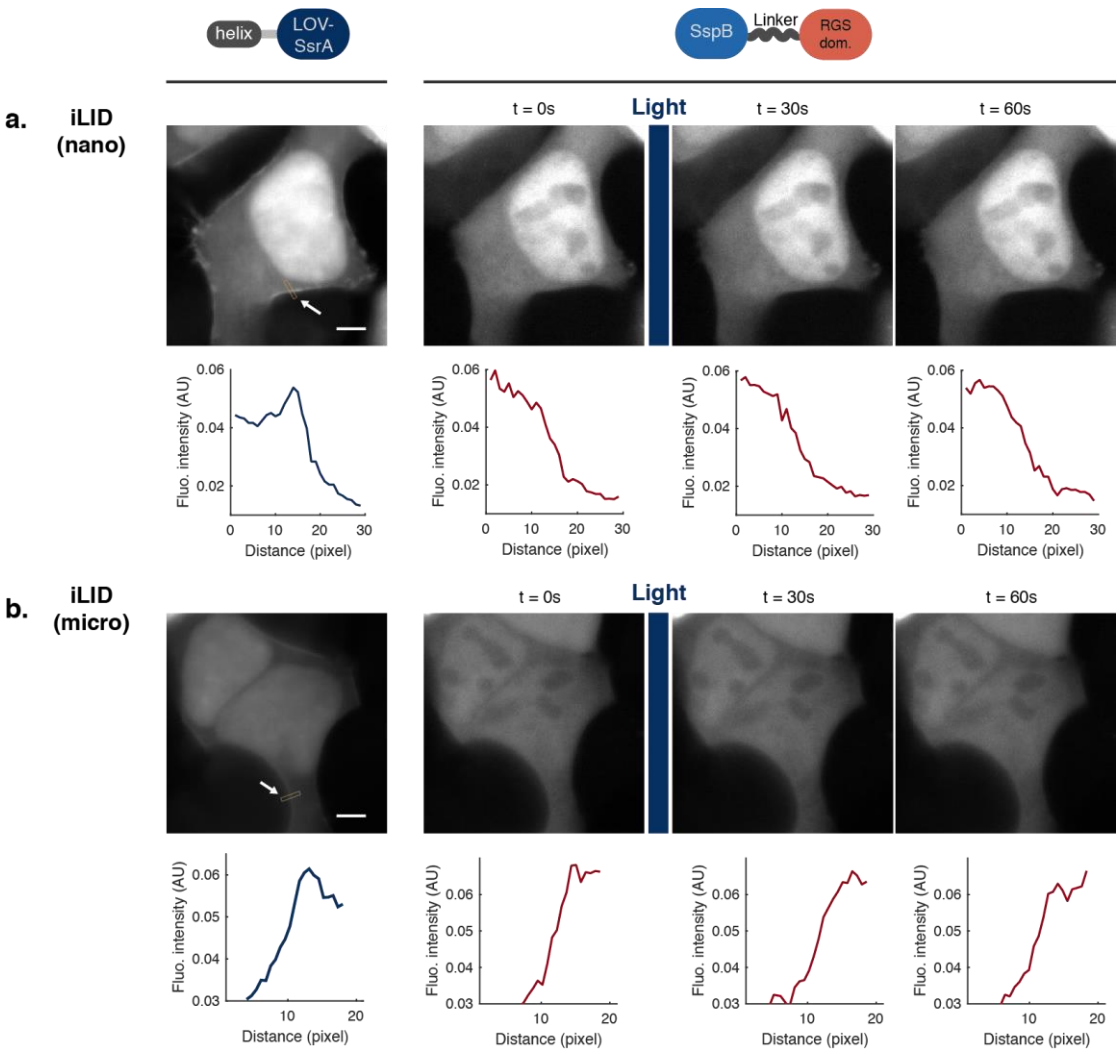

Figure 2.5. Light-induced membrane recruitment of iLID-based opto-RGS2 system.

(A) Analysis of light induced translocation of the iLID nano variant and (B) the iLID micro variant. (*Top panel*) Fluorescence micrographs of HEK293t cells co-expressing GFP-tagged α-helix-LOV-SsrA and mCherry-tagged SspB-RGS2box. Scale bar = 5 μm. Cells were exposed to blue illumination epoch (λ = 475 nm, 0.5s every 5s) after t = 0s. (*Bottom panel*) Corresponding fluorescence intensity profiles across the cell segment within the highlighted box.

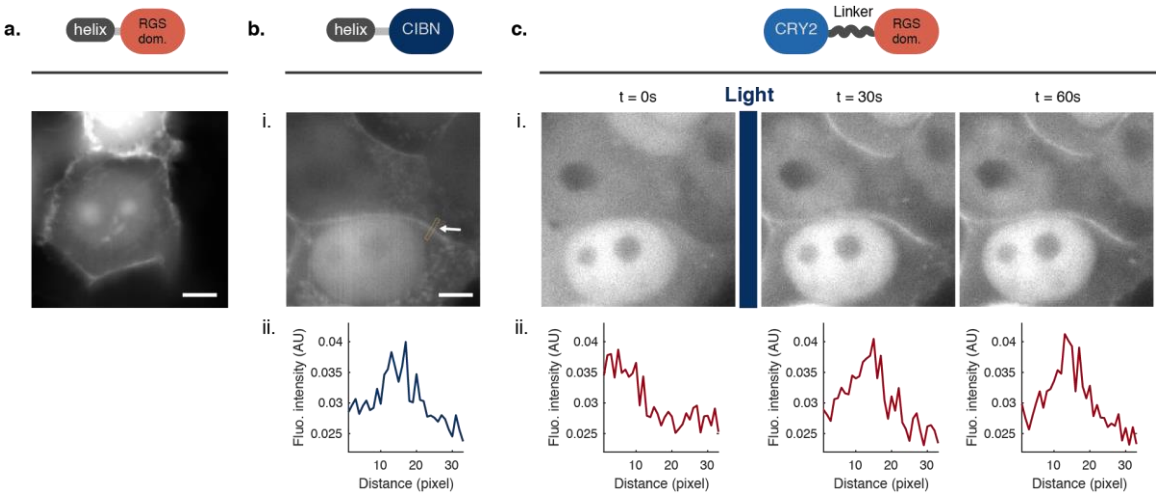

Figure 2.6 Light-induced membrane recruitment of cryptochrome-based opto-RGS2 system.

(A) Fluorescence micrograph of HEK293t cells expressing GFP-tagged hRGS2.
(B-C) Example HEK293t cells co-expressing GFP-tagged α-helix-CIBN and mCherry-tagged CRY2-R2box. Upon blue-light illumination (λ = 475 nm, 7.37 mW/mm2), CRY2-R2box translocated to the plasma membrane to dimerize with α-helix-CIBN. Bottom panel (b.ii, c.ii) shows corresponding intensity profile plots across a segment of the cell membrane (marked with white arrow). The intensity profile plot of the CRY-R2 becomes more similar to that of α-

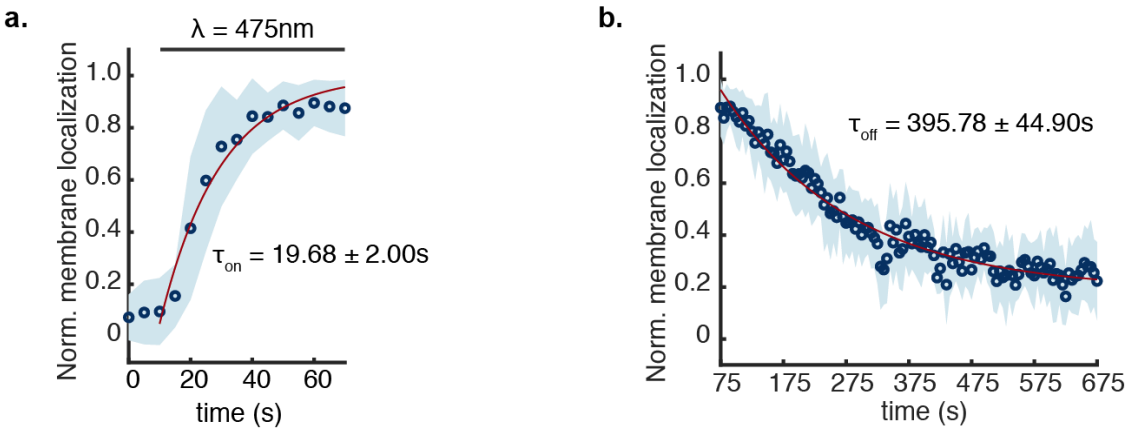

Figure 2.7 Light-induced membrane translocation and dark reversion kinetics of cryptochrome-based opto-RGS2.

(A) Membrane translocation kinetics of CRY2-R2box. Illumination epoch (λ = 475nm, 0.5s ON, 5s OFF) was delivered starting at t = 15s.
(B) Dark reversion kinetics of CRY2-R2box. CRY2-R2box slowly diffuses back to cytosol once the illumination was withdrawn.

We then sought to quantify the kinetics of the cryptochrome-based opto-R2 which is an important characteristic that defines the temporal resolution of the tool and is useful information for guiding subsequent experimental designs of calcium inhibition. Similar membrane translocation protocol was employed where a 60s-blue illumination epoch was delivered to induce CRY2-R2box membrane translocation. The increase in accumulation of CRY2-R2box at the membrane was quantified as a measure of association kinetics. The analysis was performed over 20 cells, and the association constant was estimated to be 19.68 ± 2.00s (**Figure 2.7A**). The illumination was then turned off to allow quantification of the dark reversion kinetic. CRY2-R2box slowly dissociated from the membrane and redistributed to the cytosol. The dissociation constant was calculated to be 395.78 ± 44.90s **(Figure 2.7B)**. Because the cryptochrome-based opto-R2 showed successful translocation upon illumination and dark reversibility with reasonably fast kinetics, we selected the cryptochrome-based system over iLID as the final design of our opto-R2.

2.2.3 Correlation analysis and machine learning guided cell selection

To assess the efficiency of opto-RGS2 in suppressing calcium signaling and identify its determinant factors, intracellular calcium elevations were induced through carbachol-stimulation (30 uM CCh) of endogenous M3 muscarinic receptors in HEK cells and monitored by single-cell GCaMP6f imaging (**Figure 2.8A-B**). A CRY2 “dark mutant” or “blind mutant”, which harbors a D387A mutation to prevent uptake of the optically active flavin cofactor necessary for photo-induced signaling (*100*), was used as a control to account for the effects of metabolic load and illumination. The degree of calcium amplitude suppression positively correlated with translocation efficiency (inverse of

change in cytosolic mCherry (F/F_0)) and with the expression level of CRY2-R2box (mCherry tag, F_0), with Spearman's rank correlation coefficients, ρ = 0.42 and 0.37, respectively (**Figure 2.8C-D**). The CRY2-R2box translocation of the "dark mutant" (red) was minimal and, in contrast, showed poor correlation with calcium suppression (ρ = 0.15) (**Figure 2.8C**).

Given the cell-to-cell variability in transiently transfected cells, clonal cell lines are required to ensure that opto-RGS2 function is reliable. Thus, we sought quantitative criteria that would enable systematic selection of high-performing clones, while maintaining tractable cell line selection throughput. Machine learning (logistic regression) was performed to identify such a parameter space that predicts reliable calcium suppression based on CRY2-R2box translocation and expression level (**Figure 2.8E**), which are more facile screening parameters to obtain than calcium dynamics. The model was able to predict the magnitude of optogenetic response with a true positive rate as high as 80%, meaning that cells within the gray-shaded "predicted responsive" region are 80% likely to be "strongly inhibited" (defined in Figures 2.8C-D) experimentally. Note that as the model was built to maximize the true positive prediction for efficient cell line generation, the minimization of false negative predictions was not of interest.

To test the prediction criteria, calcium suppression assays were performed using transfected opto-RGS2 cells that were distinct from the machine learning training set. As expected in "predicted responsive" cells, opto-RGS2 activation efficiently suppressed calcium elevations and to a similarly near-complete extent as over-expressed hRGS2, whereas the dark mutant showed no inducible suppression identical to the wild-type

HEK cells (**Figure 2.8F**). The validated criteria were then deemed suitable for clonal selection.

2.2.4 Inhibition of calcium signaling using genetically engineered cell line

Opto-RGS2 cell lines (**Figure 2.9A**) were then created by lentivirus-mediated co-transduction of the hetero-dimerizing components and clonal selection based on the machine learning-identified parameters. Experiments were performed where opto-RGS2 cells were illuminated after the oscillation was established (**Figure 2.9B-C**, not simultaneously as in Figure 1). This single-cell paradigm enabled the light-induced dampening of the oscillation to be normalized to its own initial dark response to account for variability. A single illumination epoch was sufficient for opto-R2 activation because the CRY2 off-kinetics was long relative to the imaging duration (τ_{off} = 396s ± 45 s, τ_{on} = 19.7s ± 2.0 s, **Figure 2.7**). Oscillations (100 uM CCh-evoked) were dampened by a single illumination epoch, with significant reductions in frequency, amplitude, and duty ratio, the latter as a general suppression measure that encompasses the other two parameters ($p < 0.001$ for all; **Figure 2.9D-F**). The Cohen's d effect size (d) was calculated to contextualize the significance, and the duty ratio suppression was of medium effect size (d_{duty} = 0.55). As seen in the example traces (**Figure 2.9B-C**), individual cells varied in their respective responses, where the suppression often manifested itself as a change primarily in amplitude (d_{amp} = 0.33) or in frequency (d_{freq} = 0.39), and, thus, duty ratio effects were more pronounced across the population as a parameter.

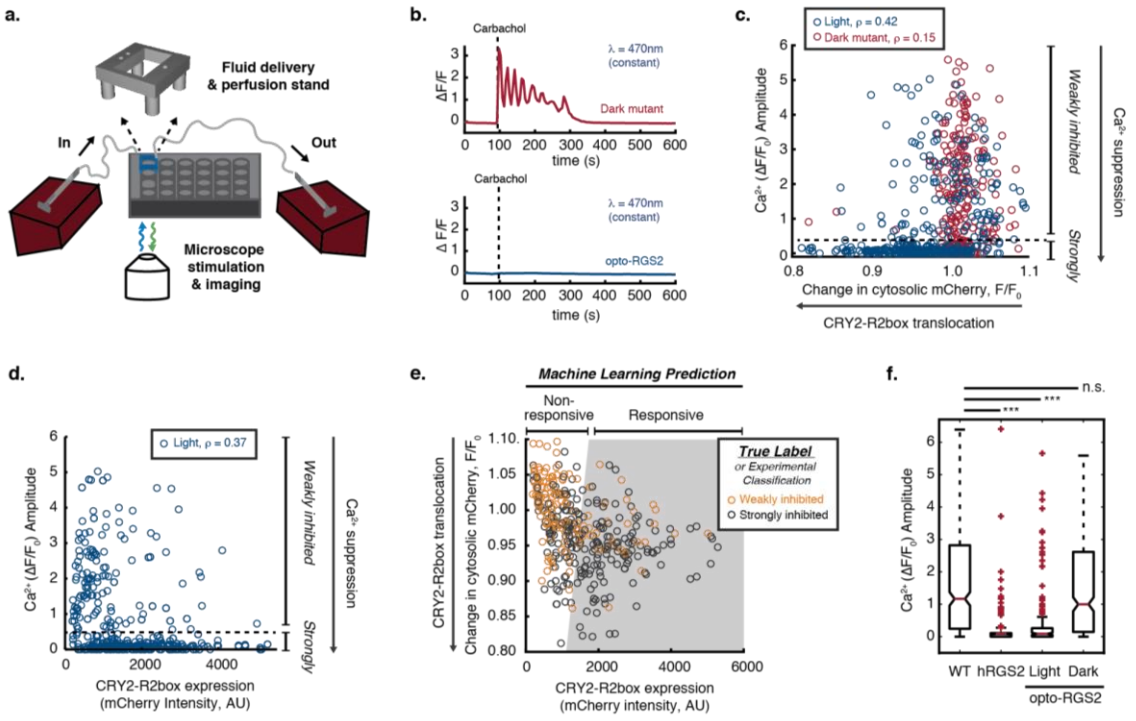

Figure 2.8. Opto-RGS2 functional determinants in transfected HEK cells.

(A) Experimental setup for single-cell functional assays of optogenetic suppression of carbachol-induced oscillations.
(B) GCamp6f imaging traces of exemplar 30 uM carbachol (CCh)-induced calcium oscillations and optogenetic suppression. (Top) Red = Illuminated opto-RGS2 dark mutant or optically insensitive apoprotein control. (Bottom) Blue = Illuminated opto-RGS2 or flavin holoprotein.
(C) Correlation analysis between oscillation suppression and CRY2-R2box translocation (inverse of change in cytosolic mCherry intensity (F/F_0)). ρ = Spearman's rank correlation coefficient. Cells with strong calcium suppression (calcium amplitude lower than 0.5, beneath the dashed line) are considered "strongly inhibited".
(D) Correlation analysis between oscillation suppression and CRY2-R2box expression.
(E) Machine learning-predicted decision boundary for discriminating cells likely to suppress calcium levels robustly (predicted responsive, gray-shaded area) based on translocation efficiency and CRY2-R2box expression level. True Label = Classification from experimental data shown in panels c-d as training set. The boundary was optimized to maximize the true positive prediction with 80% precision, where 80% of "predicted responsive" cells are "strongly inhibited" experimentally.
(F) Box-and whisker plot of calcium oscillation peak amplitude in wild-type HEK cells, constitutively active hRGS2 cells, opto-RGS2 dark mutant, and opto-RGS2 cells selected by the machine learning criteria from panel e (dataset distinct from the training set). N = 174-367.

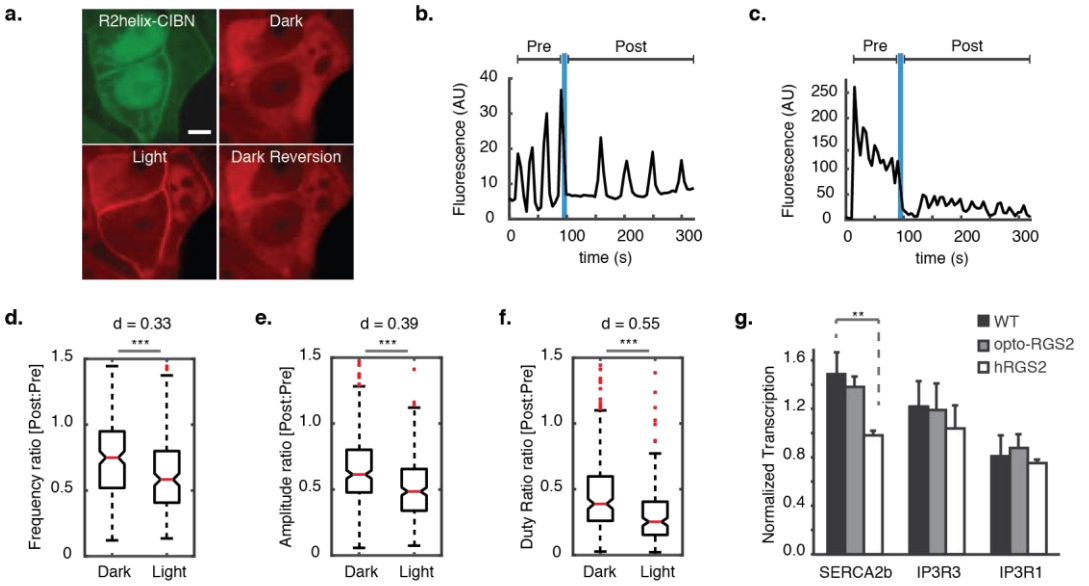

Figure 2.9. Inhibitory regulation of calcium oscillations in opto-RGS2 cell lines.

(A) Fluorescence micrographs of light-induced translocation of mCherry-tagged CRY2-R2box (red) in opto-RGS2 cell lines. (top left) GFP-tagged R2helix-CIBN is membrane- and nuclear-localized, consistent with known R2helix distribution patterns. (top right) CRY2-R2box in the cytoplasm of the same cell, (bottom left) membrane localization 30 seconds after brief (1 s) blue light stimulation, and (bottom right) thermal reversion back to the cytoplasm in the dark (900 s post-illumination). Scale = 5 um.
(B) Example X-rhodamine calcium imaging traces of dynamic suppression of 100 uM CCh-induced oscillations in response to a single epoch of blue light. Optogenetic dampening primarily decreased the frequency.
(C) Same as panel b, except where optogenetic dampening primarily decreased the amplitude.
(D) Single epoch of blue light dynamically reduced oscillation frequency. Post-illumination parameter values were normalized to pre-illumination values of the same oscillation in the same cell, as in panel a. (*** $p < 0.001$, d = Cohen's effect size)
(E) Same as panel d, except for amplitude.
(F) Same as panel d, except for duty ratio.
(G) Quantitative PCR measurements of SERCA2b and IP3R transcripts. SERCA2b level was altered in hRGS2 cells to compensate for long-term reduction in calcium load ($p < 0.01$), but not in opto-RGS2 cells.

A consequence of reversibility is that opto-RGS2 expression should not induce compensatory physiological changes to maintain calcium load (*vs*. wild-type) that would otherwise confound calcium encoding studies. Such changes are known to occur with traditional genetic manipulation, where knockout of hRGS2 alters IP_3R (inositol triphosphate receptor) and SERCA2b (sarco/endoplasmic reticulum calcium ATPase) levels to maintain the intracellular calcium load (*171*). In contrast, mRNA levels of these proteins measured here by qPCR were not altered by opto-RGS2, thus leaving basal transcriptional profiles undistorted unlike the over-expression of constitutively active hRGS2, which altered SERCA2b levels in cell lines (**Figure 2.9G**). Given that opto-RGS2 permits light *vs.* dark comparisons with less genetic variability than comparisons made between multiple populations of traditional genetic mutants *vs.* wild-type cells, it is valuable for defining cell circuits and their dynamic features.

2.2.5 Roles of RGS2 in feedback inhibition and stochasticity

One such undefined circuit in calcium encoding is the feedback circuit that regulates the synchronicity of oscillations, which is critical to coordinating multiple calcium-dependent processes evoked by ligand-stimulation of $G\alpha_q$-coupled GPCRs (*123*, *133*, *162*, *163*) (**Figure 2.10A-B**). It is known that the timing of an intracellular calcium oscillation spike does not depend on the previous one, and is thus stochastic, where stochasticity (α_{Ca2+}) is defined as the ratio of the standard deviation of the inter-spike interval (ISI, T) over the average period (T_{av}) (*162*, *163*). The oscillation signal-to-noise (SNR, $1/\alpha_{Ca2+}$) can be enhanced by a negative feedback loop (*21*). It has been suggested that the oscillation feedback occurs at the GPCR-source level because the

stochasticity is unchanged by manipulation of IP_3R and phospholipase C, which respectively operate at the ER-level or before it (*162*).

We hypothesized that RGS2 may be this regulator (**Figure 2.10C**), given that it (i) provides GPCR-source level inhibition, (ii) is coupled to global calcium elevations *via* Ca^{2+}-bound calmodulin-mediated (Ca^{2+}/CaM) relief of RGS2 inhibition by phosphatidylinositol-(3,4,5)-triphosphate (PIP_3) (*127*, *171*), and (iii) is important for generating oscillations (*101*, *171*). Analysis of the oscillation suppression data in Figure 3 showed that the spike timing was highly stochastic in the dark, where $\alpha_{dark} = 0.79 \pm 0.14$ ($\alpha = 1$ is fully stochastic) (**Figure 2.10D**), while became more synchronized with light-activated opto-RGS2, $\alpha_{light} = 0.51 \pm 0.14$ (**Figure 2.10E**). This finding showed that increasing RGS2-mediated inhibitory drive enhanced the regularity and SNR of the oscillation. RGS2 likely limits the degree of negative regulation in the proposed circuit diagram, because if the activated Ca^{2+}/CaM were not in excess, the increased inhibitory drive from opto-RGS2 activation would be poorly feedback coupled to the global calcium elevation and would not decrease α_{Ca2+}.

Accordingly, to confirm that RGS2 is feedback coupled *via* CaM, the assays were performed in the presence of the CaM peptide antagonist, CALP2, which we hypothesized would uncouple the inhibition from the calcium elevation. Pharmacological interference of the putative coupling mechanism indeed increased the stochasticity in illuminated cells, $\alpha_{light/CALP2} = 0.90 \pm 0.16$ (**Figure 2.10F**), and thus, RGS2 inhibitory feedback is calmodulin-dependent. Variance of α_{Ca2+} was estimated by statistical resampling or bootstrapping, and the results were significant at the 95% confidence level

(**Figure 2.10G**). Thus, this optogenetic analysis defines a negative feedback circuit for modulating the stochasticity of calcium oscillations, and consequently, the reliability of the signals they encode.

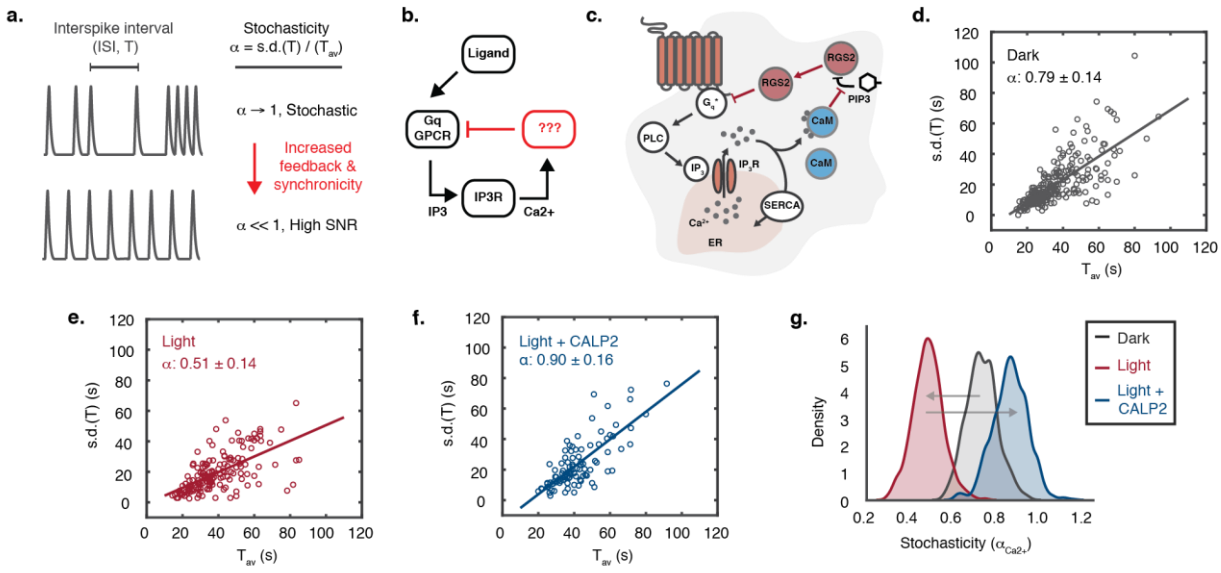

Figure 2.10. Opto-RGS2 inhibitory feedback reduces stochasticity of calcium oscillation spike timing.

(A) Interspike intervals of ligand-induced oscillations become less stochastic with feedback.
(B) The negative feedback regulator and its coupling mechanism to global elevations in calcium are still unknown as reflected in the lump circuit diagram.
(C) Proposed RGS2-mediated negative feedback loop, where inhibition of G□q-signaling is coupled to global calcium elevations through relief of PIP3 inhibition of RGS2 by calcium-activated calmodulin (CaM).
(D) Stochasticity (α) of 100 uM CCh-induced calcium oscillations in non-illuminated opto-RGS2 cell lines.
(E) Opto-RGS2 activation decreased the stochasticity in response to a single blue light epoch (as in Figure 3).
(F) The Inhibitory feedback is uncoupled from the global calcium elevation by CaM-antagonism by CALP2 peptide.
(G) Statistical bootstrapping or resampling analysis of variance (N = 1000 trials) for panels d-f.

2.3 Conclusion

The ability to dynamically recapitulate RGS2 function is important because the creation of selective agonists is hindered by the conservation of the catalytic RGS-box across subtypes (*80*, *86*, *132*, *147*). Given such conservation, the engineering design here preserved the R2-helix instead of an isoprenylated peptide for membrane localization (*117*), which is non-specific. However, not all performance-related issues were a function of protein-level design alone. The performance of hetero-dimerization systems exhibits great cell-to-cell variability, but proper selection of a homogenous population with respect to screening parameters of expression and translocation efficiency provided the requisite reliability for calcium encoding studies. Thus, this work emphasizes the cellular engineering techniques required to successfully engineering a molecular tool, beyond the transgene sequence itself.

Opto-RGS2 is a key addition to the optogenetic toolbox for studying GPCRs and second messenger signaling. The ability to potently suppress calcium is absent from the toolbox, and thus, the functionality complements existing capabilities in GPCR-level elevation of calcium and elevation/suppression of cyclic AMP (*2*, *6*, *58*, *91*, *118*). The functionality is powerful given the ubiquitous importance of GPCRs and calcium signaling in eukaryotes, and it led to the elucidation of a feedback circuit that regulates the stochasticity of agonist-evoked oscillations. This increase in oscillation synchronicity by up-regulated RGS2 suggests that RGS2-feedback has coordinative roles in calcium encoding, important for coincidence detection or multiplexing of the downstream calcium effectors (*98*, *174*). In summary, opto-RGS2 advances understanding of calcium

encoding principles and RGS/GPCR signaling dynamics in environmental sensory processing.

2.4 Future direction

2.4.1 Opto-RGS2 specificity

As briefly discussed, RGS is a large protein family. Most RGS members share similar domain architecture to RGS2, consisting of unique N-terminal targeting domain and highly conserved C-terminal RGS domain. Because the RGS domain is highly conserved across the RGS family, the RGS proteins rely on their N-terminal domain to determine their interaction partners and regulate the specificity. Given that our opto-RGS2 improved upon the previously created optogenetic RGS by incorporation of the RGS N-terminus, our design should show higher specificity and therefore better recapitulate the activity of the native RGS. Future experiments to evaluate the specificity of our opto-R2 design should be valuable to support the advantage of our design. The following approaches can be employed for assessment of the specificity.

2.4.1.1 Receptor co-localization

RGS2 has been shown to localize around the membrane through its N-terminal interaction with the third loop of the muscarinic receptor 1,3, and 5 (*9*). Mutating the amino acid residues at the muscarinic receptor interaction site or genetic knockout of the receptor gene should abolish the interaction, relieving RGS2 from the plasma membrane and therefore unable to inhibit the Gq signaling. With the presence of the R2-alpha helix,

our opto-R2 should behave similar to the native RGS2 in contrast to the existing design where the RGS2 N-terminus is absent.

2.4.1.2 Binding partner characterization with mass spectrometry

RGS2 proteins are also known to interact with proteins other than membrane receptors. Methods such as co-immunoprecipitation together with mass spectrometry can identify similarity between RGS2 and opto-R2 binding partners (*39*).

2.4.2 Effects of calcium stochasticity on calcium decoding

As we have demonstrated that RGS2 has a crucial role in calcium encoding where it regulates the stochasticity of the calcium oscillations, it will be worthwhile to next investigate how such stochasticity affects the activities of the calcium effectors and cellular decisions. The question is particularly applicable to transcription factors that are regulated by the calcium spike timing or by integration of multiple signals. Absence of signal pulses at the right timing could potentially impair the functions of these effectors and results in cellular malfunctions. Future studies on such decoding questions will further elucidate the importance of calcium stochasticity and emphasize the significance of RGS2 in calcium encoding and decoding.

2.5 Materials and methods

2.5.1 Genetic constructs

Cryptochrome and RGS-related plasmids used during this study are summarized in Table 2.1. They were constructed as follows:

Table 2.1. Plasmids constructed for opto-RGS2 construction

Plasmids were constructed from: pcDNA3.1-hRGS2 (Missouri S&T Resource Center, RGS0200000). pCRY2PHR-mCherryN1 (Addgene, 26866). pCIBN(deltaNLS)-pmGFP (Addgene, 26867). pEGFP-N1 (Addgene, 22047). pLJM1 (Penn Vector Core).

PLASMID	PURPOSE
Transient transfection	
P0: pcDNA 3.1-hRGS2	Sub-cloning
P1: pcDNA3.1-hRGS2-mCherry	Correlation analysis control
P2: pCRY2PHR-mCherryN1	Sub-cloning
P3: pCRY2PHR-mCherry-(GGGGS)3-hRGS2box Note = CRY2-R2box	Linker analysis Correlation analysis
P4: pCRY2PHR(D387A)-mCherry-(GGGGS)3-hRGS2box Note = Dark mutant	Correlation analysis control
P5: pNtermRGS2-GFP-CIBN, Note = R2helix-CIBN	Linker analysis Localization kinetics
P6: pNtermRGS2-CIBN, Note = R2helix-CIBN	Correlation analysis
Lentiviral transduction	
P7: pLJM1-hRGS2-mCherry	Cell line generation
P8: pLJM1-CRY2PHR-mCherry-(GGGGS)3-hRGS2box Note = CRY2-R2box	Cell line generation Stochasticity
P9: pLJM1-NtermRGS2-GFP-CIBN = R2helix-CIBN	Cell line generation Stochasticity

P0 was obtained from Missouri S&T (No. RGS0200000). ***P1*** was created by Gibson assembly (between BamHI and XbaI) of hRGS2 PCR amplified from P0, into a pcDNA3.1 plasmid containing mCherry.

P2 was obtained from Addgene. (Plasmid No. 26866). ***P3*** was constructed by Gibson assembly (between XhoI and XbaI**)** of the linker and hRGS2box into P2. hRGS2box was PCR-amplified from the cDNA sequence encoding hRGS2 aa 77-211. ***P4*** was created by site-directed mutagenesis to create a single point mutation (A1160C) on the P3 plasmid.

P5 and ***P6*** were constructed by Gibson assembly (between BamHI and XbaI) of the N-terminal helix of RGS2, EGFP, and CIBN into a pEGFP-N1 plasmid (Addgene Plasmid No. 22047). The N-terminal helix was PCR-amplified from the cDNA sequence encoding hRGS2 aa 1-76. CIBN was PCR-amplified from pCIBN(deltaNLS)-pmGFP (Addgene, Plasmid No. 26867).

P7 was created by inserting hRGS2-mCherry from P1 into a pLJM1 plasmid (between AgeI and EcoRI). ***P8*** and ***P9*** were constructed Gibson assembly (between NheI and EcoRI) of PCR-amplified transgene from P3 or P5, respectively, into the pLJM1 lentiviral plasmid.

The protein sequence of mCherry-tagged CRY2-R2box was:

1 mkmdkktivw frrdlriedn palaaaaheg svfpvfiwcp eeegqfypgr asrwwmkqsl
61 ahlsqslkal gsdltlikth ntisaildci rvtgatkvvf nhlydpvslv rdhtvkeklv
121 ergisvqsyn gdllyepwei ycekgkpfts fnsywkkcld msiesvmlpp pwrlmpitaa

181 aeaiwacsie elgleneaek psnalltraw spgwsnadkl lnefiekqli dyaknskkvv
241 gnstsllspy lhfgeisvrh vfqcarmkqi iwardknseg eesadlflrg iglreysryi
301 cfnfpftheq sllshlrffp wdadvdkfka wrqgrtgypl vdagmrelwa tgwmhnrirv
361 ivssfavkfl llpwkwgmky fwdtlldadl ecdilgwqyi sgsipdghel drldnpalqg
421 akydpegeyi rqwlpelarl ptewihhpwd apltvlkasg velgtnyakp ivdidtarel
481 lakaisrtre aqimigaaar dppvatmvsk geednmaiik efmrfkvhme gsvnghefei
541 egegegrpye gtqtaklkvt kggplpfawd ilspqfmygs kayvkhpadi pdylklsfpe
601 gfkwervmnf edggvvtvtq dsslqdgefi ykvklrgtnf psdgpvmqkk tmgweasser
661 mypedgalkg eikqrlklkd gghydaevkt tykakkpvql pgaynvnikl ditshnedyt
721 iveqyeraeg rhstggmdel ykcgrggggs ggggsggggs eltssglwse afdellasky
781 glaafraflk sefceenief wlacedfkkt kspqklsska rkiytdfiek eapkeinidf
841 qtktliaqni qeatsgcftt aqkrvyslme nnsyprfles efyqdlckkp qittephat*

The protein sequence of GFP-tagged R2helix-CIBN was:

1 mqsamflavq hdcrpmdksa gsghkseekr ekmkrtllkd wktrlsyflq nsstpgkpkt
61 gkkskqqafi kpspeeaqlw seasrefaaa qltsvskgee lftgvvpilv eldgdvnghk
121 fsvsgegegd atygkltlkf icttgklpvp wptlvttlty gvqcfsrypd hmkqhdffks
181 ampegyvqer tiffkddgny ktraevkfeg dtlvnrielk gidfkedgni lghkleynyn
241 shnvyimadk qkngikvnfk irhniedgsv qladhyqqnt pigdgpvllp dnhylstqsa
301 lskdpnekrd hmvllefvta agitlgmdel yktgggspgm ngaiggdlll nfpdmsvler
361 qrahlkylnp tfdsplagff adssmitgge mdsylstagl nlpmmygett vegdsrlsis
421 pettlgtgnf kaakfdtetk dcneaakkmt mnrddlveeg eeekskiteq nngstksikk
481 mkhkakkeen nfsndsskvt kelektdyi*

2.5.2 Cell culture

Human embryonic kidney 293 (HEK293t) cells (from the Lazzara Lab, UPenn) were cultured in Dulbecco's modified eagle medium (DMEM) with Glutamax (ThermoFisher, 10566016), supplemented with 10% heat-inactivated fetal bovine serum (FBS) (Sigma, F2442) and 1% penicillin-streptomycin (ThermoFisher, 15140122). Cells were maintained in a sterile water-jacketed mammalian cell culture incubator (Thermo/Forma, 3110), maintained at 5% CO_2 and 37 °C. HEK cell authentication by STR and mycoplasma testing by Myco-Alert were performed by Biosynthesis, Inc.

2.5.3 Transient transfection

DNA plasmid (24-well plate, 250 ng/well; 6-well plate, 1.25 ug/well) was mixed with TransIT-293 transfection reagent (24-well plate, 0.75 uL/well; 6-well plate, 3.75 uL/well) (Mirus Bio, MIR2700) in Opti-MEM I Reduced-Serum Medium (24-well plate, 100 uL/well; 6-well plate, 500 uL/well) (ThermoFisher, 31985070). The mix was incubated at room temperature for 15 minutes and was subsequently added to seeded cells. Gene expression was assessed 18-24 hours post-transfection.

2.5.4 Linker analysis

The respective expressions of pCRY2-mCherry-*linker*-RGS2box constructs and P5 were assessed by flow cytometry. Cells were seeded onto a poly-D-lysine (PDL)-treated 6-well plate 24 hours prior to co-transfection. Cells were trypsinized 24 hours post-transfection and washed three times with phosphate-buffered saline (PBS) (ThermoFisher, 14190250). Cells were re-suspended in flow buffer containing 1X Ca^{2+}/Mg^{2+}-free PBS, 5 mM EDTA, 25 mM HEPES pH 7.0, and 1% FBS. Cells were subsequently strained with a 70 µm cell strainer (Sigma, Z742103) and collected in a 5 mL polystyrene round-bottom FACS tube (Corning, 352054). The flow analyses were performed on 4-laser BD LSRII Cell Analyzer (mCherry detection: green laser with 610/20 emission filter; GFP detection: blue laser with 515/20 emission filter), at a rate of approximately 4000 events/s, with 100,000 events collected for each condition. Three gates were applied to select for live single cells with expression of both cryptochrome components.

2.5.5 Fluorescence microscopy and hardware

Cells were imaged with a Metamorph-automated Leica DMI6000B fluorescence microscope, equipped with a sCMOS camera (PCO.edge) and LED illuminator (Lumencor Spectra-X). The excitation illumination was filtered at the light source-level, and the microscope filter cubes (Chroma) used were: EGFP, $\lambda_{dichroic}$ < 495 nm and λ_{em} = 525/50 nm; mCherry, $\lambda_{dichroic}$ < 585 nm and λ_{em} = 630/75 nm). Pharmacological agents were delivered using a custom automated perfusion system consisting of a 3D-printed well-aligning scaffold and programmable syringe pumps (Brain Scientific, BS-8000), triggered by MetaMorph.

Fluorescence micrographs of light-induced opto-R2 translocation shown in Figure 3a were acquired using a Leica DMI8 inverted microscope (courtesy of the Hammer Lab, UPenn) equipped with confocal spinning disk module from Spectral Applied Research and Hamamatsu ImagEM X2 EM-CCD camera.

2.5.6 Membrane localization kinetics

Cells were seeded onto a poly-D-lysine coated 24-well glass bottom plate (Cellvis, P24-1.5H-N) and were co-transfected with CRY2-R2box and R2helix-CIBN. After 24 hours, the culture media was replaced with phenol-free CO_2-independent imaging media (phenol-free HBSS supplemented with 1% L-glutamine, 1% Penn/Strep, 2% essential amino acids, 1% non-essential amino acids, 2.5% HEPES pH 7.0, and 10% serum).

Cells were imaged with a 40X objective (0.5 s exposure time, 675 s total, using the mCherry filter cube with yellow excitation: λ = 580 nm, 24.20 mW/mm^2). CRY2-R2box imaging was first performed without blue illumination for 15 s to establish baseline before blue light induction (0.5 s every 5 s for 60 s, λ = 475 nm, 7.37 mW/mm^2). Blue light stimulation was then removed to determine dark reversion kinetics. The localization of R2helix-CIBN was acquired during the blue illumination period. Line sections of consistent length were manually drawn across selected segments of cell boundaries. The degree of CRY2-R2box membrane localization was calculated as the mCherry intensity at the pixels representing the cell membrane, normalized by the total intensity of all the pixels in the line. Rate constants were determined by an exponential fit.

2.5.7 Calcium suppression assays in transfected cells

Calcium signals in cells expressing opto-RGS2 [P3 + P6], opto-RGS2 dark mutant [P4 + P6], and hRGS2 [P1] were evaluated against the negative control cell (WT) [P2 + P6]. Intracellular calcium signals were monitored using GCaMP6f in glass-bottom 24-well plates. (Addgene, Plasmid No. 40755). Seeded cells were co-transfected with GCaMP6f plasmid and one of the plasmid combinations above. After 24 hours post-transfection, the culture media was replaced with the phenol-free CO_2 independent media. The cells were perfused with 30 uM carbachol (CCh) (Sigma, C4382) to stimulate the M3 muscarinic acetylcholine receptor (M3R). GCaMP6f fluorescence signals were monitored every 5 s for 900 s. mCherry fluorescence was imaged before GCaMP6f imaging, and again once every 60 s.

Image processing, manual cell segmentation and intensity quantifications were performed using ImageJ. The intensity data were imported to MATLAB for signal processing, peak identification, and peak prominence measurements of amplitude. Signal prominence was defined as the extent to which the peak stands out due to its intrinsic height, using the MATLAB "findpeaks()" function. The signal plotted is the relative change in fluorescence signal ($\Delta F/F_0$). Samples were considered outliers if they were greater than $q_3 + 1.5(q_3 - q_1)$ or less than $q_1 - 1.5(q_3 - q_1)$ where q_1 and q_3 represent the 25th and 75th percentiles of the sample data, respectively.

2.5.8 Correlation analysis and machine learning prediction

Spearman's rank correlation analysis was performed using the Python library pandas (pandas.Dataframe.corr()) to identify predictive parameters affecting the strength of the calcium suppression (defined as inverse of calcium prominence). Correlation between calcium prominence and the following parameters were analyzed: translocation efficiency, expression of CRY2-R2box, and expression of R2helix-CIBN. No correlation was observed for R2helix-CIBN level.

The parameter space at which cells can completely inhibit the calcium signals were identified using a machine learning method logistic regression (scikit-learn library, L2 regularization, C = 1.0, "balanced" class weight); the model parameters were optimized using GridSearchCV function to maximize prediction precision (true-positive rate) (precision = 80%). The calcium signals considered strongly inhibited had normalized prominence values of $\Delta F/F_0 < 0.5$.

2.5.9 Lentivirus production and cell line generation

Opto-RGS2 lentivirus was generated by transfecting HEK293t cells with either P8 or P9 with 3rd generation helper plasmids. The media was replaced one day after transfection, and virus-containing supernatant was collected on the second and third days. After centrifugation (1000 rpm, 5 minutes), the supernatant containing the lentivirus was filtered (0.4 um PES) and used immediately.

To generate an opto-RGS2 stable cell line, HEK293t cells were co-infected with lentiviruses carrying CRY2-R2box and R2helix-CIBN. The infected cells were grown and selected in culture media containing 0.125 ug/mL puromycin (Clontech, 631305). Individual clones expressing both components of opto-RGS2 were picked under a sterile fluorescence microscope (courtesy of the Cremins Lab, Penn) and grown in 24-well plates. Light-induced translocation of the CRY2-R2box was evaluated for each clone to select suitably responsive ones (i.e. based on correlation analysis-defined threshold). The hRGS2 stable cell line was generated similarly using P7 plasmid.

2.5.10 Calcium dynamics of stable cell lines

Opto-RGS2 stable cells seeded on a PDL-coated glass-bottom 24-well plate were loaded with 2 uM X-Rhod-1 calcium indicator dye (ThermoFisher, X14210). Cells were incubated with dye at 37 °C, and washed after 30 minutes, after which the media was replaced with CO_2-independent media. Cells were incubated at 37 °C for another 30 minutes for de-esterificaition. To ensure oscillatory activity, the media was replaced with 5.2 mM calcium-containing CO_2-independent media. Cells were perfused with 100 uM

carbachol, and time-lapse images of XRhod1 signals were acquired. After 90 s, cells were exposed to brief blue light pulses (10 s total, 0.5 s ON, 0.5 s OFF).

Image processing, manual cell segmentation, and intensity quantification were performed in ImageJ. The intensity measurements were passed into automated custom MATLAB scripts for signal processing, peak identification (20% above baseline threshold), and to compute reported oscillation parameters. The frequency ratio was calculated by dividing post-illumination (t = 100 – 250s) oscillation frequency by pre-illumination (t = 0 – 100s) frequency. Student t-test, and Cohen's d-test were performed to evaluate the significance and the effect size of the light-induced change. Identical analyses were performed with amplitude and duty ratio.

2.5.11 qPCR

RNA was extracted using standard TRIzol RNA extraction procedures. Cells were crushed with a pestle in 1 mL (per 5 x 10^6 cells) TRIzol (ThermoFisher, 15596026) and incubated at room temperature for 5 minutes. 200 mL chloroform (Sigma, B9673) was added and the sample was centrifuged at 12,000 *x* g at 4 °C for 15 minutes. The RNA-containing aqueous phase was isolated and added to 500 uL cold isopropanol. The sample was incubated at room temperature for 10 minutes and centrifuged at 12,000 *x* g at 4 °C for another 10 minutes to precipitate the RNA. After the supernatant was removed, the RNA pellet was washed with cold 80% ethanol and re-suspended in DEPC-treated water (Ambion, 9906). The RNA concentration was measured using a NanoDrop ND2000 Spectrophotometer.

For RT-PCR, 1 uL of random primers (100 ng/uL) and 1uL of dNTP mix (10mM) (ThermoFisher, 18427013) were added to each of the 0.5 ug RNA samples. Samples were heated at 65 °C for 5 minutes, and then mixed with 1 uL RNaseOUT (40units/uL, ThermoFisher, 10777019), 4 uL 5X First-Strand Buffer, 1 uL DTT (0.1M), and 1 uL SuperScript III RT (200 units/u, ThermoFisher, 18080093). The mix was incubated at 25 °C for 5 minutes, 50 °C for 40 minutes, and 70 °C for 15 minutes. The product was diluted with 60 uL TE buffer and stored at -20 °C.

qPCR was performed using SYBR green. 1.5 uL RT-PCRed sample was mixed with 12.5 uL SYBR green master mix (2X) (Applied Biosystems, 4367659), 0.375 uL forward primer (20 uM) (IDT), 0.375 uL reverse primer (20 uM) (IDT), and 10.25 uL water. The wild-type standard curve spanned a 0.008-5X equivalent(s) range. Each qPCR measurement was calibrated against the standard curve, and normalized by the level of the housekeeping gene, GAPDH, to determine the final expression value. All measurements were performed in duplicates, with 5-6 samples per cell line/condition. The primers used to quantify RNA encoding SERCA2b, IP3R1, and IP3R3 proteins are listed in Table 2.2.

Table 2.2. Primers used for qPCR.

PROTEIN	GENE	REFSEQ	PRIMER	SEQUENCE (5'→3')
SERCA2b	ATPA2	NM_001681	Forward	GGGCAAAGTGTATCGACAGG
			Reverse	TCAGCAGGAACTTTGTCACC
IP3R1	ITPR1	NM_002222	Forward	AACCGGGGACCTTAACAATC
			Reverse	TTTCCAGAACTGCTTTTGGG
IP3R3	ITPR3	NM_002224	Forward	GTCAATGGCTTCATCAGCAC
			Reverse	GAGGCAGTCACGGAACTTCT
GAPDH	GAPDH	NM_002046	Forward	AAGGTGAAGGTCGGAGTCAA
			Reverse	AATGAAGGGGTCATTGATGG

2.5.12 Stochasticity analysis

Assay and data processing were performed as described in Section 10 above. 50 uM of CALP2 (Tocris, 2319) was added to the media 1 hour prior to calcium imaging to inhibit calmodulin activity. Stochasticity was assessed based on the variability of the interspike intervals (ISI, or T) within a signal relative to its mean (Tav). Linear regression analysis was performed using the MATLAB function LinearModel.fit to derive the estimated stochasticity. 450-1000 cells were analyzed for each experimental condition. The 95% bootstrap confidence interval was calculated using bias corrected and accelerated percentile methods, with 1000 bootstrap samples.

CHAPTER 3 : Optogenetic Control of Calcium Oscillations for the Study of Calcium Decoding

3.1 Introduction

Calcium acts as a secondary messenger to coordinate multiple cellular functions in response to the external stimuli. Despite its universality, calcium signaling achieves specificity through dynamic patterns of its oscillation waveforms which encode the strength and identity of the external stimuli. A number of calcium effectors can distinctively decode these signaling dynamics and, as a result, individually trigger specific cellular responses. We are particularly interested in calcium-dependent transcription factors, which are the calcium effectors that regulate critical functions in proliferation, development, stress response, and synaptic transmission.

It is known that the transcriptional activity of calcium-dependent transcription factors is enhanced by increasing calcium oscillation frequency (*18*, *37*, *38*, *121*, *135*, *150*, *166*). However, cells decode oscillatory biochemical signals based on not only the peak amplitude and frequency as principle components of the waveform, but also the duty cycle (or duty ratio). Here, duty cycle is defined as the cumulative load of calcium concentration elevated above basal levels with respect to time, normalized to a steady-state load of equal peak amplitude (*135*). Oscillation duty cycle can serve as a measure of cumulative load that influences transcriptional signaling (*128*) (**Figure 3.2A**).

To understand whether cells decode each dynamical component of the calcium signal and initiate responses that are specific to those components, it is necessary to understand how frequency and duty cycle of calcium oscillations each affect transcription independently (*76*, *141*). However, experimental analyses tend to stimulate cells with fixed calcium pulse-widths and, under those conditions, frequency and duty cycle change concomitantly. Thus, it remains unclear whether calcium-dependent transcription factors primarily act as signal integrators of cumulative load delivered by pulsatile signals or whether they selectively respond to specific oscillation frequencies. In principle, these ‘‘decoding principles’’ can be experimentally discerned by matching calcium duty cycle across frequencies, and vice versa, to respectively isolate the contributions that frequency and duty cycle each make to transcriptional activation levels.

We will first review the mechanisms by which different calcium-dependent transcription factors are regulated and the similarity they share in their general circuit topology. Then, we will present how we employed a novel set of techniques to uncover a primary mechanism of transcription factor decoding mechanism.

3.1.1 Calcium-dependent transcription factors

3.1.1.1 NF-κB

NF-κB (Nuclear factor kappa-light-chain-enhancer of activated B cells) is a transcription factor prevalent in the immune and nervous systems. It plays a key role in

regulating immune response to antigens, neuroplasticity, and learning and memory. NF-κB is a protein dimer consisting of one or two of the following subunits: p105, p100, p50, p52, RELA, c-REL and RELB. The canonical form of NF-κB complex is a heterodimer of p50 and RELA, with their amino-terminal containing REL-homology domain (RHD) responsible for DNA binding, dimerization, and interaction with the IκB family of NF-κB inhibitors. RELA carries additional transactivation domains (TADs) on its carboxy-terminus that allows NF-κB to initiate transcription (*25*, *64*). In an inactive state, IκB binds to cytoplasmic NF-κB, shielding its nuclear localization signal. In the presence of external stimuli, calcium elevations, along with other signaling molecules, activate protein kinase, IKK, which subsequently proceeds to phosphorylate IκB. Phosphorylated IκB then undergoes proteasomal degradation, freeing NF-κB to translocate to the nucleus (*27*, *65*, *89*, *113*, *124*, *159*, *172*) (**Figure 3.1A**) and initiating transcription of the genes involved in inflammation and plasticity (*25*, *64*).

Additionally, NF-κB modulates transcription of IκB and A20 genes which code for the direct inhibitor of NF-κB and the inhibitor of IKK, respectively. IκB and A20 proteins are then synthesized to re-form a complex with NF-κB and inhibit activation of NF-κB (*27*, *65*, *89*, *113*, *124*, *159*, *172*). The production of such inhibitors functions as a negative feedback that limits NF-κB activities to certain calcium oscillation waveforms (**Figure 3.1A**). If calcium oscillation frequency is faster than the negative feedback rate, NF-κB will integrate the calcium signals resulting in its nuclear accumulation and transcription. On the other hand, if the oscillations are too slow such that the next signal spikes fail to arise in time before the NF-κB inactivation, NF-κB will be unable to integrate the signals and, instead, respond to individual signal spikes (*121*, *128*, *150*).

3.1.1.2 CREB

CREB (cyclic AMP-responsive element binding protein) is a transcription factor mediating transcription of the genes involved in formation of long-term memory (*17*, *106*, *173*). Increase in synaptic activity triggers elevation of intracellular calcium which then binds to calcium binding calmodulins (CaM) and activates it. Ca^{2+}/CaM proceeds to activate protein kinase CaMKIV that phosphorylates CREB, permitting it to initiate transcription (*173*). In addition to CaMKIV, Ca^{2+}/CaM can also activate a protein

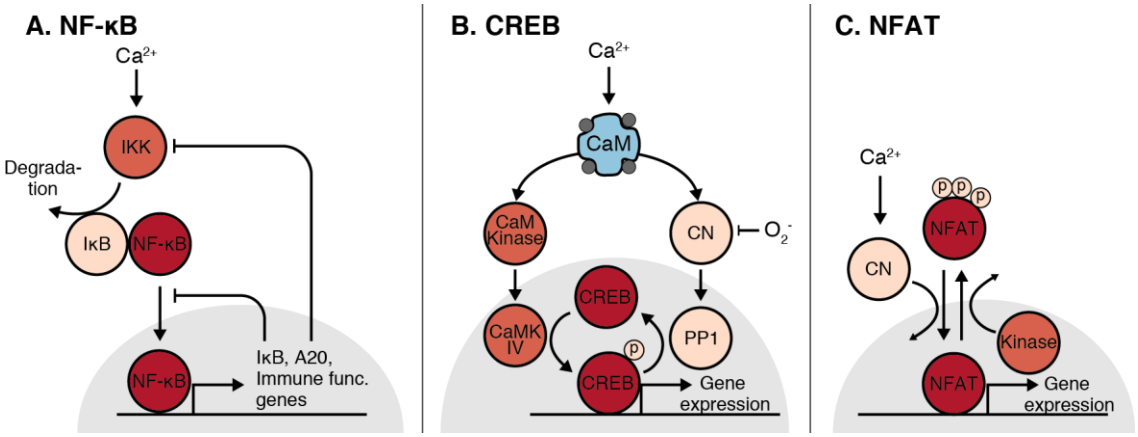

Figure 3.1. Calcium activation mechanisms of calcium-dependent transcription factors.

(A) Calcium elevation promotes degradation of NF-κB inhibitor IκB, allowing NF-κB to translocate into the nucleus and initiate transcription. IκB and A20 genes, along with other genes, are transcribed by NF-κB and translated to form functional proteins to inhibit NF-κB activities.
(B) Upon calcium elevation, Ca^{2+}/CaM stimulates phosphorylation of CREB permitting it transcriptional ability. The Ca^{2+}/CaM, at the same time, activates phosphatase PP1 which functions to de-phosphorylate CREB and terminate its function. Prolonged calcium elevation promotes production of O_2^- that inhibits CREB dephosphorylation, allowing CREB to remain activated.
(C) Increases in calcium levels result in dephosphorylation of NFAT, allowing it to shuttle into the nucleus and initiate transcription. Nuclear kinases, on the other hand, re-phosphorylate NFAT, returning it to the cytosol.

phosphatase phosphor-inhibitor-1, through calcineurin (CN), which functions to dephosphorylated active CREB, terminating its activity. However, prolonged calcium stimulation promotes production of superoxide anions (O_2^-) that, in turn, inactivates CN and relieve CREB from the negative regulation (*17*) (**figure 3.1B**). With this mechanism, CREB is minimally active under a brief stimulation or short calcium pulse, but becomes significantly active under a prolonged stimulation or long calcium duration.

3.1.1.3 NFAT

NFAT regulates immune response to infection (*33*, *47*, *66*, *103*, *110*) and promotes the development of cardiac, skeletal muscle (*29*, *31*, *33*, *146*) and the neuronal system (*33*, *115*). In response to extracellular stimuli, cytoplasmic calcium concentration increases and activates the calcium-dependent phosphatase, CN. CN, in turn, dephosphorylates cytoplasmic NFAT to expose its nuclear localization signal; dephosphorylated (activated) NFAT then shuttles to the nucleus, binds its cognate promoter, and initiates transcription (**Figure 3.2A**; we call this nuclear translocation rate α). Activated NFAT is constitutively phosphorylated within the nucleus and subsequently exported from it in a phosphorylation-dependent manner (we call the nuclear export rate β in **Figure 3.2A**). When cytoplasmic calcium levels fall, CN activity decreases and the phosphorylated form of NFAT accumulates in the cytoplasm, halting NFAT-dependent transcription (*33*, *66*). Because nuclear export is the rate-limiting step in returning NFAT activity to baseline (*29*, *76*, *166*, *179*), NFAT accumulates in the nucleus when the calcium oscillation frequency (we call this frequency v in **Figure 3.2A**) exceeds export frequency, resulting in increases in transcriptional activities.

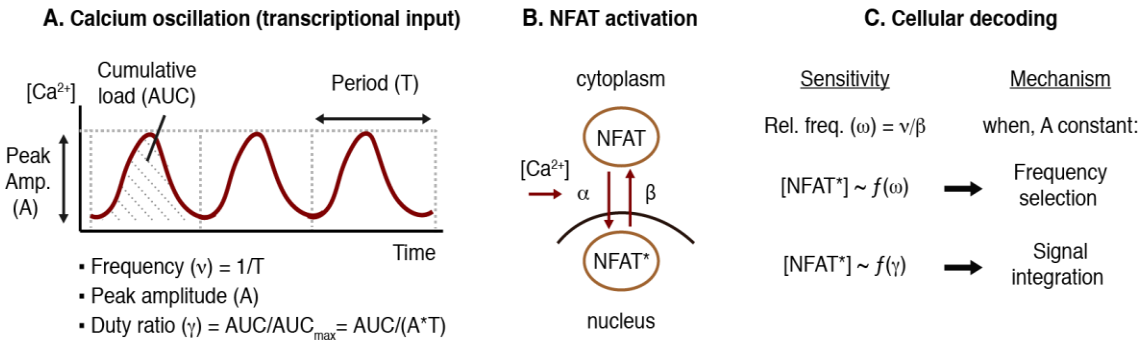

Figure 3.2. NFAT decoding principles

(A) Calcium oscillations encode information in their frequency, peak amplitude, and duty ratio. (B) Elevated calcium induces NFAT translocation and transcriptional activation at rate α. Nuclear export at rate β deactivates transcriptional signaling (inactive form, NFAT and active form, NFAT*).
(C) Calcium signal processing is frequency-selective when transcription is enhanced at specific oscillation frequencies (absolute ν, or relative ω = ν/β). Alternatively, NFAT is a signal integrator if the enhancement is attributable to duty ratio.

3.1.2 Problem statement

As described in the earlier section, calcium-coupled transcription factors are regulated by extremely complex and dynamic regulatory circuits. The timing and magnitude of the calcium signals would significantly affect the activation state of these transcription factors. However, the complexity of the circuits limits our understanding in how the transcription factors are regulated or decode these calcium oscillatory signals. Therefore, we set out to apply our proposed duty-cycle-matching and frequency-matching oscillation paradigms, together with mathematical modeling, optogenetics, and synthetic biology approaches, to resolve the primary decoding principles of calcium-dependent transcription. While NF-κB and CREB can be cross-activated by other signaling molecules, NFAT is regulated exclusively by calcium signaling, and one can therefore ensure that the alteration in the observed transcriptional behaviors are resulted

solely from our imposed calcium waveforms. As a result, we chose to focus our calcium decoding study on NFAT transcription factor, crucial to immune cell function, development, stem cell differentiation, and tumor progression (*67*, *103*, *104*, *115*).

3.2 Results and discussion

3.2.1 Mathematical model of NFAT activation

We first constructed a simplified mathematical model describing NFAT activation by calcium oscillations to identify determinant parameters of the calcium waveform and limit the state space for our experimental studies. Our final simplified model was developed through the following process and assumptions. Increases in calcium signal activate phosphatase calcineurin (CN), which in turn binds and dephosphorylates

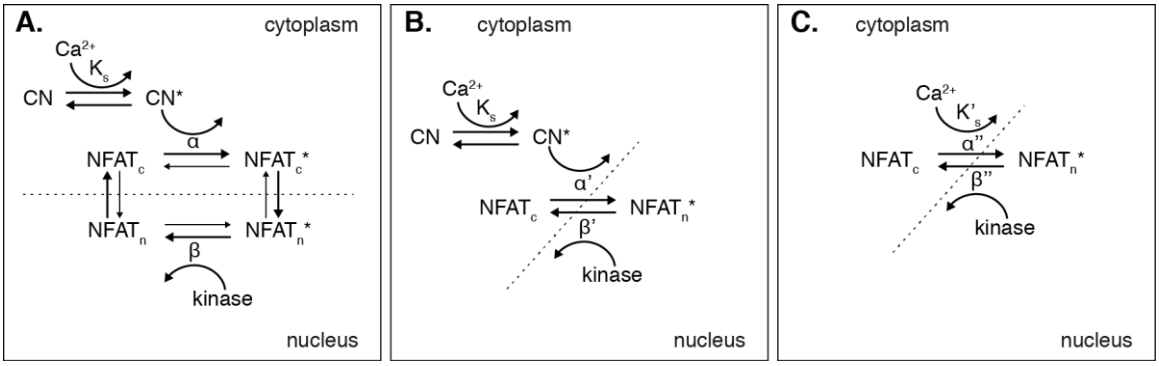

Figure 3.3. Mathematical model describing calcium-induced NFAT nuclear shuttling.

(A) Model in which NFAT de/re-phosphorylation is separated from a nuclear import/export.
(B) Simplified model in which de/re-phosphorylation is lumped with translocation as an activation/deactivation step.
(C) Minimal model assuming fast calcium-calcineurin binding and steady-state calcineurin (CN) concentrations, which was used to analyze the sensitivity of NFAT activity to frequency and duty ratio.

cytoplasmic NFAT, exposing its nuclear localization signal for nuclear translocation and transcriptional initiation. Nuclear NFAT is re-phosphorylated by kinases resulting in translocation back to cytoplasm (**Figure 3.3A**). The de-phosphorylation and nuclear import of NFAT can be lumped into one step and described as NFAT activation, and likewise re-phosphorylation and nuclear export of NFAT can be lumped as an inactivation step (**Figure 3.3B**). Because calcium-calcineurin binding is generally much faster than NFAT de-phosphorylation, we assume steady-state CN levels, yielding the simplified model shown Figure 3.3C and Figure 3.2.

To derive an analytical solution for average NFAT activity in response to oscillatory calcium, the oscillation is modeled as a square-wave (*135*), and average NFAT activity as time approaches infinity is described as ($\bar{X}$):

$$\bar{X} = \gamma + \left[\frac{\omega\sigma}{1+\sigma} \cdot \frac{(1-e^{-\gamma(1+\sigma)/\omega})(1-e^{-(1-\gamma)/\omega})}{1-e^{-(1+\gamma\sigma)/\omega}}\right], \; where \qquad \textit{Equation 1}$$

$$The\ effective\ activation\ rate\colon\ \sigma = \frac{\alpha''}{\beta''} \cdot \frac{(A/K'_s)^n}{1+\ (A/K'_s)^n}$$

$$Relative\ oscillation\ frequency\colon \omega = \frac{1}{\beta'' T}$$

$$Duty\ ratio\colon \gamma = \frac{\Delta}{T}$$

A, T, and Δ are calcium peak amplitude, period, and spike width, respectively. NFAT half-saturation constant and Hill coefficient were identified experimentally as described in Section 3.5.10, and the import rate (α) and the export rate (β) were obtained from experimental reports (*78*, *179*).

Using this derived analytic model, we performed a sensitivity analysis to identify the individual effect of specific parameters on the NFAT response. We calculated the mean NFAT transcriptional activity as a function of either relative calcium oscillation frequency (ω) or duty ratio (γ) while holding the remaining components constant. The relative oscillation frequency is the determinant frequency parameter suggested by the model and is defined as oscillation frequency (ν) relative to the NFAT nuclear export rate (β). This analysis (**Figure 3.4**) spanned a physiological range of peak calcium amplitude (A) at either an optimal duty ratio or an optimal relative frequency.

NFAT sensitivity to relative frequency was evaluated using Equation 1, with ω spanning 0 to 3. The sensitivity is high at low duty ratios, and maximized at an optimal duty ratio of (*135*):

$$\gamma_{opt} = \frac{\sqrt{1+\sigma}-1}{\sigma}. \qquad \textit{Equation 2}$$

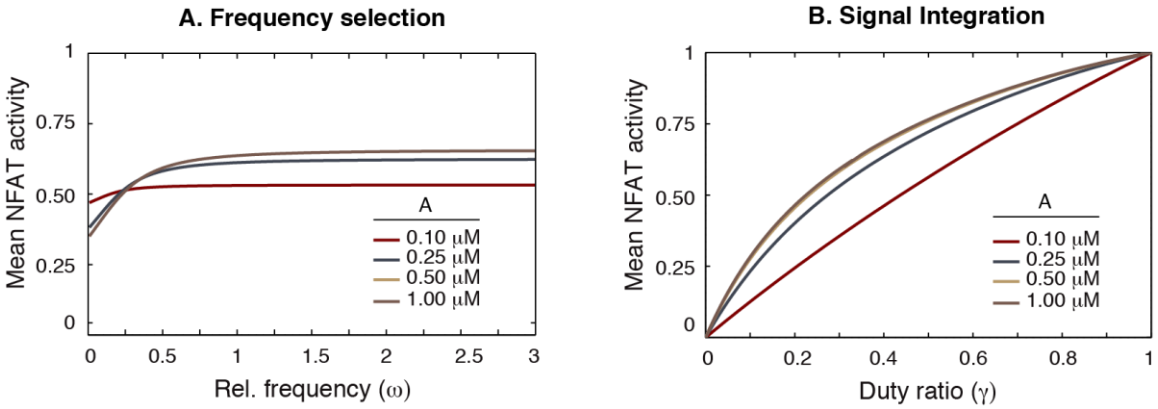

Figure 3.4. NFAT sensitivity analysis with mathematical modeling

Mathematical models of NFAT sensitivity to (A) calcium frequency and (B) duty ratio suggest it is primarily an integrator of cumulative calcium delivered by pulsatile loads regardless of peak amplitude, as the duty ratio-response spans the whole activation range, whereas frequency dependence is more modest. Note that the models for 0.5 and 1.0 mM calcium overlap.

The analysis revealed that frequency sensitivity over the physiologically relevant range (ω = 0–3) using the optimal duty ratio is confined to the lower range of relative frequency (ω < 1), with a maximum frequency-dependent enhancement of ~30% (**Figure 3.4A**). However, duty cycle has a more pronounced effect that spans the entire range of transcriptional activation regardless of oscillation amplitude (**Figure 3.4B**). The model thus suggests that NFAT is more sensitive to duty cycle than specific frequency and, consequently, is primarily an integrator of cumulative calcium load. Importantly, the analysis also informed our experimental design by identifying the parameter regimes in which the NFAT response is most sensitive to, as well as estimating the maximum change in NFAT activity as a function of these individual parameters.

3.2.2 Optogenetic approach for controlling calcium oscillations

Next, we sought to test these analytic results directly by optogenetically controlling intracellular calcium in HeLa cells and correlating the oscillation waveforms to transcriptional activity in multiplexed gene expression assays. To allow creation of calcium oscillations with physiological characteristics, we first looked to select an appropriate optogenetic tool with (i) fast kinetics with ability to mediate oscillations with the periods as small as 100s, (ii) high sensitivity that can elevate intracellular calcium concentration by at least 200 nM, and (iii) prolonged photostability that remains sensitive through hours of repeated illuminations. Of all the existing optogenetic tools discussed in section 1.2, G_q-coupled opsins exhibit highest sensitivity and show properties that meet all these criteria.

3.2.2.1 Selection of G_q-coupled opsins

G_q-coupled opsins are highly sensitive as the signals from the opsins are amplified through cascade of proteins signaling (*102*). However, the off kinetics of the existing human OPN4 can be relatively slow compared to the LOV-based optogenetic tools, we then wished to examine additional OPN4 homologs from other organisms to explore possibility of further improve the opsin kinetics. Five G_q-coupled opsins were selected for screening, including *A. cerana* (honey bees), *E. scolopes* (squids), *R. rutilus* (fish), *P. dumerilii* (worm), and *H. sapiens* (human) opsins. Cells expressing the opsins were stimulated with a brief 10s blue light pulse of sub-saturation intensity (10^{15} photons/cm^2/s). Calcium changes were monitored using X-Rhod-1 Ca^{2+} indicator to minimize crosstalk and plotted in figure 3.5A. Analyses suggested that *A. cerana*, *E. scolopes*, and *P. dumerilii* opsins are relatively insensitive as less than 2% increase in fluorescent level was observed in response to the light stimulus. *R. rutilus* and *H. sapiens* opsins, on the other hand, exhibit profound sensitivity triggering fluorescent change by more than 10% (**Figure 3.5A**). They also exhibit reasonably high speed, turning off the calcium response by 30 seconds after the light stimulation. *R. rutilus* opsin was, however, poorly expressed in mammalian cells in relative to human melanopsin (Data not shown). We, therefore, decided to move forward with human melanopsin for our subsequent experiments.

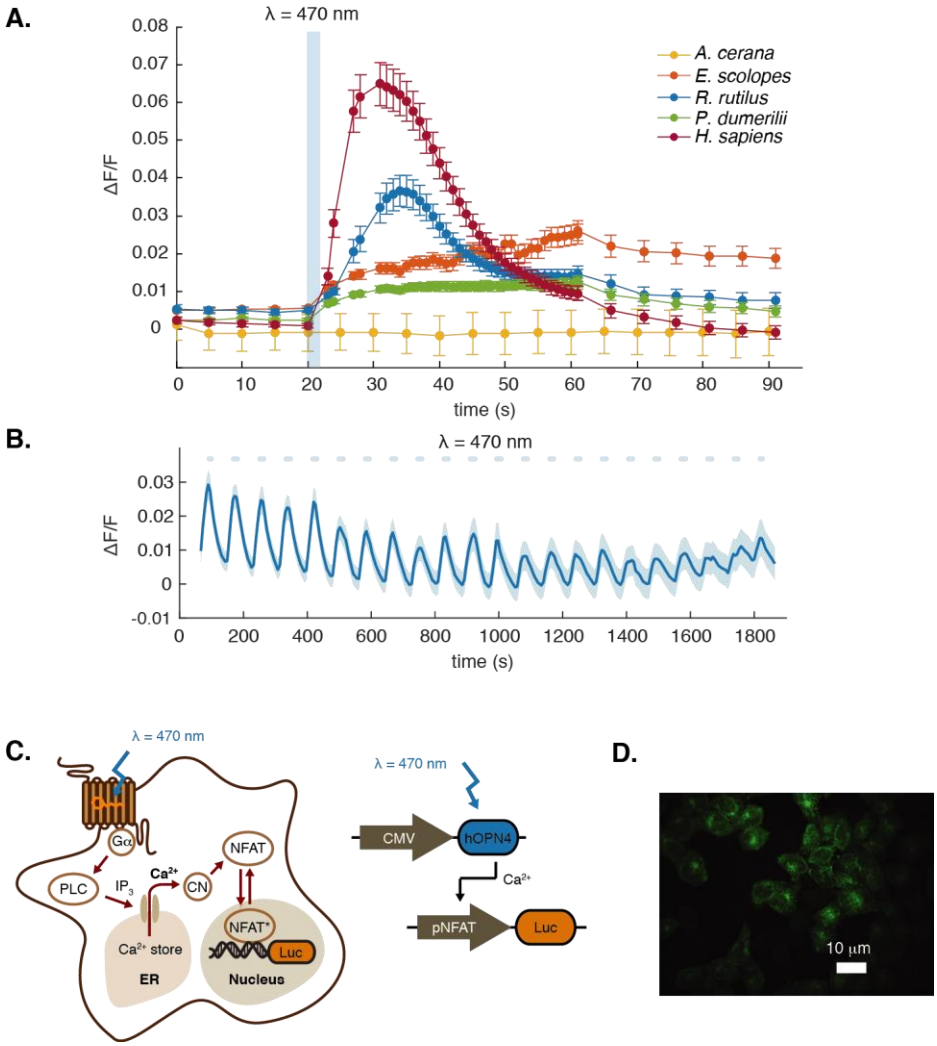

Figure 3.5. Optogenetic approach for controlling calcium signals.

(A) Light-induced (λ = 470, 3.8 mW/cm^2) calcium signals mediated by different G_q-coupled opsins. Each trace corresponds to the mean calcium signals averaged over the cell population expressing respective opsins (N>30).
(B) Human melanopsin-mediated calcium signal under 30-minute repeated blue illumination (λ = 470, 3.8 mW/cm^2, 1s ON 60s OFF).
(C) Signaling pathways and genetic circuit diagram of a synthetic optogenetic transcription device for decoding calcium encoding in HeLa cells. The calcium oscillations are optically created by melanopsin-mediated store-operated release, activating NFAT via Calcineurin (CN). The transcriptional activity of the specific oscillation is reported by luciferase under the NFAT promoter.
(D) Confocal micrograph of engineered HeLa cells stably expressing melanopsin, visualized by a C-terminal GFP tag.

We next further examined kinetics of human melanopsin to assess possibility of its use in prolonged calcium encoding. The human melanopsin was stimulated with a 10s-pulse of half-saturation intensity, 10^{15} photons/cm^2/s, and its calcium-coupled kinetics was then evaluated. The amplitude of calcium spike, τ_{on}, and τ_{off} was calculated to be 966.8 nM, 13.75s, and 26.75s, respectively. The calcium rise is sufficiently high for creating the desired oscillation determined earlier. τ_{on}, and τ_{off} are also less than 30 seconds which is more than enough for mediating the target frequent oscillation of 100s period. Human melanopsin was also shown to be reasonably stable as it remains activated as long as 30 minutes in response to the repeated stimulation of 60-s interval (**Figure 3.5B**). The data suggests that it was feasible to use human melanopsin for clamping the target calcium encodings.

2.2.2.2 Cell line generation for minimization of signal variability

To achieve homogeneous calcium responses among the cell population, we engineered HeLa cells to stably express the selected human melanopsin (hOPN4) for robust optogenetic control of store-operated release of calcium from the endoplasmic reticulum (ER). Twenty-four clonal cells were assayed to select for the clone of most uniform hOPN4 expression and calcium responses (**Figure 3.5D**). Luciferase reporter was then placed under the regulation of the NFAT promoter such that NFAT activities under varying patterns of calcium oscillation can be assessed through the expression of the luciferase reporter (**Figure 3.5C**). HeLa cells were chosen because they primarily express one isoform (NFAT4) that dominates the frequency sensitivity (**Figures 3.6**), thereby simplifying modeling and model-to-data correlations.

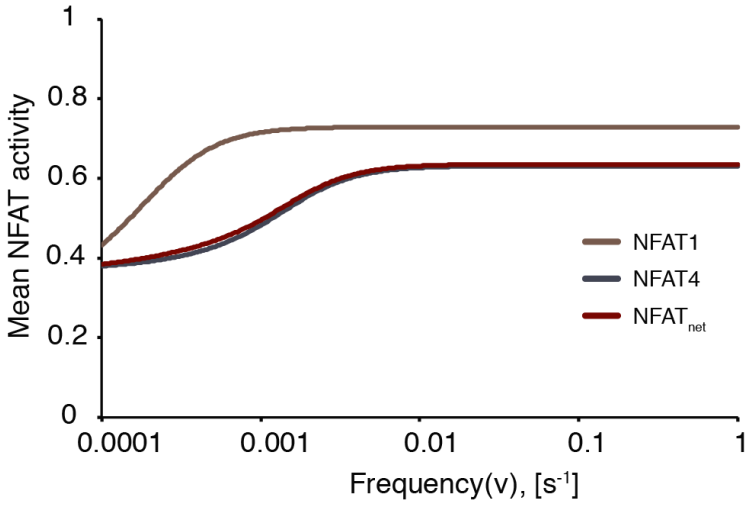

Figure 3.6. Isoform specific and isoform weighted-average NFAT activation sensitivity.

The net NFAT activity or expression-weighted average activity of the NFAT1 and NFAT4 isoforms found in HeLa cells resembles the activity of NFAT4, suggesting that the frequency sensitive-response is dominated by NFAT4.

As previously suggested, different NFAT isoforms exhibit distinct nuclear translocation kinetics (*179*). To evaluate the total NFAT activity averaged over the isoform repertoire, weighted sensitivity analysis was performed using a reported isoform expression ratio in HeLa cells of 0.83 $\log_{10}$(ppm) NFAT1 vs. 2.0 $\log_{10}$(ppm) NFAT4 (*139*). The net NFAT sensitivity (**Figure 3.6**) is relatively similar to that of NFAT4, suggesting that the frequency response in HeLa cells is dominated by NFAT4, and thus for simplicity, use the export rate of NFAT4 as the lump export rate in our system.

2.2.2.3 Identification of optical stimulation paradigms

Calcium waveforms in individual cells were evoked by optical stimulation and measured via calcium imaging with X-Rhod-1. We identified stimulation conditions that yielded calcium transients of identical peak concentrations (amplitudes) while varying

areas-under-the-curve (AUCs) (**Figure 3.7A**). Figure 3.7A shows the three waveforms and the empirically derived optical pulse-trains to reliably generate them. Repeated short pulses (1 s-long every 5 s, blue dots in **Figure 3.7A**) were used to prevent photoreceptor bleaching by constant illumination. Transcriptional induction epochs are created by repeating individual calcium transients and adjusting the inter-peak period in order to either match duty cycle across varying frequencies or match frequency across varying duty cycles (**Figure 3.9**). The highest oscillation frequency that allows calcium elevation to completely decay to the baseline was v ~8 mHz, and thus, optogenetic calcium clamping had sufficient temporal precision to ensure NFAT nuclear accumulation.

To ensure that the created calcium waveforms exhibit amplitude large enough for activation of NFAT, we assessed the level of NFAT activities at varying levels of constant calcium elevation. The analysis showed that calcium half-saturation concentration for NFAT activation is at 0.20 uM (**Figure 3.7B**). The identified matching peak amplitudes of 0.27 uM exceeded the half-saturation concentration for NFAT activation, and were, therefore, sufficient for triggering NFAT activities.

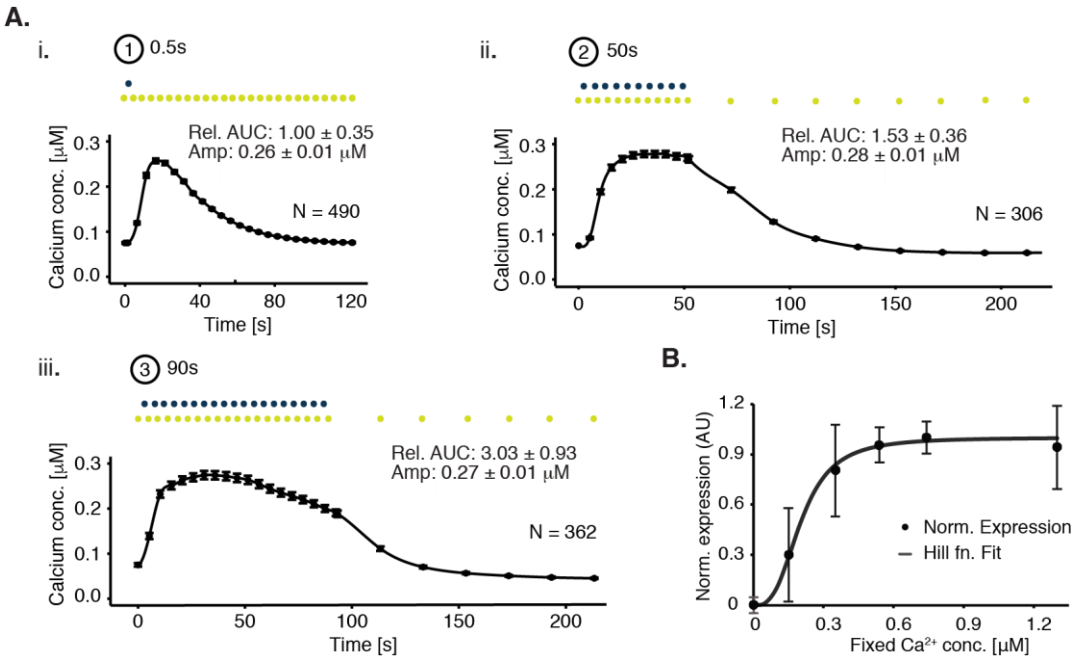

Figure 3.7. Characterization of calcium waveforms under varying illumination paradigms.

(A) Calcium transients of identical peak amplitude, but varying AUC (presented as Rel. AUC, relative to the AUC of 0.5 s-stimulation) created by melanopsin stimulation, as measured by calcium indicator X-Rhod-1 imaging. The colored dots represent optical stimulation pulses. The data are represented as mean ± SEM (with 306–490 cells per averaged trace).
(B) Waveforms generated in (A) exhibit amplitude sufficient for NFAT activation. NFAT transcriptional activity as a function of steady-state calcium concentration in engineered melanopsin-HeLa cells, assessed by first fixing or clamping calcium concentration in the dark, and then quantifying the expression of luciferase under the NFAT promoter (normalized, ± s.d.). Hill function fit estimated the NFAT half-calcium activation to be 0.2 uM.

3.2.3 Construction of programmable illuminators for high-throughput gene expression assay

We constructed programmable illuminators to enable consistent delivery of pulsing paradigms and high-throughput assay of NFAT activities. The illuminators designed for uniform light delivering to individual wells in a 24-well plate. The irradiance and pulse timing of each LED column can be respectively controlled via potentiometers and programmed through microcontrollers (**Figure 3.8**). To replicate the exact illumination conditions employed during the paradigm identification, an illuminator delivering yellow light pulses together with an illuminator delivering blue light pulses were used for each 24-well setup.

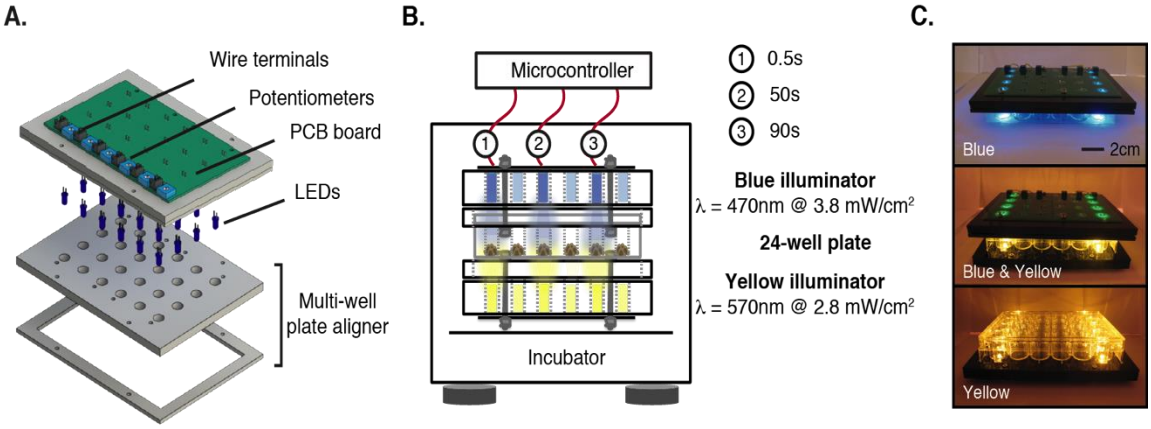

Figure 3.8. Experimental setup of the high-throughput transcriptional assays

(A) Schematic of custom illuminator to deliver identical stimulation as used in calcium imaging experiments, using a variable potentiometer and microcontroller to respectively tune irradiance and control timing per row of LEDs (see also Figure 2.9).
(B) Schematic for multiplexed optogenetic transcription assays in a multiwell plate (blue illuminator, melanopsin stimulation and yellow illuminator, recapitulation of X-Rhod-1 imaging).
(C) Photograph of the experimental setup, here shown outside of the tissue culture incubator.

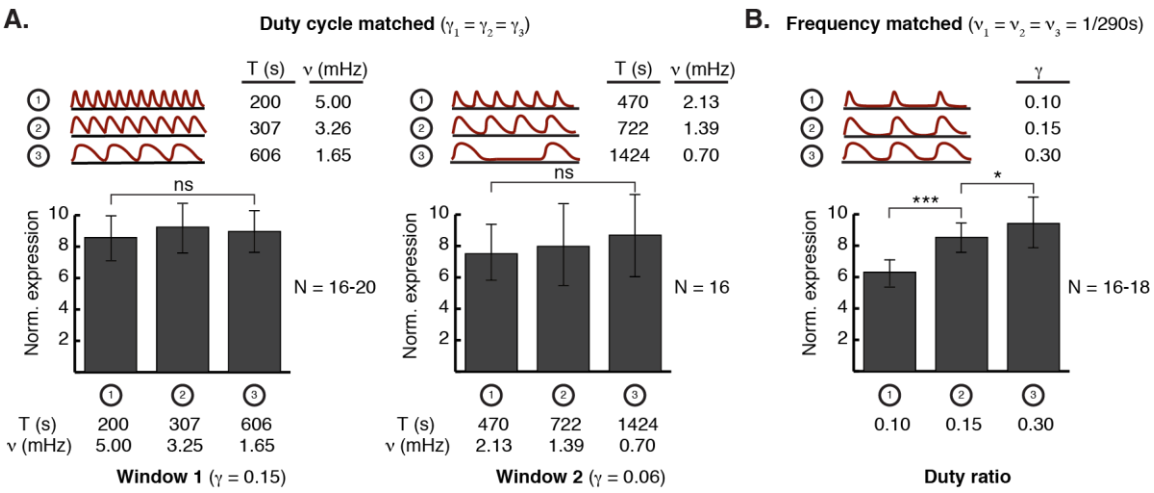

Figure 3.9. Parametric analysis of calcium oscillation frequency and duty cycle on NFAT transcriptional signaling

(A) Isolating the role of calcium frequency on NFAT transcriptional activity by optogenetic duty-cycle matching at fixed peak amplitude. The luciferase reporter expression under the transcriptional regulation of NFAT is optogenetically induced by melanopsin stimulation (refer to Figure 2.4C). The transcriptional activity is normalized to non-illuminated cells that are otherwise identical. No statistically significant difference is observed between frequencies at a given duty ratio (unpaired t test).
(B) Isolating the role of duty cycle under frequency-matched conditions at fixed peak amplitude. The transcriptional activity increases with duty ratio with sta- tistical significance (unpaired t test, * = $p < 0.05$, and *** = $p < 0.001$), suggesting that NFAT is primarily an integrator of cumulative load. In (E) and (F), data are represented as mean ± SD.

2.2.4 Gene expression assay

To isolate the specific contribution of frequency on NFAT transcriptional activity, we matched the duty ratio by adjusting the period between repeated peaks from Figure 3.7A. Two frequency windows of interest (1.65–5 and 0.70–2.1 mHz) encompassed the most frequency-sensitive regime (ω = 0.3–1.0; Figure 3.4A), based on reported $1/\beta_{NFAT4}$ of 3.0–7.6 min (*78*, *179*). Multiplexed transcription studies were performed in 24-well plates using custom illuminators that reproduce the calcium imaging conditions, for both melanopsin stimulation and X-Rhod-1 excitation, by controlling light-emitting diodes

(LEDs) via potentiometers (irradiance) and microcontrollers (timing) (**Figures 3.9**). No statistically significant difference in transcriptional activity was observed within either duty cycle-matched window (**Figure 3.9A**). Note that to limit cell variation and basal luciferase expression, all data within a particular frequency window were collected simultaneously, but the two distinct frequency windows draw from different cell passages. The duty cycle-matched assays suggest that NFAT is not primarily a frequency-selective decoder of calcium oscillations, as initially proposed by others (*37*, *38*).

To determine whether NFAT is instead primarily an integrator of cumulative load, we assessed the effect of duty cycle on transcriptional activity, at fixed frequency and amplitude (**Figure 3.9B**). All data in figure 3.9B were acquired simultaneously, but the frequency-matched data set was generated with different cell passages than the duty cycle-matched one. The same waveforms in figure 3.7A were used to span a 3-fold duty cycle range in a regime (γ = 0.1–0.3) chosen to maximize sensitivity based on the model in figure 3.4B. Statistically significant differences were observed across this range. Similar-fold increases in cumulative load are sufficient to fundamentally alter cellular dynamics, including transitions between poised and actively proliferating stem cell states (*36*). The increased sensitivity to duty cycle over spike timing suggests that NFAT behaves as a signal integrator, as suggested by the mathematical model and hypothesized by others (*11*, *14*, *29*, *77*). Importantly, previous studies using paired pulses of calcium in rat basophilic leukemia cells (RBL) confirmed that NFAT activation indeed integrates calcium elevations that are coincident within an inter-pulse temporal cutoff (*77*). The results here reveal that such decoding-by-integration is in fact the dominant mechanism for NFAT.

3.2.5 Discussion

As the study was conducted in HeLa cells which predominantly express one of the NFAT isoform, NFAT4, the question subsequently raised is then to what extent this mechanism of decoding can be generalized to other isoforms and other cell types. NFAT family comprises of five protein members: NFAT1-NFAT5. All of which carry conserved phosphorylation sites and calcineurin binding regions allowing NFAT nuclear shuttling to be similarly regulated through phosphorylation (*66*). Each isoform, however, has slight variation in these conserved regions resulting in distinct nuclear translocation kinetics and calcineurin binding affinity. Despite the differences in their molecular properties, all the isoforms undergo similar regulation through phosphorylation and de-phosphorylation, and should, in theory, exhibit similar decoding mechanism. Based on our mathematical model, the difference in translocation kinetics should only shift the sensitive frequency range, but have no effect on the degree of sensitivity. While increased calcineurin binding affinity within physiological range may slightly raise the frequency sensitivity, the duty ratio should though predominate the NFAT regulation. As a result, we believe that our findings should be applicable to all the NFAT isoforms.

NFAT behaviors in different cell types mostly differ by NFAT isoform composition and NFAT nuclear kinases. One cell type may express certain NFAT isoforms more than another; because all isoforms are fundamentally regulated with similar mechanism as discussed previously, the different in isoforms should mainly affect the range of sensitive frequency and minimally impact the frequency sensitivity. Likewise, NFAT nuclear kinases are responsible for controlling NFAT nuclear export rates which will only have an effect on the sensitive window and not on the degree of sensitivity. Consequently, the

decoding mechanism revealed here should hold true for other cell types, and not exclusive to our model cell type.

Furthermore, the finding is consistent with related studies on NFκB in immune cells (*152*, *184*) and the stimulus duration-dependent switching of cAMP-response element binding protein (CREB) in neurons (*17*, *18*), thus suggesting that decoding-by-integration is a general transcriptional principle applicable to many mammalian calcium-responsive activators. However, because these transcription factors differ from NFAT in terms of the presence of negative feedback loops mediated by IκB in NFκB signaling (*92*, *159*) and in terms CREB responsiveness to additional second messenger beyond calcium (*143*), one should keep attuned to signaling network-specific differences in the decoding principles employed by different calcium-dependent transcription factors.

Systematically isolating the contributions of individual waveform parameters to calcium-dependent transcriptional activity clarifies the role of frequency in studies performed with steady-state loads and/or unmatched duty cycles. Previously observed enhancements with shortening periods were likely attributable to consequent differences in cumulative load. This distinction does not imply frequency insensitivity, since excited cells typically increase their calcium spike frequency (*141*), but rather shifts the attributable source of enhancement to better reflect the decoding principle, from specific frequency or peak timing, to frequency-coupled cumulative load.

NFAT signaling relies on pulsatile calcium to coordinate with other regulators to direct diverse signaling outputs (*128*) and to achieve selectivity by temporal cutoff filtering (of isoform-specific translocation rates (*92*, *179*)), in addition to distinct spatial

calcium signatures within cells. Single-cell studies on calcium-dependent transcription factors have shown that nuclear translocation occurs in pulsatile bursts of increasing output frequency with increasing steady-state calcium input (*23*, *78*, *92*, *159*, *179*), so that coordinated gene expression under one promoter depends on the fraction of localization time, but not exact timing or true frequency (frequency-modulated (FM) coordination (*23*, *92*)). Since fraction of localization time is also a duty ratio, the optogenetic findings here are consistent with the general FM-coordination principle, but now applied to the upstream, non-steady-state oscillatory input.

3.3 Conclusions

In total, this work defines a workflow for using mathematical modeling, optogenetics, and mammalian synthetic biology to isolate the decoding principles at work in dynamical regulation of transcription. By resolving this experimental confound in interpreting the roles of interdependent components of an oscillatory signal, this parameterized analysis refines a key decoding principle of frequency modulated calcium-dependent transcription to better explain how mammalian cells dynamically respond to complex stimuli.

3.4 Future directions

3.4.1 Decoding of irregular calcium oscillations

So far, we have assumed that the calcium oscillation frequency is consistent throughout the course of signaling. However, within each individual cells, large variation in the period between calcium spikes (Interspike interval, ISI) has been widely observed (*45*, *148*, *149*). Cells including astrocytes, microglia, PLA, and HEK cells exhibited oscillation with up to 89% coefficient of variation in ISI. It is, therefore, interesting to examine how NFAT and other calcium-dependent transcription factors respond to calcium oscillations of irregular interspike intervals, signaling paradigms more closely resembled the physiological observations.

3.4.2 Roles of calcium spike timing

Our study demonstrated that cumulative load of calcium oscillations is a primary determinant factor regulating NFAT activities, which is consistent with the decoding mechanism of other calcium-dependent transcription factors. The finding then raises a question of whether the spike timing plays an important role under any particular conditions or for any type of special regulation. For instance, if the amount of calcium being released is limited, does the pattern of calcium mobilization, such as release all at once or space out with certain duration, matter and what pattern optimizes the transcription factor activation? This particular circumstance can be applicable to the cells subjected to the absence of extracellular calcium environment where calcium is pooled exclusively for the ER internal store.

The signal timing can also play a crucial role for coordination of multiple signal inputs. Certain transcription factors including NF-κB and CREB integrate additional input

such as cAMP and PKC (*19*, *106*, *138*, *173*) where calcium spike and cAMP (or PKC) signal are required to emerge concurrently in order for the transcription factors to initiate transcription of certain genes. It is therefore worthwhile to extend this similar experimental approach to study transcriptional response to such concomitant inputs.

3.5 Materials and methods

3.5.1 Genetic constructs

The pLJM1-melanopsin-GFP plasmid was constructed by subcloning human melanopsin (hOPN4, provided by the Boyden Lab, MIT) fused to a C-terminal EGFP reporter with an enhanced-trafficking signal between the NheI and EcoRI restriction sites of lentiviral vector pLJM1-EGFP (provided by the Gadue Lab, Penn). The plasmid was propagated in NEB Stable cells, and purified using a QIAGEN plasmid maxi kit to generate lentivirus. The NFAT luciferase reporter plasmid pGL4.30[luc2P/NFAT-RE/Hygro] (Promega E8481) was propagated in DH5 cells, and purified using QIAGEN plasmid maxi kit (Qiagen 12165). Unless stated otherwise, all oligonucleotides were synthesized by IDT and cloning was sequence verified by Sanger sequencing (Penn Cell Center).

3.5.2 Cell culture

HeLa cells (provided by the Raj Lab, Penn) were grown in Dulbecco's modified Eagle's medium (DMEM) with GlutaMAX (Invitrogen 10566016), supplemented with 10%

heat-inactivated fetal bovine serum (FBS) (Seradigm 1500-500) and 1% Penicillin-Streptomycin (Invitrogen 15140122). Cells were maintained in a standard water-jacketed mammalian cell culture incubator (Thermo/Forma 3110).

3.5.3 Lentiviral generation of stable cell lines

To generate lentivirus, HEK293T cells (provided by the Lazzara Lab, Penn) were transfected with pLJM1-melanopsin-EGFP and 3rd generation packaging system plasmids (or helper plasmids). The media was replaced one day after transfection, and virus-containing supernatant was collected on the second and the third days. After centrifugation (1000 rpm, 5 minutes), the supernatant was filtered (0.4um PES) and used immediately or stored at 4°C for <7 days. HeLa cells were lentivirally infected and selected using 1 ug/ml Puromycin (Clontech 631305). Individual clones expressing melanopsin-EGFP were picked under a sterile fluorescence microscope (courtesy of the Cremins Lab, Penn) and grown in 24-well plates. Optogenetic performance or light-induced store operated release was assessed for each clone by calcium imaging (see **Section 3.5.4: Calcium imaging**), in order to select a suitable clone with high light responsiveness and minimal signal attenuation by repeated illuminations. Membrane localization was assessed by confocal microscopy (Leica SP5, courtesy of the Meaney Lab, Penn).

3.5.4 Calcium imaging

Calcium imaging was performed on an automated Leica DMI6000B fluorescence microscope (custom Chroma dichroic filter cube, λ_{ex} < 575nm and λ_{em} > 580nm),

equipped with a sCMOS camera (pco.edge) and LED illuminator (Lumencor Spectra-X) for fluorescence imaging and optogenetic stimulation, all under Metamorph software control. Cells seeded on collagen-coated German glass coverslips (24 hours in advance) were incubated with 2μM X-Rhod-1 (Invitrogen X-14210) for 30 minutes at 37°C, and then washed and replaced with phenol-free CO_2-independent media (phenol-free HBSS supplemented with 1% L-glutamine, 1% Penn/Strep, 2% essential amino acids, 1% non-essential amino acids, 2.5% HEPES pH 7.0, and 10% serum), supplemented with 2μM all-trans retinal (Sigma-Aldrich R2500). After incubating cells for 30 minutes for dye de-esterification, the coverslip was transferred to a perfusion chamber (Autom8, with a Harvard Apparatus Syringe Pump) for imaging. It should be noted that genetically encoded calcium indicators were not employed because those with red-shifted excitation from melanopsin, such as RCaMP (*3*), required imaging irradiances that saturated melanopsin signaling despite the spectral separation, and bioluminescent indicators lacked sufficient temporal resolution in our hands (*134*).

Time-lapse images of dye-loaded cells were taken with 0.5s exposures on a 20x air objective (λ_{ex} = 570nm, 2.8mW/cm^2). Melanopsin stimulation paradigms (λ_{ex} = 470nm, 3.8mW/cm^2) were developed after scanning ranges of individual pulse duration (0.1 - 50s), pulse interval (1 - 5s), and total pulse train duration (1 – 90s). Stimulation epochs were repeated three times per imaging trial to assess for photoreceptor bleaching, and traces shown in main text Figure 2 are derived from the average per trial. A single 0.5s pulse was sufficient to saturate the optogenetic store-operated release response, and the longer stimulation paradigms (50s and 90s) reported in main text were chosen such that the resulting period-adjusted calcium duty ratios were matched over a three-fold

frequency range. Image processing, cell segmentation, and measurements of fluorescence intensity of individual cells were performed using ImageJ and Metamorph.

To convert relative fluorescence to absolute calcium concentration, minimum (F_{min}) and maximum fluorescence (F_{max}) signals were obtained immediately after imaging every cover slip, and then input into Equation 3 (refer to **Section 3.5.5: Calcium calibration**, below). To obtain F_{min}, cells were washed with calcium-free HBSS three times, and then were incubated with F_{min}-buffer for 10 minutes (HBSS, 5μM calcium ionophore (IM, Sigma-Aldrich C7522), and 3μM EGTA (Sigma-Aldrich E8145)) to allow complete EGTA sequestration of calcium prior to acquiring the F_{min} image. Similar washing and incubation protocols were used to subsequently obtain F_{max} images after 5-minute perfusion with F_{max}-buffer (HBSS, 5μM IM, and 10mM $CaCl_2$). Calcium conversion from fluorescence and the calculations of waveform parameters were performed in MATLAB.

3.5.5 Calcium calibration

Stable HeLa-melanopsin cells were grown on collagen-coated coverslips and dye-loaded as described in Section 3.5.4: Calcium imaging. Cells were perfused with buffer containing 5μM IM and calcium calibration samples prepared from stock calibration standard (Biotium 59100), and imaged as described above. Fluorescence intensities of individual cells were averaged, and the natural logarithm of normalized fluorescence measurements were plotted against that of calcium concentration. A linear regression was fit to the data in Excel to derive Equation 3 (R-squared of 0.93).

$$ln\left[\frac{F-F_{min}}{F_{max}-F}\right] = 0.7618 \cdot ln\,[Ca^{2+}] + 0.149$$ *Equation 3*

3.5.6 Data analyses and calculation of calcium waveform parameters

Data analyses were performed using MATLAB. Fluorescence intensity of an individual cell was converted to absolute calcium concentration using its corresponding F_{min} and F_{max} (Equation 3). The average trace for each illumination paradigm was calculated by averaging the signal from individual cells for each sample. The area under the curve (AUC) was calculated from the baseline-corrected trace over the two minutes following melanopsin stimulation initiation (or the typical fall to baseline). The mean AUC and peaks for each experiment were calculated by averaging the AUC and peaks of all single-cell traces from 6 coverslips (3 epochs per cell, 306-490 cells in total).

3.5.7 Transcriptional Efficiency

Cells were seeded in clear-bottom black 24-well plates (Perkin Elmer 1450-605) at a density of 100,000 cells/well. After 24 hours, cells were transfected with 0.5μg of pGL4.30 plasmid per well using TransIT-LT1 transfection reagent (Mirus Bio 2305) in Opti-MEM (Invitrogen 31985070). At 24-hours post-transfection, the cell media was replaced with phenol-free DMEM containing 2μM all-trans retinal. The plates were placed under custom illuminators (See **Section 3.5.9: Illuminator construction and programming**), which were programmed through Arduino microcontroller to deliver light that recapitulated calcium imaging irradiance and pulse sequences to create calcium transients of matching duty ratio or frequency after period adjustment. The cells were

irradiated for 6 hours in a humidified incubator at 37°C and 5% CO_2, and subsequently collected for luciferase reporter quantification (Promega E1501, according to manufacturer protocol) after chemically cell lysing with cell culture lysis reagent (Promega E1531). Luminescence measurements were performed in white 96-well plates (Greiner Bio-One T-3025-14), using a Tecan M200 plate reader (5s integration time).

3.5.8 Identification of NFAT Ca^{2+} half-saturation binding

HeLa-melanopsin cells were bathed in calibration buffer and assayed for steady-state transcriptional efficiency using a luciferase reporter under the regulatory control of the NFAT promoter (see **Section 3.5.9: Transcriptional efficiency**), in the absence of optical stimulation. The calibration buffer contains HBSS, 0.2% BSA, 1mM MgCl2, 0.5mM EGTA, 5μM IM, and varying concentrations of $CaCl_2$ yielding free calcium concentrations of 0, 0.16, 0.35, 0.54, 0.74, and 1.3 μM. The assay was performed in triplicate for each buffer. Expression was normalized to the minimum and maximum luminescence signals, $[(R-R_{min})/(R_{max}-R_{min})]$ (**Figure 3.7B**). The data were fit to a Hill equation, with best-fit values of Hill coefficient (n) = 3.01 and calcium half-saturation binding (K_s) = 0.20 μM (R-squared of 0.99).

3.5.9 Illuminator construction and hardware programming

The illuminator consists of two layers of acrylic scaffold for a plate positioning and LED alignment, and two custom PCBs designed for independent control of each LED column via Arduino automation of pulse sequences and tuning of irradiance (measured on a ThorLabs PM100D power meter with S120 sensor) using

potentiometers (Trimpot, 3362H-102LF). The acrylic layers (**Figure 3.10D**) were designed in Solid-Works and laser-cut (Universal Laser Systems, Model No. VLS 3.50), to align 5mm dome-cap LEDs to a standard 24-well plate (Joe Knows Electronics, 5-Round-B-100). The PCB boards were designed in Eagle CAD and printed by Custom Circuit Board LLC, with each column possessing four parallel-connected LEDs, a 1kΩ variable potentiometer, and wire terminal for microcontroller-interfacing (**Figure 3.10C**). All LEDs were quality-controlled prior to assembly for similar output, as measured by an optical power meter. The individual layers were aligned using laser-cut holes assembled with 2-56 machine screws and narrow hex nuts, as shown in Figure 3.8.

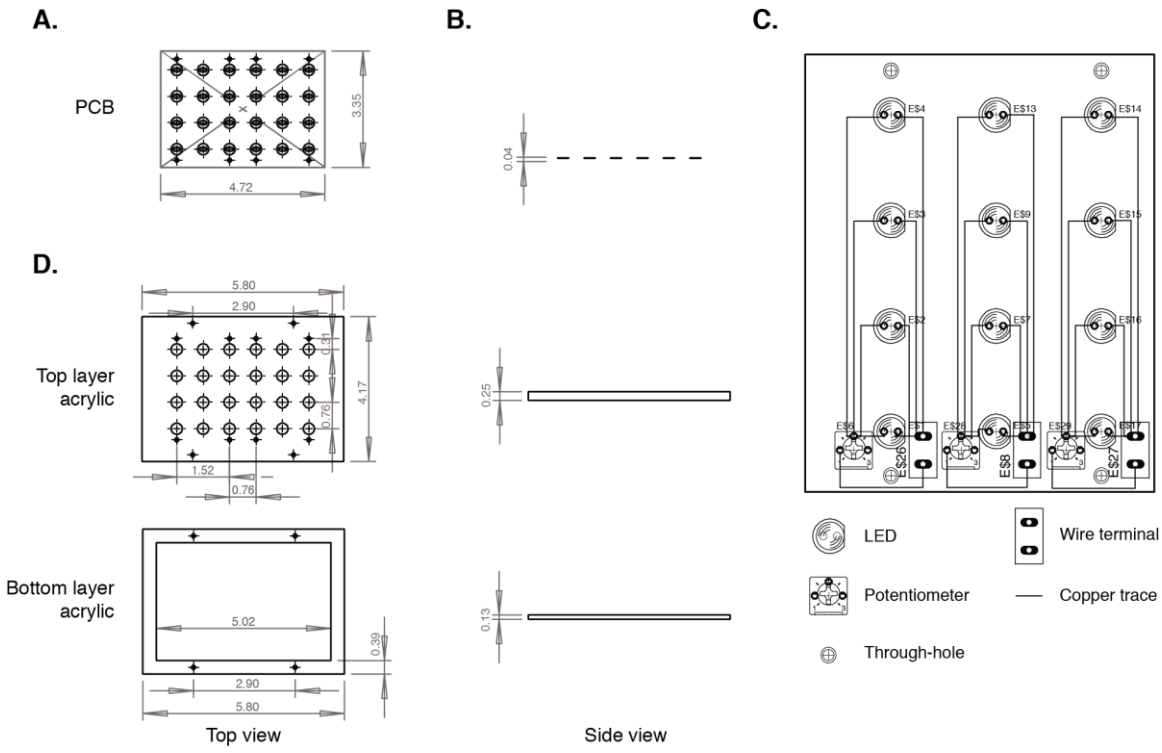

Figure 3.10. CAD schematics of custom illuminator for multiplexed optogenetic transcriptional induction (scale in inches).

(A) Top view of PCB with six independent columns of LEDs per 24-well plate.
(B) PCB layout with 3 columns shown. Each column contains four LEDs connected in parallel with a 1kΩ variable potentiometer, and a wire terminal.
(C) Circuit diagram of a single LED column on the PCB.
(D) Top view of acrylic positioning plates.

CHAPTER 4 : Conclusions and Future Directions

4.1 Conclusions

To maintain proper function and survival, cells consistently adapt to their changing environments by sensing and responding to external cues. These external cues pass along information through a series of intracellular signaling cascades to inform appropriate cell decision. The information is often carried through common signaling pathways, such as calcium, that are shared among multiple external stimuli. In calcium signaling, the intensity and identity of the stimuli are encoded in the temporal patterns of the calcium oscillations (*10*, *42*, *52*, *54*) which are, in turn, decoded downstream to trigger selective cellular responses (*29*, *37*, *38*, *44*, *121*, *137*, *150*). The dynamics of the signals expands capabilities of the calcium signaling pathway and enables discriminatory cell responses.

Despite the significance of the calcium signaling dynamics, the principles of how the information is encoded and decoded remain largely unanswered, partly due to the limitation of the tools that perturb calcium signaling in temporally precise manners. To overcome this hurdle, we developed novel bi-directional optogenetic approaches for precise manipulation of calcium signals and perturbation of signaling circuitry and applied them to resolve the unanswered questions in calcium encoding and decoding.

4.1.1 An optogenetic tool for resolving calcium encoding circuitry

We devoted the first portion of the thesis to investigating a key question in calcium encoding to determine a global negative feedback in the calcium oscillation circuit. Based upon past experimental evidences, we identified a regulator of G-protein signaling (RGS) protein as a potential global negative regulator of the calcium oscillation signaling circuit, created a novel optogenetic RGS for dynamic manipulation of RGS activities, and utilized it for uncovering the role of RGS in regulation of oscillation periodicity and stochasticity.

We created optogenetic RGS (opto-RGS), a main negative regulator of G proteins, with a specific focus on RGS2 subtype highly specific to $G_{\alpha q}$ isoform. Opto-RGS2 was constructed from split RGS2 in which its C-terminal RGS2-box and N-terminal α-helix were respectively fused to *Arabidopsis* cryptochrome 2 (CRY2) and its binding partner, CIBN. The two components are apart and inactive in the dark. Blue light illumination induces dimerization of the cryptochrome pair, bringing the C-terminal RGS2-box to its N-terminal α-helix at the membrane and, therefore, reconstituting the functional full-length RGS2. This optogenetic design offers improved specificity by incorporation of the RGS α-helix that is responsible for targeting and specific subcellular localization. Unlike the previous design with non-specific membrane targeting signal (*118*), opto-RGS2 should act specifically on the $G_{\alpha q}$ signaling and show minimal activity towards other G protein pathways.

To obtain a uniform behavior, we generated a stable HEK293t cell line expressing opto-RGS2. We established a novel machine learning-guided approach that

allows high-throughput selection of clonal populations with desired functional properties. The most optimal clonal line was selected, and the opto-RGS2 calcium inhibition activities of the clone were verified to functionally resemble those of the native RGS2. Opto-R2 suppressed agonist-evoked calcium oscillation amplitude, frequency and duty ratio in a light-dependent manner. In addition, the dark control showed minimal or no basal inhibition activities disregarding the concerns associated with cryptochrome-based optogenetic tools. Quantitative PCR analyses also verified that stable expression of opto-RGS2 did not perturb the basal calcium homeostasis previously observed with traditional perturbation approaches such as RGS2 genetic knockouts. Together, opto-RGS2 served as a novel perturbation tool that is highly specific, reversible, and functionally indistinguishable from the native RGS2.

We utilized opto-RGS2 to investigate the role of RGS2 in regulating calcium oscillation feedback and stochasticity. We evoked calcium oscillations through ligand stimulation and assessed the coefficient of variation (α), a measure of stochasticity, of the interspike interval (ISI) of the observed oscillations. Illuminated cells (active RGS2) exhibited significantly lower ISI variation than the non-illuminated cells (inactive RGS2). This suggests that RGS2 reduced the ISI variation and therefore lowered the signal stochasticity. To confirm the role of RGS2, we examined how the ISI coefficient of variation changed with inhibited calcium binding protein calmodulin CaM as previous studies suggested that RGS coupled to the calcium feedback through CaM. The ISI coefficient of variation in cells with CaM inhibition returned to the original value observed in the non-illuminated cells. This analysis confirmed that RGS2 was coupled to the calcium elevation through Ca^{2+}/CaM, and together act as a regulator of the calcium oscillation stochasticity.

Our experimental results support the stochastic view of calcium signaling and the role of RGS2 as a global negative feedback regulator of calcium oscillations. The coefficient of variations of the receptor-mediated calcium ISI were too high (~80%) for the signaling to be deterministic, consistent with the observations by a number of calcium encoding studies (*45*, *148*). In addition, we identified RGS2 as a potential global negative feedback that controls long-period oscillations, the phenomena unexplained by previous calcium encoding models. Under the stochastic framework, theoretical analyses predicted that the signal-to-noise ratio should remain constant if the perturbation does not affect the global feedback mechanism (*149*, *161*). The fact that RGS2 altered oscillation signal-to-noise ratio and modified average ISI indicated that RGS2 played a key role in the global negative feedback. Our finding is consistent with the hypothesis proposed by Thurley et al. that the global feedback should be upstream and closer to G protein or G-protein coupled receptors (*162*).

The RGS2 negative feedback can be combined with the class I calcium encoding model to describe calcium oscillation phenomena. Class I model hypothesized that IP_3R altered its sensitivity by the calcium levels which forms the basis of how calcium oscillations are created (*4*, *35*, *40*, *96*, *157*). The model is strongly supported by the discovery of the IP_3R biphasic property, but lacks explanation for the long ISI observed experimentally (*42*). Because RGS inhibition of G-protein signaling can be in the scale of tens of seconds or minutes (*101*), our finding of RGS2 negative feedback can be incorporated to the model to potentially explain the circuit component responsible for extended oscillation periodicity.

4.1.2 An optogenetic approach for study calcium decoding

The second portion of the thesis shifted the focus towards the investigation of a calcium decoding principle of a calcium-dependent transcription factor NFAT. We developed a novel optogenetic approach for precise generation of calcium oscillation waveforms, built a mathematical model to explain the NFAT decoding behaviors, and applied the optogenetic method to experimentally uncover the NFAT decoding principles.

To establish the novel optogenetic approach, we (i) experimentally identified the most sensitive and fast kinetics calcium-coupled receptor, melanopsin, for light-induced generation of calcium signals, and (ii) created a synthetic optogenetic transcription device consisting of HeLa cells stably expressing melanopsin and NFAT-driven luciferase reporter. The creation of a stable cell line reduced response variability while the circuit connection with the luciferase reporter offered a more scalable and robust approach for monitoring calcium-mediated NFAT transcriptional activities through measurement of luciferase expression, (iii) identified the illumination paradigms for shaping calcium waveforms of desired characteristics, and (iv) fabricated custom illuminators with programmable irradiance and pulse timing for high-throughput assay of NFAT activities. These collective steps comprised an approach for precise clamping of calcium oscillation waveforms and reliable high-throughput assessment of calcium-coupled NFAT transcriptional activities.

The established optogenetic approach was applied to resolve the main calcium decoding question as to whether NFAT is a true frequency decoder that can discriminate

the signals solely based on frequency or is primarily a signal integrator that is more sensitive to the signal duty ratio. We used our developed optogenetic method to create calcium oscillation signals with either matching frequency or matching duty ratio and assess NFAT transcriptional activities under these conditions. Our analyses suggested that NFAT showed no significant change in transcriptional efficiency across physiological frequency range with constant duty ratio. On the other hand, NFAT transcriptional efficiency substantially improved with increasing duty ratio of a fixed frequency. The results indicated that NFAT acted predominantly as a signal integrator as opposed to a frequency decoder perceived by a conventional view. This is consistent with our mathematical model predicting duty ratio as a primary oscillation characteristic that determines NFAT transcriptional activities.

Decoding by signal integration may be a general decoding principle of calcium-activated transcription factors, as similar decoding behaviors were observed in NF-κB and CREB transcription factors. NF-κB transcriptional activities are far more sensitive to the cumulative calcium spike duration compared to the spike frequency (*152*, *184*), whereas extended duration of calcium elevations maintains CREB in an active state (*17*, *18*). These transcription factors respond more prominently to the change in calcium load rather than oscillation frequency.

As frequency and duty ratio are often coupled in physiological conditions, this finding does not suggest that frequency has no role in regulation of cell decision, but rather shifts the weight more towards calcium load or duty ratio. Studies demonstrated that the calcium-activated transcription factors show their highest transcription efficiency at different frequency-coupled duty ratio ranges. NFAT exhibited highest activity at low

duty ratio (0.2-0.3 at 20 mHz frequency) while NF-κB performed most optimally towards a higher duty ratio range (0.8 - 0.9 at 10 mHz frequency) (*150*). This notion suggests that frequency-coupled duty ratio may be the determinant oscillation characteristic that elicits cell response specificity.

This finding points to the next question that if frequency is not the major component in determining specificity, what could potentially be the functional roles of the repetitive calcium pulsing or the timing of the signals. Recent studies suggest that signal pulsing may facilitate coordination of gene expressions under different promoters (*23*). Pulsing enables genes of related roles to be expressed with a consistent proportion regardless of the variability in the signaling inputs. Additionally, pulsing may also be crucial for transcription factors that require integration of multiple signaling inputs in which signals from multiple signaling pathways must be present concurrently to initiate transcription (*92*).

In sum, our finding on the NFAT decoding mechanism is consistent with related studies on similar transcription factors and emphasized the importance of duty ratio as an additional factor when considering dynamics of oscillation signals.

4.2 Future directions

The optogentic technologies and the understanding of calcium dynamics developed in this thesis can be useful for further applications in the context of both reverse and forward engineering.

4.3.1 Reverse engineering

Intracellular signaling is extremely dynamic, and multiple signaling pathways oftentimes cross-interact with each other to regulate particular cell responses. While studies in the past two decades have gained substantial insights regarding signaling dynamics, many questions in the functional roles of pulsing and oscillations are still unanswered. Because of their fast, sensitive, and specific properties required for studying dynamic systems, optogenetic approaches are valuable technologies that can be used to elucidate other functions and circuit topology of signal transductions.

The optogenetic approaches developed here are specialized for controlling of calcium signaling and circuit. They can be transferred to study many other questions in calcium signaling dynamics. Moreover, these tools can become more powerful if combined with other optogenetic tools that allow simultaneous manipulation of multiple pathways useful for the study of cellular processes regulated under multiple signaling inputs.

One other question in calcium signaling is the role of stochasticity in the calcium ISI. As we have showed, agonist-evoked calcium oscillations are stochastic and highly irregular in periodicity. This raises a question as to what could potentially be the advantages of the stochastic behavior and how that affects the downstream calcium effectors and cellular decision. Similar to the approach described in chapter 2, our melanopsin-mediated optogenetic approach can be used to generate trains of calcium pulses with irregular intervals similar to what is observed physiologically, and transcriptional efficiencies of calcium-activated transcription factors can then be

monitored under these conditions. The roles of calcium stochasticity can then be elucidated.

Another example is on investigating potential roles of pulse timing for integration of concurrent signaling inputs. Many transcription factors such as CREB can be regulated by multiple signaling pathways. Calcium and cAMP messengers have been shown to influence the activation state of CREB (*105*). As both messengers are known to exhibit diverse pulsing dynamics (*128*), it is noteworthy to understand the individual and synergistic roles of the signals, and whether the timing of two signals matters for regulating CREB activities. In this circumstance, our optogenetic calcium control approach can be used together with a tool for optogenetic modulation of cAMP such as bPAC (*1*, *155*) or optoPKA (*116*) to precisely coordinate the timing of calcium and cAMP signals. Combination of these optogenetic tools offers a powerful approach for studying target proteins under combinatorial regulation, a more complex decoding mechanism observed in signal transductions.

4.3.2 Forward engineering

The notion of signaling dynamics is valuable in the context of synthetic biology. Synthetic circuits constructed in the past mostly consider continuous-based interactions (*111*). However, as we has presented, biological signaling is in fact extremely dynamic, and these dynamic components demonstrate a number of benefits over constant signaling. The temporal patterns expand signaling pathway capabilities, integrate multiple signaling inputs, coordinate proportional expression of related genes, and maximize use of limited resources (*92*). More optimal synthetic circuits can potentially be

built by taking advantage of dynamic knowledge learned from the natural encoding and decoding principles.

One potential synthetic circuit can be built based on the versatility of the calcium signaling. As described in chapter 3, a few transcription factors are regulated by dynamics of calcium signaling. Our study suggested that these transcription factors decode the signals primarily by the calcium load or oscillation duty ratio, and they exhibit sensitivity towards different ranges of duty ratio. With this knowledge, one can construct an optogenetic multiplexing transcriptional circuit in which different sets of calcium-activated transcription factors can be activated depending on the oscillation characteristics of the optogenetically-mediated calcium inputs.

APPENDIX 1: Photo-Activated RGS Chimera – an Alternative Design to Optogenetic Control of RGS Proteins

A1.1 Introduction

Optogenetics has proved extraordinarily useful as a tool for dissecting intracellular signal transductions. In chapter 2, we discussed our development of optogenetic RGS2 that took advantage over light-inducible dimerization proteins and functionally subcellular localization nature of RGS proteins; light induces translocation of the catalytic RGS-box to the location where it can interact with its target proteins, G proteins (**Figure A1.1A**). While this design performed well in our HEK293t cell lines, it is a two-component system in which their relative expressions may need to be properly tuned for each individual host cell line. We, therefore, considered an alternative single-component design that relied on a light-switchable property of a different class of photoreceptor, LOV domain. With this strategy, light induces conformational change in the LOV photoreceptor, relieving and exposing the previously concealed signaling domain to interact with its partners (**Figure A1.1B**). RGS serves as the signaling domain or effector in this design. If engineered successfully, this design can serve as an alternative option to our original opto-RGS2. Under this chapter, we will discuss this alternative LOV-RGS design and its light-inducible function for calcium inhibition.

One challenge that comes with engineering optogenetic tools using light-switchable strategy is designing proper LOV-effector interface for light-induced release of the effector. LOV is usually consisted of a PAS domain and a J_{α}-helix that links the

PAS domain to its effector. In the dark state, the effector is held close to the PAS domain through a few interaction sites which are altered in the lit-state, resulting in the release of the effector. These interacting surfaces of the PAS domain and the effector are responsible for the light-switchable property. To date, generalized principle of which residues accounted for the property has not been identified; they have to be evaluated empirically for each effector including RGS. As this approach of engineering can be inefficient and laborious, instead of engineering LOV-RGS from the ground up, we rationally modified functional LOV-RGS proteins, BcRGS5, found naturally in a species of fungus.

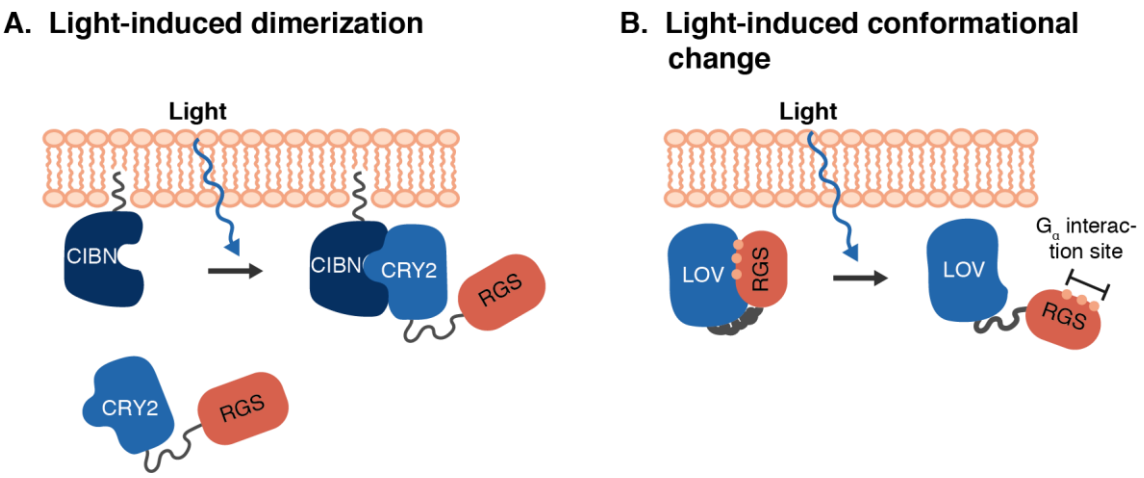

Figure A.1. Two strategies for creating optogenetic RGS.

(A) Light-induced dimerization photoreceptor brings RGS to a specific subcellular localization where it can interact with G_α proteins.
(B) Light-induced conformational change in photoreceptor relieves the RGS domain and, in turn, free the hidden G_α interaction site to engage G_α proteins.

A1.2 Results and Discussion

To modify the BcRGS5 to interface with human Gaq pathway similar to human RGS2 (hRGS2), we can either (i) replace the BcRGS5 residues responsible for G_α interaction with the hRGS2 amino acid sequence (Figure A.1A) or (ii) replace the entire RGS domain within the BcRGS5 with hRGS2 (Figure A.1B). We employed both approaches to create four variants of BcRGS5-hRGS2 chimera (Figure A.1C).

Variant 1 was created using the first mutation approach. The mutation sites were identified by aligning BcRGS5 amino acid sequence with the reference hRGS2 and hRGS4. The crystal structures and the G_α interacting sites for these two human RGSs have already been identified. We, therefore, mutated the discrepancy residues within the sites to those of hRGS2 (Figure A.1C.ii). Variant 2-4 were constructed using the second approach of domain swapping. To maintain or minimally disturb the BcRGS5 function, the hRGS2 has to be swapped in such that it preserves the original secondary structure of the BcRGS5. As BcRGS5 is newly discovered and the crystal structure is not yet resolved, we used protein bioinformatics tools including JPred, Phyre2, and ExPASy to predict the BcRGS5 secondary structure. Based on the computational predictions, three variants were made to conserve the alpha-helix structure at the N- and C-terminal ends of the fungal RGS (Figure A.1C.iii-v). Additional GS-rich linker was added between hRGS2 and LOV domain of variant 3 in order to maintain consistent spacing.

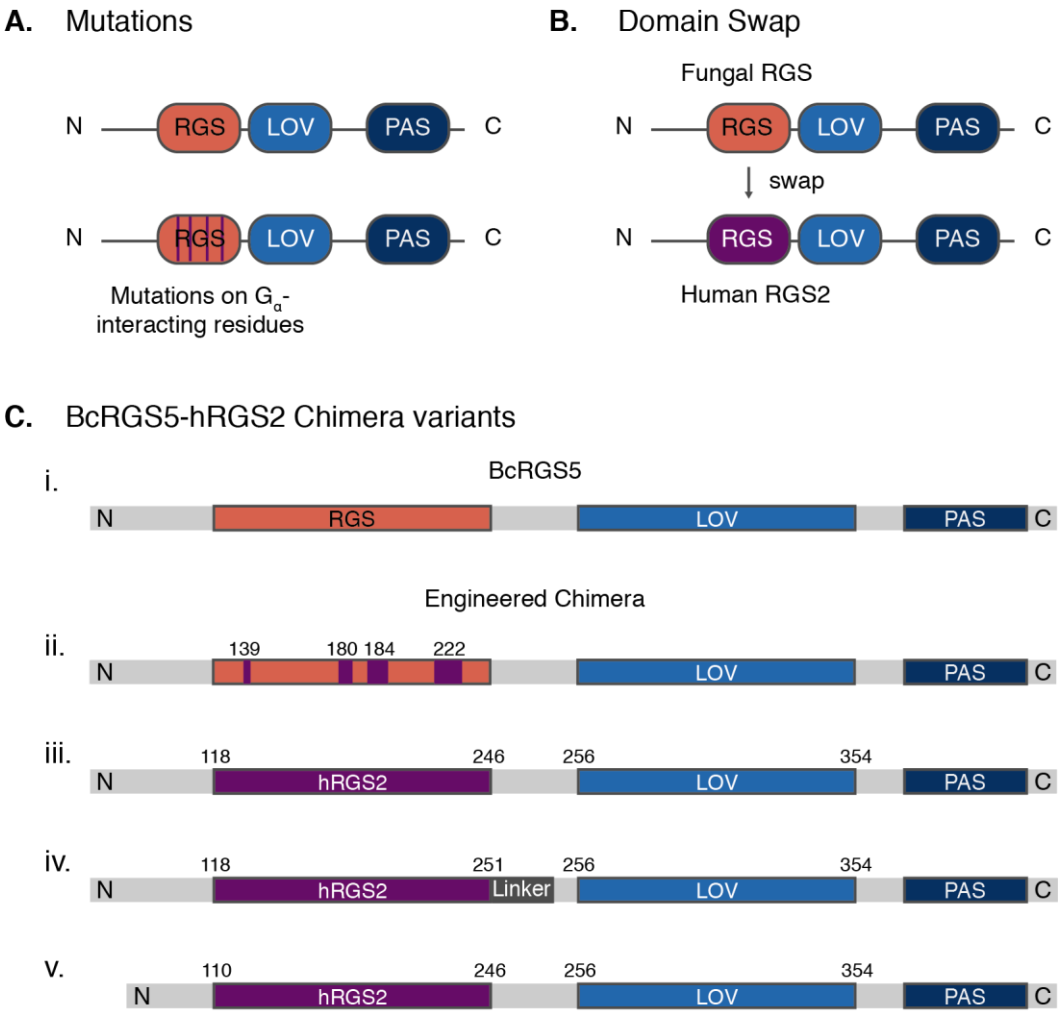

Figure A.2. Construction of BcRGS5-hRGS2 chimeras.

(A-B) Strategies for creating BcRGS5-hRGS2 chimeras: (A) G_α-interacting site mutations and (B) domain swapping.
(C) Four different variants of BcRGS5-hRGS2 chimera in comparison to the original BcRGS5. (i) BcRGS5 (ii) Variant 1, created by the mutation strategy described in (A). (iii-v) Variant 2-4, created by the domain swapping strategy described in (B).

We next sought to evaluate the light-induced GTPase-activating protein (GAP) function of the chimeras. HeLa cells transiently expressing the chimera variants were evoked with 100uM histamine, and, using a red calcium indicator X-Rhod-1, the calcium signaling in the light and dark were assessed compared to the native hRGS2. hRGS2 completely inhibited agonist-evoked calcium signals (**Figure A.3A**). Compared to the wild-type (WT) population, the calcium amplitude in the hRGS2 expressing cells was suppressed by the cohen's d effect size of 0.67. BcRGS5 and chimera variant 1 slightly suppressed the calcium amplitude in the dark-state in relative to the WT, but showed no further suppression in the lit-state (**Figure A.3B-C**). Chimera variant 2 exhibited minimal suppression in the dark, while enhanced suppression upon exposure to light (**Figure A.3D**). However, the signal amplitude difference between the lit- and dark-state is of minimal effect size (d = 0.17). Chimera variant 3 and 4 both completely inhibited the signal in the dark- and lit-state (**Figure A.3E-F**).

Among all the variants, chimera variant 2 is the only version that showed light-inducible calcium suppression activity. The calcium signal analysis suggested that BcRGS5 was unable to engage and exert GAP activity of the human $G_{\alpha q}$ proteins. Mutations on the predicted G_{α} interacting residues were not sufficient for gaining ability to human $G_{\alpha q}$ engagement. On the other hand, replacing the fungal RGS domain with the hRGS2 appeared to be a more effective strategy. Variant 2 exhibited some shift in the calcium inhibition activity between light and dark. Though the dynamic range, as measured by the cohen's d effect size, is relatively small compared to the inhibition observed in native hRGS2. Slightly shifting the hRGS2 replacement position in BcRGS5 appeared to break the light switchability. As observed in variant 3 and 4, sliding the hRGS2 position a few residues downstream or upstream of the variant 2 hRGS2 location

disrupted the folding and its interaction with the LOV domain, causing the hRGS2 to be exposed and free to target the G_{α} proteins even prior to light exposure.

Dynamic range is important for optogentic tools, particularly optogenetic RGS. A light-inducible RGS with minimal GAP activity in the dark and large activity contrast in the light is highly preferable. BcRGS5-hRGS2 variant 2 is the only variant that exhibited increased in GAP activity in the lit-state. Its dynamic range is nonetheless fairly small, which may not be sufficiently robust for noisy applications such as calcium encoding. Given the better dynamic range of cryptochrome-based opto-RGS2 described in chapter 3, we decided to move forward with the opto-RGS2 instead of the BcRGS5-hRGS2 chimera system.

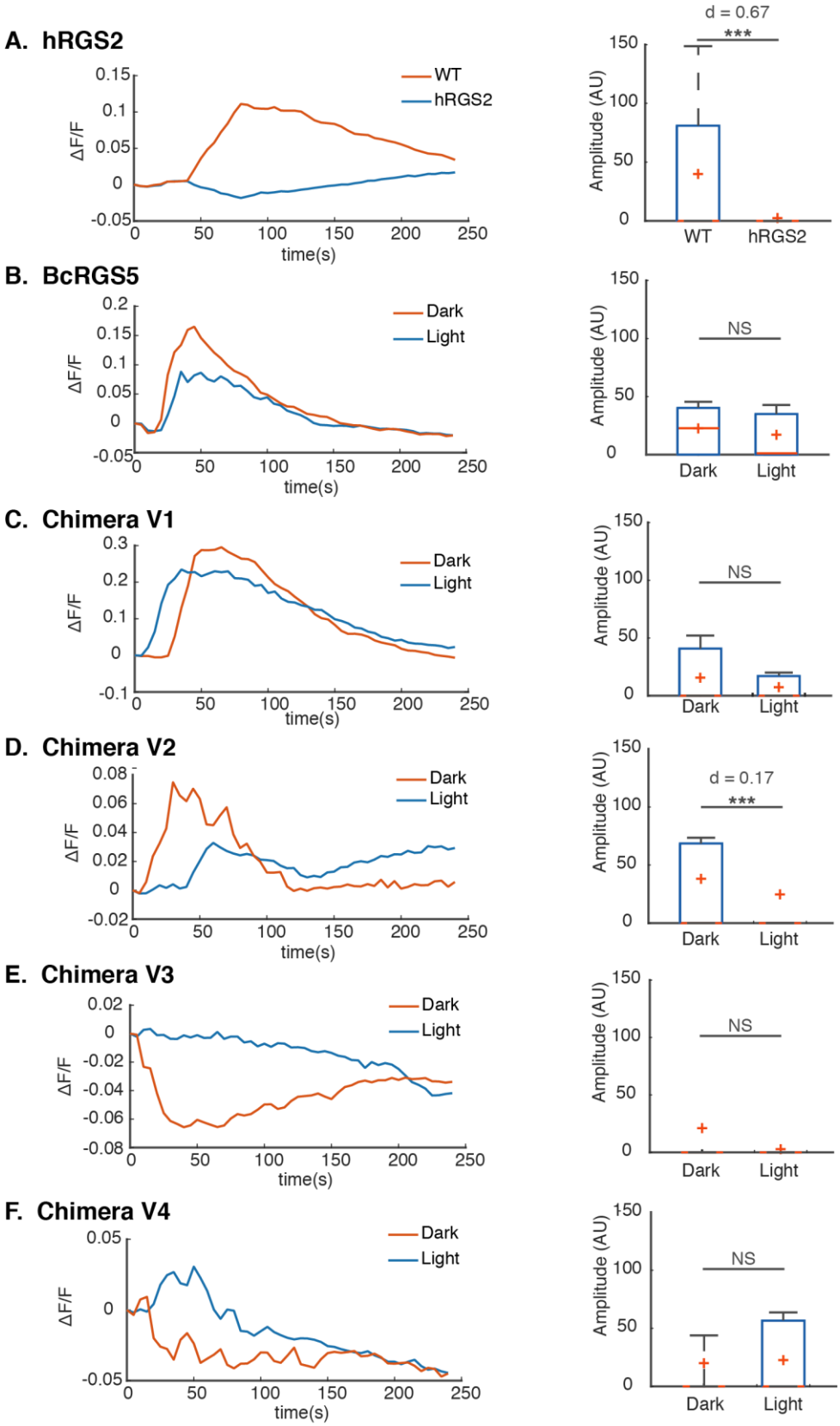
A. hRGS2
WT
hRGS2
ΔF/F
time(s)
d = 0.67
***
Amplitude (AU)
WT
hRGS2
B. BcRGS5
Dark
Light
NS
C. Chimera V1
D. Chimera V2
d = 0.17
E. Chimera V3
F. Chimera V4

A1.3 Conclusions

We sought to create an alternative single-component optogenetic RGS2 tool using a light-induced conformational change based strategy. Using natural fungal BcRGS5 as a scaffold, four versions of BcRGS5-hRGS2 chimeras were constructed to allow engagement of the RGS to the human $G_{\alpha q}$ proteins. One of the variants (variant 2) showed some extent of light-inducible $G_{\alpha q}$-mediated calcium inhibition. Its dynamic range is, however, relatively small compared to the cryptochrome-based opto-RGS2. As a result, we discontinued our further development on the chimera and rather focused on the cryptochrome-based opto-RGS2.

Figure A.3. Histamine-evoked calcium signaling in HeLa cells expressing native hRGS2 and engineered RGS chimeras.

Histamine-induced calcium signals observed in HeLa cells transiently expressing (A) hRGS2 (B) BcRGS5 (C) Chimera variant 1 (D) Chimera variant 2 (E) Chimera variant 3 (F) Chimera variant 4. The left panel shows mean calcium signal traces averaged over > 30 cells, represented by change in fluorescence signal of calcium indicator X-Rhod-1 (ΔF/F). The right panel shows raw signal amplitude of the corresponding calcium signals on the left. (unpaired t-test, ** = p-value < 0.01, *** = p-value < 0.001, NS = not siginificant), d denotes Cohen's d effect size.

BIBLIOGRAPHY

1. E. M. Adler, Using Light to Increase cAMP. *Sci. Signal.* **4**, ec17 (2011).

2. R. D. Airan, K. R. Thompson, L. E. Fenno, H. Bernstein, K. Deisseroth, Temporally precise in vivo control of intracellular signalling. *Nature*. **458**, 1025–9 (2009).

3. J. Akerboom *et al.*, Genetically encoded calcium indicators for multi-color neural activity imaging and combination with optogenetics. *Front. Mol. Neurosci.* **6**, 1–29 (2013).

4. A. Atri, J. Amundson, D. Clapham, J. Sneyd, A Single-Pool Model for Intracellular Calcium Oscillations and Waves in the Xenopus laevis Oocyte. *Biophys. J. Vol.* **65**, 1727–1739 (1993).

5. W. Bacchus, M. Fussenegger, The use of light for engineered control and reprogramming of cellular functions. *Curr. Opin. Biotechnol.* **23**, 695–702 (2012).

6. H. J. Bailes, L.-Y. Zhuang, R. J. Lucas, Reproducible and Sustained Regulation of Gαs Signalling Using a Metazoan Opsin as an Optogenetic Tool. *PLoS One*. **7**, e30774 (2012).

7. M. Behar, A. Hoffmann, Understanding the temporal codes of intra-cellular signals. *Curr. Opin. Genet. Dev.* **20**, 684–93 (2010).

8. M. L. Bernhardt *et al.*, Regulator of G-protein signaling 2 (RGS2) suppresses premature calcium release in mouse eggs. *Development*. **142**, 2633–2640 (2015).

9. L. S. Bernstein *et al.*, RGS2 binds directly and selectively to the M1 muscarinic acetylcholine receptor third intracellular loop to modulate Gq/11alpha signaling. *J. Biol. Chem.* **279**, 21248–21256 (2004).

10. J. Berridge, Calcium Oscillations. *J. Biol. Chem.* **265**, 9583–9566 (1990).

11. M. J. Berridge, Remodelling Ca2+ signalling systems and cardiac hypertrophy. *Biochem. Soc. Trans.* **34**, 228–31 (2006).

12. M. Berridge, Heirarchical Calcium signaling system in HeLa cells. *J. Physiol.* **499**, 307–314 (1997).

13. M. J. Berridge, Spatial and Temporal Aspects of Signalling. *Cell Signal. Biol.*, 1–49 (2009).

14. M. J. Berridge, M. D. Bootman, H. L. Roderick, Calcium signalling: dynamics, homeostasis and remodelling. *Nat. Rev. Mol. Cell Biol.* **4**, 517–29 (2003).

15. M. Berridge, P. Lipp, M. Bootman, The versatility and universality of calcium signaling. *Nat. Rev. Mol. Cell Biol.* **1**, 11–21 (2000).

16. llya Bezprozvanny, J. Watras, B. E. Ehrlich, Bell-shaped calcium-response

curves of Ins(l,4,5)P3- and calcium-gated channels from endoplasmic reticulum of cerebellum. *Nature*. **351**, 751–754 (1991).

17. H. Bito, K. Deisseroth, R. W. Tsien, CREB phosphorylation and dephosphorylation: A Ca2+- and stimulus duration-dependent switch for hippocampal gene expression. *Cell*. **87**, 1203–1214 (1996).

18. H. Bito, K. Deisseroth, R. W. Tsien, Ca2+-dependent regulation in neuronal gene expression. *Curr. Opin. Neurobiol.* **7**, 419–429 (1997).

19. M. Blonska, X. Lin, NF- κ B signaling pathways regulated by CARMA family of scaffold proteins. *Nat. Publ. Gr.* **21**, 55–70 (2010).

20. M. D. Bootman, M. J. Berridge, P. Lipp, Cooking with calcium: the recipes for composing global signals from elementary events. *Cell*. **91**, 367–73 (1997).

21. O. Brandman, T. Meyer, Feedback loops shape cellular signals in space and time. *Science*. **322**, 390–5 (2008).

22. L. J. Bugaj, A. T. Choksi, C. K. Mesuda, R. S. Kane, D. V Schaffer, Optogenetic protein clustering and signaling activation in mammalian cells. *Nat. Methods*. **10**, 249–52 (2013).

23. L. Cai, C. K. Dalal, M. B. Elowitz, Frequency-modulated nuclear localization bursts coordinate gene regulation. *Nature*. **455**, 485–90 (2008).

24. E. Carafoli, L. Santella, D. Branca, M. Brini, Generation, control, and processing of cellular calcium signals. *Crit. Rev. Biochem. Mol. Biol.* **36**, 107–260 (2001).

25. L.-F. Chen, W. C. Greene, Shaping the nuclear action of NF-kappaB. *Nat. Rev. Mol. Cell Biol.* **5**, 392–401 (2004).

26. X. Chen, J. L. Zaro, W. C. Shen, Fusion protein linkers: Property, design and functionality. *Adv. Drug Deliv. Rev.* **65**, 1357–1369 (2013).

27. R. Cheong, A. Hoffmann, A. Levchenko, Understanding NF-kappaB signaling via mathematical modeling. *Mol. Syst. Biol.* **4**, 192 (2008).

28. D. E. Clapham, Calcium Signaling. *Cell*. **131**, 1047–1058 (2007).

29. M. Colella *et al.*, Ca2+ oscillation frequency decoding in cardiac cell hypertrophy: role of calcineurin/NFAT as Ca2+ signal integrators. *Proc. Natl. Acad. Sci. U. S. A.* **105**, 2859–64 (2008).

30. L. Combettes *et al.*, Rapid filtration studies of the effect of cytosolic Ca2+ on inositol 1,4,5-trisphosphate-induced Ca2+ release from cerebellar microsomes. *J. Biol. Chem.* **269**, 17561–71 (1994).

31. M. T. Cooling, P. Hunter, E. J. Crampin, Sensitivity of NFAT cycling to cytosolic calcium concentration: implications for hypertrophic signals in cardiac myocytes. *Biophys. J.* **96**, 2095–104 (2009).

32. S. J. Coultrap, K. U. Bayer, CaMKII regulation in information processing and storage. *Trends Neurosci.* **35**, 607–18 (2012).

33. G. R. Crabtree, E. N. Olson, NFAT signaling: choreographing the social lives of cells. *Cell*. **109 Suppl**, S67-79 (2002).

34. K. S. Cuthbertson, T. R. Chay, Modelling receptor-controlled intracellular calcium oscillators. *Cell Calcium*. **12**, 97–109 (1991).

35. G. W. De, Y. And, J. Keizer, A single-pool inositol 1,4,5-trisphosphate-receptor-based model for agonist-stimulated oscillations in Ca2+ concentration. *Biophysics (Oxf).* **89**, 9895–9899 (1992).

36. H. Deng, A. A. Gerencser, H. Jasper, Signal integration by Ca 2+ regulates intestinal stem-cell activity. *Nature*. **528**, 212–217 (2015).

37. R. E. Dolmetsch, K. Xu, R. S. Lewis, Calcium oscillations increase the efficiency and specificity of gene expression. *Nature*. **392**, 933–6 (1998).

38. R. Dolmetsch, R. Lewis, C. Goodnow, J. Healy, Differential activation of transcription factors induced by Ca2+ response amplitude and duration. *Nature*. **386**, 855–858 (1997).

39. B. Domon, R. Aebersold, Mass spectrometry and protein analysis. *Science*. **312**, 212–7 (2006).

40. G. Dupont, S. Swillens, Quantal release, incremental detection, and long-period Ca2+ oscillations in a model based on regulatory Ca2+-binding sites along the permeation pathway. *Biophys. J.* **71**, 1714–1722 (1996).

41. G. Dupont, A. Abou-Lovergne, L. Combettes, Stochastic aspects of oscillatory Ca2+ dynamics in hepatocytes. *Biophys. J.* **95**, 2193–202 (2008).

42. G. Dupont, L. Combettes, G. S. Bird, J. W. Putney, Calcium oscillations. *Cold Spring Harb. Perspect. Biol.* **3**, 1–18 (2011).

43. G. Dupont, C. Erneux, Simulations of the effects of inositol and activities on Ca * + oscillations. **22**, 321–331 (1997).

44. E. Fabbri *et al.*, α2 Neurosci Biobehav Rev adrenergic receptor dysregulation in depressive disorders: implications for the neurobiology of depression and antidepressant therapy. *Glia*. **17**, 14997–15002 (2010).

45. M. Falcke, On the role of stochastic channel behavior in intracellular Ca2+ dynamics. *Biophys. J.* **84**, 42–56 (2003).

46. E. A. Finch, T. J. Turner, S. M. Goldin, Calcium as a coagonist of inositol 1,4,5-trisphosphate-induced calcium release. *Science*. **252**, 443–6 (1991).

47. W. G. Fisher, P.-C. Yang, R. K. Medikonduri, M. S. Jafri, NFAT and NFkappaB activation in T lymphocytes: a model of differential activation of gene expression. *Ann. Biomed. Eng.* **34**, 1712–28 (2006).

48. J. K. Foskett, C. White, K.-H. Cheung, D.-O. D. Mak, Inositol trisphosphate receptor Ca2+ release channels. *Physiol. Rev.* **87**, 593–658 (2007).

49. D. Fraiman, B. Pando, S. Dargan, I. Parker, S. P. Dawson, Analysis of Puff Dynamics in Oocytes: Interdependence of Puff Amplitude and Interpuff Interval. *Biophys. J.* **90**, 3897–3907 (2006).

50. N. Fukuda, T. Matsuda, T. Nagai, Optical control of the Ca2+ concentration in a live specimen with a genetically encoded Ca2+-releasing molecular tool. *ACS Chem. Biol.* **9**, 1197–1203 (2014).

51. A. Ghosh, M. Greenberg, Calcium signaling in neurons: molecular mechanisms and cellular consequences. *Science.* **268**, 239–247 (1995).

52. a Goldbeter, G. Dupont, M. J. Berridge, Minimal model for signal-induced Ca2+ oscillations and for their frequency encoding through protein phosphorylation. *Proc. Natl. Acad. Sci. U. S. A.* **87**, 1461–5 (1990).

53. A. Goldbeter, Computational approaches to cellular rhythms. *Nature*. **420**, 238–45 (2002).

54. X. Gu, N. Spitzer, Distinct aspects of neuronal differentiation encoded by frequency of spontaneous Ca2+ transients. *Nature*. **375**, 784–787 (1995).

55. G. Guntas *et al.*, Engineering an improved light-induced dimer (iLID) for controlling the localization and activity of signaling proteins. *Proc. Natl. Acad. Sci.* **112**, 112–117 (2015).

56. P. Gurung, J. R. Lukens, T. Kanneganti, Correlating in vitro and in vivo Activities of Light Inducible Dimers: a Cellular Optogenetics Guide. **21**, 193–201 (2016).

57. M. W. Hankins, S. N. Peirson, R. G. Foster, Melanopsin: an exciting photopigment. *Trends Neurosci.* **31**, 27–36 (2008).

58. P. Hannanta-Anan, B. Y. Chow, Optogenetic Control of Calcium Oscillation Waveform Defines NFAT as an Integrator of Calcium Load. *Cell Syst.* **2**, 283–288 (2016).

59. L. He *et al.*, Near-infrared photoactivatable control of Ca2+signaling and optogenetic immunomodulation. *Elife*. **4**, 1–25 (2015).

60. J. R. Hepler, Emerging roles for RGS proteins in cell signalling. *Trends Pharmacol. Sci.* **20**, 376–382 (1999).

61. S. P. Heximer, H. Lim, J. L. Bernard, K. J. Blumer, Mechanisms governing subcellular localization and function of human RGS2. *J. Biol. Chem.* **276**, 14195–14203 (2001).

62. S. P. Heximer, N. Watson, M. E. Linder, K. J. Blumer, J. R. Hepler, RGS2/G0S8 is a selective inhibitor of Gqalpha function. *Proc. Natl. Acad. Sci. U. S. A.* **94**, 14389–93 (1997).

63. S. P. Heximer *et al.*, G protein selectivity is a determinant of RGS2 function. *J. Biol. Chem.* **274**, 34253–34259 (1999).

64. a Hoffmann, G. Natoli, G. Ghosh, Transcriptional regulation via the NF-kappaB signaling module. *Oncogene*. **25**, 6706–16 (2006).

65. A. Hoffmann, A. Levchenko, M. L. Scott, D. Baltimore, The IkappaB-NF-kappaB signaling module: temporal control and selective gene activation. *Science*. **298**, 1241–5 (2002).

66. P. G. Hogan, L. Chen, J. Nardone, A. Rao, Transcriptional regulation by calcium, calcineurin, and NFAT. *Genes Dev.* **17**, 2205–32 (2003).

67. V. Horsley, A. O. Aliprantis, L. Polak, L. H. Glimcher, E. Fuchs, NFATc1 Balances Quiescence and Proliferation of Skin Stem Cells. *Cell*. **132**, 299–310 (2008).

68. T. Ingi *et al.*, Dynamic regulation of RGS2 suggests a novel mechanism in G-protein signaling and neuronal plasticity. *J. Neurosci.* **18**, 7178–88 (1998).

69. M. Ishii, S. Fujita, M. Yamada, Y. Hosaka, Y. Kurachi, Phosphatidylinositol 3,4,5-trisphosphate and Ca2+/calmodulin competitively bind to the regulators of G-protein-signalling (RGS) domain of RGS4 and reciprocally regulate its action. *Biochem J*. **385**, 65–73 (2005).

70. M. Ishii, A. Inanobe, Y. Kurachi, PIP3 inhibition of RGS protein and its reversal by Ca2+/calmodulin mediate voltage-dependent control of the G protein cycle in a cardiac K+ channel. *Proc Natl Acad Sci U S A*. **99**, 4325–4330 (2002).

71. M. Ishii, Y. Kurachi, Assays of RGS protein modulation by phosphatidylinositides and calmodulin. *Methods Enzymol.* **389**, 105–118 (2004).

72. T. Ishii *et al.*, Light generation of intracellular Ca(2+) signals by a genetically encoded protein BACCS. *Nat. Commun.* **6**, 8021 (2015).

73. R. Jacob, Calcium oscillations in electrically non-excitable cells. *Biochim. Biophys. Acta*. **1052**, 427–438 (1990).

74. A. A. Kaberniuk, A. A. Shemetov, V. V Verkhusha, A bacterial phytochrome-based optogenetic system controllable with near-infrared light. *Nat. Methods*. **13**, 591–597 (2016).

75. J. Kach, N. Sethakorn, N. O. Dulin, A finer tuning of G-protein signaling through regulated control of RGS proteins. *AJP Hear. Circ. Physiol.* **303**, H19–H35 (2012).

76. A. Kalo, Y. Shav-Tal, Acting on impulse: dissecting the dynamics of the NFAT transcriptional response. *Genome Biol.* **14**, 102 (2013).

77. P. Kar, C. Nelson, A. B. Parekh, CRAC channels drive digital activation and provide analog control and synergy to Ca(2+)-dependent gene regulation. *Curr. Biol.* **22**, 242–7 (2012).

78. P. Kar, A. B. Parekh, Distinct Spatial Ca^{2+} Signatures Selectively Activate

Different NFAT Transcription Factor Isoforms. *Mol. Cell*. **58**, 232–243 (2015).

79. W. K. A. Karunarathne, P. R. O'Neill, N. Gautam, Subcellular optogenetics - controlling signaling and single-cell behavior. *J. Cell Sci.* **128**, 15–25 (2015).

80. K. Kaur, J. M. Kehrl, R. A. Charbeneau, R. R. Neubig, RGS-insensitive Gα subunits: Probes of gα subtype-selective signaling and physiological functions of RGS proteins. *Methods Mol. Biol.* **756**, 75–98 (2011).

81. F. Kawano, H. Suzuki, A. Furuya, M. Sato, Engineered pairs of distinct photoswitches for optogenetic control of cellular proteins. *Nat. Commun.* **6**, 6256 (2015).

82. J. H. Kehrl, S. Sinnarajah, RGS2: A multifunctional regulator of G-protein signaling. *Int. J. Biochem. Cell Biol.* **34**, 432–438 (2002).

83. M. J. Kennedy *et al.*, Rapid blue-light-mediated induction of protein interactions in living cells. *Nat. Methods*. **7**, 973–5 (2010).

84. B. N. Kholodenko, J. F. Hancock, W. Kolch, Signalling ballet in space and time. *Nat. Rev. Mol. Cell Biol.* **11**, 414–26 (2010).

85. A. J. Kimple *et al.*, Structural determinants of G-protein alpha subunit selectivity by regulator of G-protein signaling 2 (RGS2). *J. Biol. Chem.* **284**, 19402–19411 (2009).

86. A. J. Kimple, D. E. Bosch, P. M. Giguere, D. P. Siderovski, Regulators of G-Protein Signaling and Their G alpha Substrates: Promises and Challenges in Their Use as Drug Discovery Targets. *Pharmacol. Rev.* **63**, 728–749 (2011).

87. S. Kleinlogel *et al.*, Ultra light-sensitive and fast neuronal activation with the Ca^2+-permeable channelrhodopsin CatCh. *Nat. Neurosci.* **14**, 513–8 (2011).

88. P. De Koninck, Sensitivity of CaM Kinase II to the Frequency of Ca2+ Oscillations. *Science.* **279**, 227–230 (1998).

89. S. Krishna, M. H. Jensen, K. Sneppen, Minimal model of spiky oscillations in NF-kappaB signaling. *Proc. Natl. Acad. Sci. U. S. A.* **103**, 10840–10845 (2006).

90. T. Kumbalasiri, M. D. Rollag, M. C. Isoldi, a M. D. L. Castrucci, I. Provencio, Melanopsin triggers the release of internal calcium stores in response to light. *Photochem. Photobiol.* **83**, 273–9 (2007).

91. T. Kyung *et al.*, Optogenetic control of endogenous Ca(2+) channels in vivo. *Nat. Biotechnol.* **33**, 1092–6 (2015).

92. J. H. Levine, Functional Roles of Pulsing. *Science.* **342**, 1193–1200 (2013).

93. A. Levskaya, O. D. Weiner, W. a Lim, C. a Voigt, Spatiotemporal control of cell signalling using a light-switchable protein interaction. *Nature*. **461**, 997–1001 (2009).

94. R. S. Lewis, Calcium signaling mechanisms in T lymphocytes. *Annu. Rev. Immunol.* **19**, 497–521 (2001).

95. X. Li *et al.*, Arabidopsis cryptochrome 2 (CRY2) functions by the photoactivation mechanism distinct from the tryptophan (trp) triad-dependent photoreduction. *Proc. Natl. Acad. Sci. U. S. A.* **108**, 20844–9 (2011).

96. Y.-X. Li, J. Rinzel, Equations for InsP3 Receptor-mediated [Ca2+]i Oscillations Derived from a Detailed Kinetic Model: A Hodgkin-Huxley Like Formalism. *J. Theor. Biol.* **166**, 461–473 (1994).

97. Z. Li *et al.*, Graded activation of CRAC channel by binding of different numbers of STIM1 to Orai1 subunits. *Cell Res.* **21**, 305–15 (2011).

98. Y. Lin, C. H. Sohn, C. K. Dalal, L. Cai, M. B. Elowitz, Combinatorial gene regulation by modulation of relative pulse timing. *Nature*. **527**, 54–58 (2015).

99. J. Liou, M. Fivaz, T. Inoue, T. Meyer, Live-cell imaging reveals sequential oligomerization and local plasma membrane targeting of stromal interaction molecule 1 after Ca2+ store depletion. *Proc. Natl. Acad. Sci. U. S. A.* **104**, 9301–6 (2007).

100. H. Liu *et al.*, Photoexcited CRY2 interacts with CIB1 to regulate transcription and floral initiation in Arabidopsis. *Science.* **322**, 1535–1539 (2008).

101. X. Luo, S. Popov, a K. Bera, T. M. Wilkie, S. Muallem, RGS proteins provide biochemical control of agonist-evoked [Ca2+]i oscillations. *Mol. Cell*. **7**, 651–60 (2001).

102. G. Ma *et al.*, Optogenetic toolkit for precise control of calcium signaling. *Cell Calcium*. **64**, 36–46 (2017).

103. F. Macian, NFAT proteins: key regulators of T-cell development and function. *Nat. Rev. Immunol.* **5**, 472–84 (2005).

104. M. Mancini, A. Toker, NFAT proteins: emerging roles in cancer progression. *Nat. Rev. Cancer*. **9**, 810–20 (2009).

105. P. Marambaud, U. Dreses-Werringloer, V. Vingtdeux, Calcium signaling in neurodegeneration. *Mol. Neurodegener.* **4**, 20 (2009).

106. B. Mayr, M. Montminy, Transcriptional regulation by the phosphorylation-dependent factor CREB. *Nat. Rev. Mol. Cell Biol.* **2**, 599–609 (2001).

107. C. R. McCudden, M. D. Hains, R. J. Kimple, D. P. Siderovski, F. S. Willard, G-protein signaling: Back to the future. *Cell. Mol. Life Sci.* **62**, 551–577 (2005).

108. Z. Melyan, E. E. Tarttelin, J. Bellingham, R. J. Lucas, M. W. Hankins, Addition of human melanopsin renders mammalian cells photoresponsive. *Nature*. **433**, 741–5 (2005).

109. T. Meyer, L. Stryer, Molecular model for receptor-stimulated calcium spiking.

Biochemistry. **85**, 5051–5055 (1988).

110. S. Monticelli, A. Rao, NFAT1 and NFAT2 are positive regulators of IL-4 gene transcription. *Eur. J. Immunol.* **32**, 2971–2978 (2002).

111. T. S. Moon, C. Lou, A. Tamsir, B. C. Stanton, C. a Voigt, Genetic programs constructed from layered logic gates in single cells. *Nature*. **491**, 249–53 (2012).

112. M. R. Nance *et al.*, Structural and functional analysis of the regulator of G protein signaling 2-Gαq complex. *Structure*. **21**, 438–448 (2013).

113. D. E. Nelson *et al.*, Oscillations in NF-kappaB signaling control the dynamics of gene expression. *Science*. **306**, 704–8 (2004).

114. R. R. Neubig, D. P. Siderovski, Regulators of G-protein signalling as new central nervous system drug targets. *Nat. Rev. Drug Discov.* **1**, 187–97 (2002).

115. T. Nguyen, S. Di Giovanni, NFAT signaling in neural development and axon growth. *Int. J. Dev. Neurosci.* **26**, 141–145 (2008).

116. C. P. O'Banion *et al.*, Design and Profiling of a Subcellular Targeted Optogenetic cAMP-Dependent Protein Kinase. *Cell Chem. Biol.* **25**, 100–109.e8 (2018).

117. P. R. O'Neill, N. Gautam, Optimizing optogenetic constructs for control over signaling and cell behaviours. *Photochem. Photobiol. Sci.* **14**, 1578–85 (2015).

118. P. R. O'Neill, N. Gautam, Subcellular optogenetic inhibition of G proteins generates signaling gradients and cell migration. *Mol. Biol. Cell*. **25**, 2305–14 (2014).

119. E. Oancea, T. Meyer, Protein kinase C as a molecular machine for decoding calcium and diacylglycerol signals. *Cell*. **95**, 307–18 (1998).

120. S. Panda *et al.*, Illumination of the melanopsin signaling pathway. *Science*. **307**, 600–4 (2005).

121. A. B. Parekh, Decoding cytosolic Ca2+ oscillations. *Trends Biochem. Sci.* **36**, 78–87 (2011).

122. A. B. Parekh, J. W. P. Jr, Store-Operated Calcium Channels. *Physiol. Rev.* **85**, 757–810 (2005).

123. M. Perc, A. K. Green, C. J. Dixon, M. Marhl, Establishing the stochastic nature of intracellular calcium oscillations from experimental data. *Biophys. Chem.* **132**, 33–38 (2008).

124. N. D. Perkins, Post-translational modifications regulating the activity and function of the nuclear factor kappa B pathway. *Oncogene*. **25**, 6717–30 (2006).

125. E. Pham, E. Mills, K. Truong, A synthetic photoactivated protein to generate local or global Ca(2+) signals. *Chem. Biol.* **18**, 880–90 (2011).

126. A. Politi, L. D. Gaspers, A. P. Thomas, T. Höfer, Models of IP3 and Ca2+ oscillations: frequency encoding and identification of underlying feedbacks. *Biophys. J.* **90**, 3120–33 (2006).

127. S. G. Popov, U. Murali Krishna, J. R. Falck, T. M. Wilkie, Ca2+/calmodulin reverses phosphatidylinositol 3,4,5-trisphosphate- dependent inhibition of regulators of G protein-signaling GTPase-activating protein activity. *J. Biol. Chem.* **275**, 18962–18968 (2000).

128. J. E. Purvis, G. Lahav, Review Encoding and Decoding Cellular Information through Signaling Dynamics. *Cell*, 945–956 (2013).

129. X. Qiu *et al.*, Induction of photosensitivity by heterologous expression of melanopsin. *Nature*. **433**, 745–9 (2005).

130. D. Renard, J. Poggioli, B. Berthon, M. Claret, How far does phospholipase C activity depend on the cell calcium concentration? A study in intact cells. *Biochem. J.* **243**, 391–8 (1987).

131. M. Rollag, Opsins : Not Just for Eyes Online. **339** (2013).

132. D. L. Roman *et al.*, Identification of small-molecule inhibitors of RGS4 using a high-throughput flow cytometry protein interaction assay. *Mol. Pharmacol.* **71**, 169–175 (2007).

133. S. Rüdiger, Stochastic models of intracellular calcium signals. *Phys. Rep.* **534** (2014), pp. 39–87.

134. K. Saito *et al.*, Luminescent proteins for high-speed single-cell and whole-body imaging. *Nat. Commun.* **3**, 1262 (2012).

135. C. Salazar, A. Z. Politi, T. Hofer, Decoding of calcium oscillations by phosphorylation cycles: analytic results. *Biophys J*. **94**, 1203–1215 (2008).

136. C. Salazar, T. Höfer, Allosteric Regulation of the Transcription Factor NFAT1 by Multiple Phosphorylation Sites: A Mathematical Analysis. *J. Mol. Biol.* **327**, 31–45 (2003).

137. J. J. Saucerman, D. M. Bers, Calmodulin mediates differential sensitivity of CaMKII and calcineurin to local Ca2+ in cardiac myocytes. *Biophys. J.* **95**, 4597–612 (2008).

138. M. Savignac, R. Gomez-villafuertes, J. R. Naranjo, C. N. De Biotecnologı, Ca 2+ - Operated Transcriptional Networks : Molecular Mechanisms and In Vivo Models. *Physiol. Rev.* **88**, 421–449 (2008).

139. C. Schaab, T. Geiger, G. Stoehr, J. Cox, M. Mann, Analysis of High Accuracy, Quantitative Proteomics Data in the MaxQB Database. *Mol. Cell. Proteomics*. **11**, M111.014068 (2012).

140. A. M. Scharenberg, L. a Humphries, D. J. Rawlings, Calcium signalling and cell-fate choice in B cells. *Nat. Rev. Immunol.* **7**, 778–89 (2007).

141. S. Schuster, M. Marhl, T. Höfer, Modelling of simple and complex calcium oscillations. From single-cell responses to intercellular signalling. *Eur. J. Biochem.* **269**, 1333–55 (2002).

142. J. Selimkhanov *et al.*, Accurate information transmission through dynamic biochemical signaling networks. *Science*. **346**, 1370–3 (2014).

143. A. J. Shaywitz, M. E. Greenberg, CREB: A Stimulus-Induced Transcription Factor Activated by A Diverse Array of Extracellular Signals. *Annu. Rev. Biochem.* **68**, 821–861 (1999).

144. Y. Shichida, W. L. Davies, M. W. Hankins, R. G. Foster, Photosensitive retinal pigments Vertebrate ancient opsin and melanopsin : divergent irradiance detectors †. *Photochem. Photobiol. Sci.* **9**, 1444–1457 (2010).

145. Y. Shichida, T. Matsuyama, Evolution of opsins and phototransduction. *Philos. Trans. R. Soc. Lond. B. Biol. Sci.* **364**, 2881–95 (2009).

146. S.-Y. Shin, H. W. Yang, J.-R. Kim, W. Do Heo, K.-H. Cho, A hidden incoherent switch regulates RCAN1 in the calcineurin-NFAT signaling network. *J. Cell Sci.* **124**, 82–90 (2011).

147. B. Sjögren, R. R. Neubig, Thinking outside of the “RGS box”: new approaches to therapeutic targeting of regulators of G protein signaling. *Mol. Pharmacol.* **78**, 550–7 (2010).

148. A. Skupin *et al.*, How does intracellular Ca2+ oscillate: by chance or by the clock? *Biophys. J.* **94**, 2404–11 (2008).

149. A. Skupin, H. Kettenmann, M. Falcke, Calcium Signals Driven by Single Channel Noise. *PLoS Comput. Biol.* **6**, e1000870 (2010).

150. E. Smedler, P. Uhlén, Frequency decoding of calcium oscillations. *Biochim. Biophys. Acta - Gen. Subj.* **1840**, 964–969 (2014).

151. J. Soboloff, B. S. Rothberg, M. Madesh, D. L. Gill, STIM proteins: dynamic calcium signal transducers. *Nat. Rev. Mol. Cell Biol.* **13**, 549–65 (2012).

152. S. Song *et al.*, Irregular Ca(2+) oscillations regulate transcription via cumulative spike duration and spike amplitude. *J. Biol. Chem.* **287**, 40246–55 (2012).

153. M. Soundararajan *et al.*, Structural diversity in the RGS domain and its interaction with heterotrimeric G protein alpha-subunits. *Proc. Natl. Acad. Sci. U. S. A.* **105**, 6457–62 (2008).

154. S. M. Spangler, M. R. Bruchas, Optogenetic approaches for dissecting neuromodulation and GPCR signaling in neural circuits. *Curr. Opin. Pharmacol.* **32**, 56–70 (2017).

155. M. Stierl *et al.*, Light modulation of cellular cAMP by a small bacterial photoactivated adenylyl cyclase, bPAC, of the soil bacterium Beggiatoa. *J. Biol. Chem.* **286**, 1181–8 (2011).

156. D. Strickland *et al.*, TULIPs: tunable, light-controlled interacting protein tags for cell biology. *Nat. Methods*. **9**, 379–84 (2012).

157. Y. Tang, J. L. Stephenson, H. G. Othmer, Simplification and analysis of models of calcium dynamics based on IP3-sensitive calcium channel kinetics. *Biophys. J.* **70**, 246–263 (1996).

158. A. Taslimi *et al.*, Optimized second-generation CRY2–CIB dimerizers and photoactivatable Cre recombinase. *Nat. Chem. Biol.* **12**, 1–8 (2016).

159. S. Tay *et al.*, Single-cell NF-kappaB dynamics reveal digital activation and analogue information processing. *Nature*. **466**, 267–71 (2010).

160. D. Thomas *et al.*, Microscopic properties of elementary Ca2+ release sites in non-excitable cells. *Curr. Biol.* **10**, 8–15 (2000).

161. K. Thurley, M. Falcke, Derivation of Ca2+ signals from puff properties reveals that pathway function is robust against cell variability but sensitive for control. *Proc. Natl. Acad. Sci.* **108**, 427–432 (2011).

162. K. Thurley *et al.*, Reliable encoding of stimulus intensities within random sequences of intracellular Ca2+ spikes. *Sci. Signal.* **7**, ra59 (2014).

163. K. Thurley, A. Skupin, R. Thul, M. Falcke, Fundamental properties of Ca2+ signals. *Biochim. Biophys. Acta*. **1820**, 1185–94 (2012).

164. D. Tischer, O. D. Weiner, Illuminating cell signalling with optogenetic tools. *Nat. Rev. Mol. Cell Biol.* **15**, 551–8 (2014).

165. J. Toettcher, C. Voigt, O. Weiner, W. Lim, The promise of optogenetics in cell biology : interrogating molecular circuits in space and time. *Nat. Methods*. **8**, 35–38 (2010).

166. T. Tomida, K. Hirose, A. Takizawa, F. Shibasaki, M. Iino, NFAT functions as a working memory of a signals in decoding a oscillation. *Embo J*. **22**, 3825–3832 (2003).

167. S. C. Tovey, G. B. Willars, Single-Cell Imaging of Intracellular Ca2+ and Phospholipase C Activity Reveals That RGS 2 , 3 , and 4 Differentially Regulate Signaling via the G alpha q / 11 -Linked Muscarinic M 3 Receptor. *Mol. Pharmacol.* **66**, 1453–1464 (2004).

168. T. Y.-C. Tsai *et al.*, Robust, tunable biological oscillations from interlinked positive and negative feedback loops. *Science*. **321**, 126–9 (2008).

169. D. Varga-Szabo, A. Braun, B. Nieswandt, Calcium signaling in platelets. *J. Thromb. Haemost.* **7**, 1057–1066 (2009).

170. L. De Vries, B. Zheng, T. Fischer, E. Elenko, M. G. Farquhar, The Regulator of G Protein Signaling Family. *Annu. Rev. Pharmacol. Toxicol.* **400**, 235–271 (2000).

171. X. Wang, G. Huang, X. Luo, J. M. Penninger, S. Muallem, Role of regulator of G

protein signaling 2 (RGS2) in Ca2+ oscillations and adaptation of Ca2+ signaling to reduce excitability of RGS2-/- cells. *J. Biol. Chem.* **279**, 41642–41649 (2004).

172. S. L. Werner, D. Barken, A. Hoffmann, Stimulus specificity of gene expression programs determined by temporal control of IKK activity. *Science*. **309**, 1857–61 (2005).

173. a E. West *et al.*, Calcium regulation of neuronal gene expression. *Proc. Natl. Acad. Sci. U. S. A.* **98**, 11024–31 (2001).

174. R. Wollman, T. Meyer, Coordinated oscillations in cortical actin and Ca2+ correlate with cycles of vesicle secretion. *Nat. Cell Biol.* **14**, 1261–1269 (2012).

175. G.-X. Xie, P. P. Palmer, How regulators of G protein signaling achieve selective regulation. *J. Mol. Biol.* **366**, 349–65 (2007).

176. X. Xu *et al.*, RGS proteins determine signaling specificity of G(q)-coupled receptors. *J. Biol. Chem.* **274**, 3549–3556 (1999).

177. T. Xue *et al.*, Melanopsin signalling in mammalian iris and retina. *Nature*. **479**, 67–73 (2011).

178. H. Ye, M. Daoud-El Baba, R.-W. Peng, M. Fussenegger, A synthetic optogenetic transcription device enhances blood-glucose homeostasis in mice. *Science*. **332**, 1565–8 (2011).

179. N. Yissachar *et al.*, Dynamic response diversity of NFAT isoforms in individual living cells. *Mol. Cell*. **49**, 322–30 (2013).

180. N. Yosef, A. Regev, Impulse control: temporal dynamics in gene transcription. *Cell*. **144**, 886–96 (2011).

181. K. Zhang, B. Cui, Optogenetic control of intracellular signaling pathways. *Trends Biotechnol.* **33**, 92–100 (2015).

182. S. L. Zhang *et al.*, STIM1 is a Ca2+ sensor that activates CRAC channels and migrates from the Ca2+ store to the plasma membrane. *Nature*. **437**, 902–5 (2005).

183. P. Zhao, W. Cladman, H. H. M. Van Tol, P. Chidiac, Fine-tuning of GPCR signals by intracellular G protein modulators*. Progress in Molecular Biology and Translational Science*. **115**, 421-453 (2013).

184. L. Zhu *et al.*, Cumulated $Ca2^{+}$ spike duration underlies $Ca2^{+}$ oscillation frequency-regulated NFκB transcriptional activity. *J. Cell Sci.* **124**, 2591–601 (2011).

185. T. Ziegler, A. Möglich, Photoreceptor engineering. *Front. Mol. Biosci.* **2**, 30 (2015).